Self-Bearing Linear-Rotary Actuators with Wireless Power Transfer for High-Purity and Precision Applications

Spasoje Mirić, Rosario V. Giuffrida, Prasad Jayathurathnage, Johann W. Kolar

Swiss Federal Institute of Technology (ETH) Zurich
Power Electronic Systems Laboratory
www.pes.ee.ethz.ch

May 15, 2023, San Francisco

Self-Bearing Linear-Rotary Actuators with Wireless Power Transfer for High-Purity and Precision Applications

Spasoje Mirić et al.

University of Innsbruck, Institute for Mechatronics
Innsbruck Drives and Energy Systems Laboratory (iDES)
www.uibk.ac.at/mechatronik/ides/

May 15, 2023, San Francisco

universität innsbruck

Outline

Part 1

- *Introduction*

- *LiRA Examples / Applications*
- *Linear Actuator with Integrated MBs*
- *Position Sensors*
- *Dynamic Modeling, Controller Design*
- *Generalized Complex Space Vector*
- *Double Stator LiRA*

- *Outlook*

Part 2

- *Introduction*

- *Application: Blood Pumps*
- *Sensors for SB-LiRAs*
- *Design Example: the ShuttlePump*

- *Outlook*

Part 3

- *Introduction*

- *WPT to Linear Actuators*
- *Orthogonal and Parallel Field Concept*
- *Supplying Multiple Receivers*
  Voltage & Current Impressed WPT

- *Outlook*

Outline

Part 1

- *Introduction*

- *LiRA Examples / Applications*
- *Linear Actuator with Integrated MBs*
- *Position Sensors*
- *Dynamic Modeling, Controller Design*
- *Generalized Complex Space Vector*
- *Double Stator LiRA*

- *Outlook*

Part 2

- *Introduction*

- *Application: Blood Pumps*
- *Sensors for SB-LiRAs*
- *Design Example: the ShuttlePump*

- *Outlook*

Part 3

- *Introduction*

- *WPT to Linear Actuators*
- *Orthogonal and Parallel Field Concept*
- *Supplying Multiple Receivers*
  Voltage & Current Impressed WPT

- *Outlook*

Introduction

Linear Rotary Actuators (LiRAs)
Applications
LiRA Examples

Linear-Rotary Actuator (LiRA)

- LiRA is conceived by coupling Linear and Rotary actuators (machines)
- Types of coupling: Mechanical, Magnetic, Double Stator

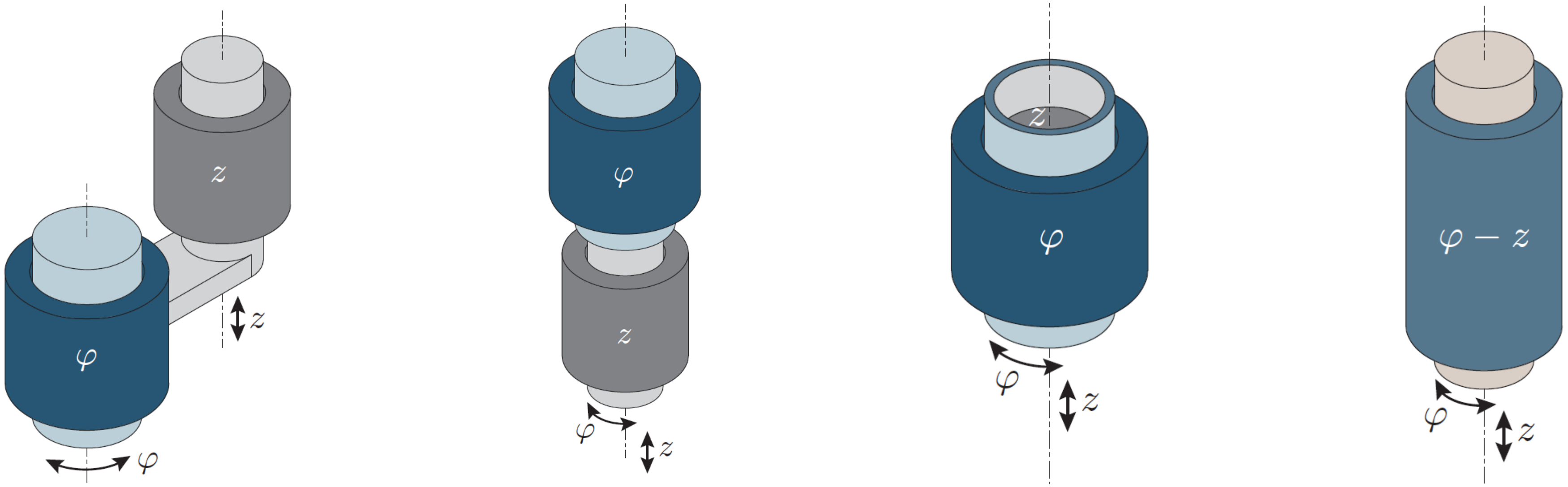

- Parallel Mechanical Coupling
- Series Mechanical Coupling
- Double Stator
- Magnetic Coupling

- Intended use determines the type of the LiRA, i.e., the type of coupling
- Parallel mechanical coupling → simple to realize, but low dynamics & moving cables

LiRA Application Examples

- A wide spectrum of application areas: servo, tools, industrial automation, robot end-effector, blood pumps

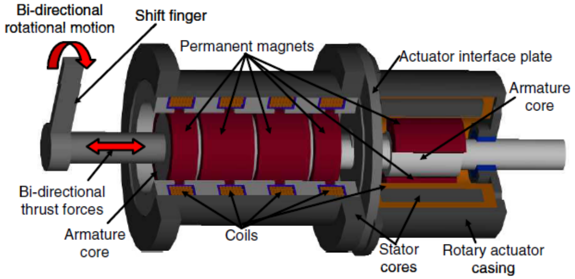

Source: IEEE

- Servo

Source: RIDGID

- Lathe

Source: FOOD manufacture

- Industry Assembly Lines

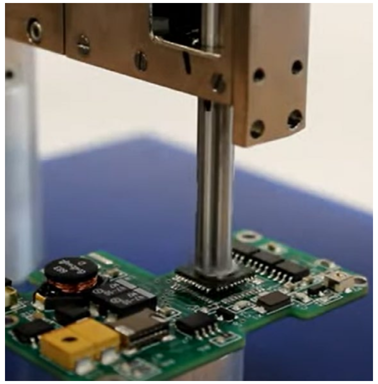

Source: SMAC Moving Coil Actuators

- Pick & Place Robot in Electronics/Semiconductor Industry

Source: camfil

- Handling/Dosing in Pharmaceutical/Chemical Industry

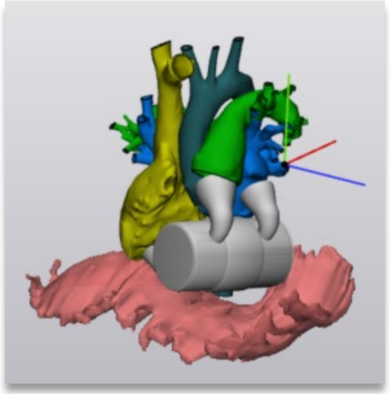

Source: Medizinische Universität Wien

- ShuttlePump

LiRA Example 1

- Series mechanical coupling → three-phase slotless PM rotary actuator (top) & linear actuator (bottom)
- Pick&Place LiRA enables rotational and translational motion for small component placement

Source: IEEE, TU/e Eindhoven University of Technology

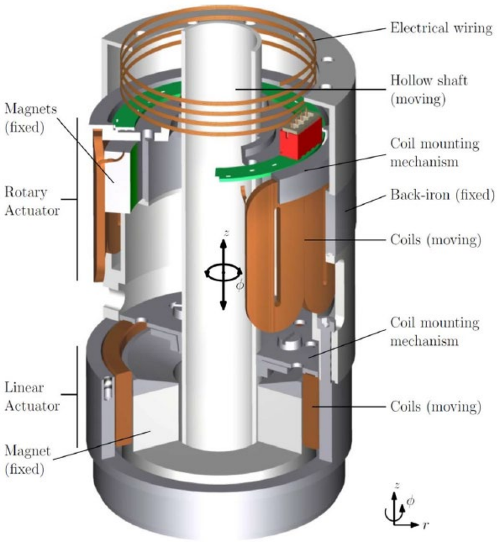

Parameter	Value
z_{stroke}	±5 mm
ϕ_{stroke}	±180° degrees
z_{err}	5 µm
ϕ_{err}	3 mrad
α_z	150 m s^{-2}
α_ϕ	7700 rad s^{-2}
v_{max}	3 m s^{-1}
ω_{max}	135 rad s^{-1}
d_z	0.22
d_ϕ	0.39
$L_{z\phi}$	105 mm
$r_{o,max}$	30 mm
$r_{i,min}$	18 mm

→ High accelerations required

→ Rather a low max. speed

- LiRA or $z\phi$-Actuator
- Specifications

- Component placement throughput → high dynamics/accelerations
- Actuator operation → low speeds due to limited stroke (acceleration/deceleration)

[ref] Overboom, T. T., et al. "Design and Optimization of a Rotary Actuator for a Two-Degree-of-Freedom $ z\phi $-Module." IEEE Transactions on Industry Applications 46.6 (2010): 2401-2409.

LiRA Example 2

- Series mechanical coupling → three-phase rotary actuator & three-phase linear actuator
- Pick&Place LiRA enables rotational and translational motion for small component placement

Source: IEEE, TU/e Eindhoven University of Technology

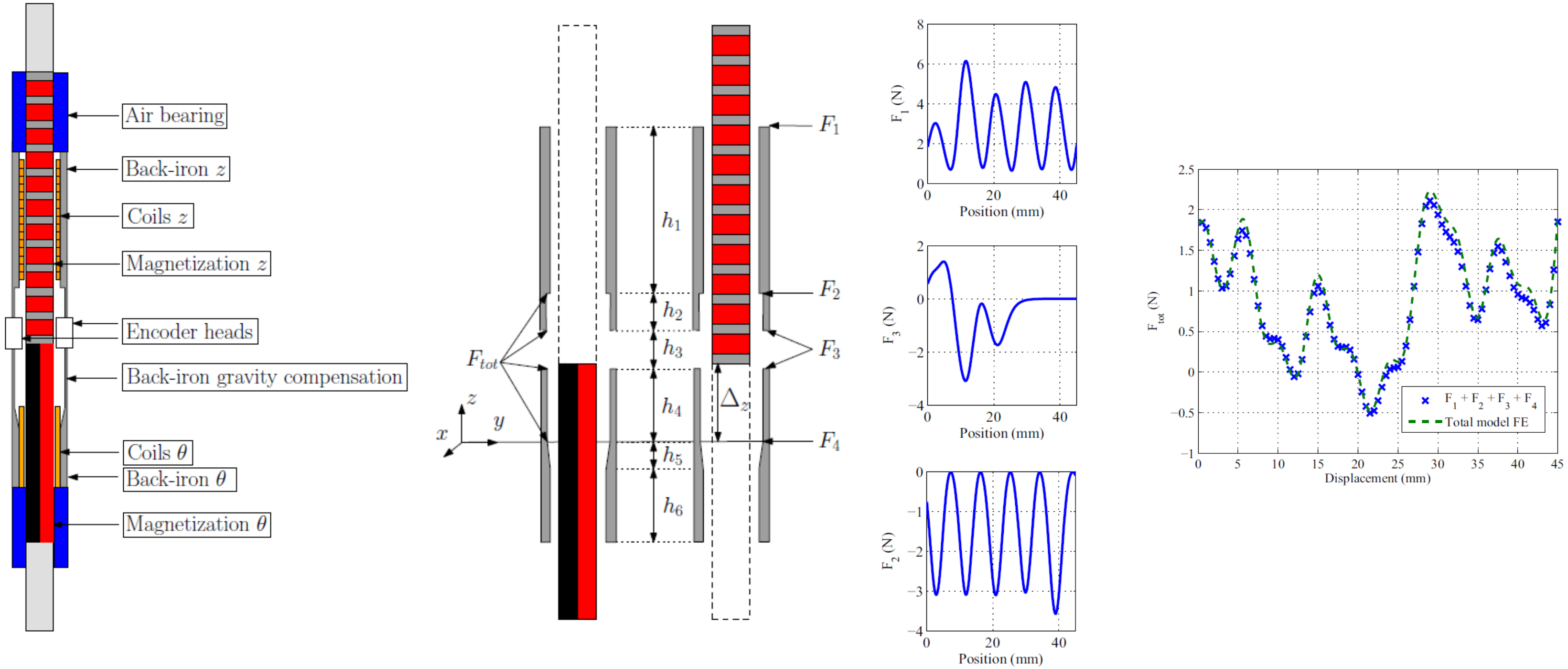

- Cogging force due to end effects → minimization by optimizing stator core geometry / placement
- Passive gravity compensation → force profile optimized in 3D-FEM by varying geometry

[ref] Meessen, K. J., J. J. H. Paulides, and E. A. Lomonova. "Analysis and design considerations of a 2-DoF rotary-linear actuator." 2011 IEEE International Electric Machines & Drives Conference (IEMDC). IEEE, 2011.

LiRA Example 3

- Three-phase rotary actuator & slotless linear actuator winding in the air gap
- Pick&Place LiRA enables rotational and translational motion for small component placement

Source: IEEE, TU/e Eindhoven University of Technology

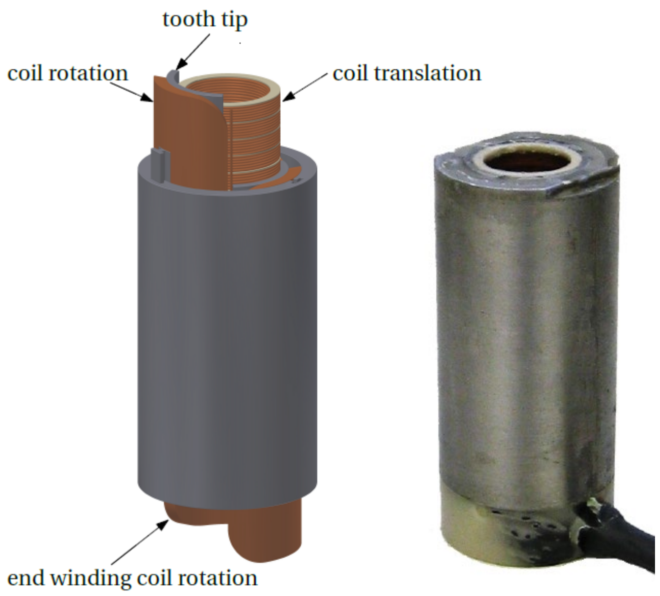

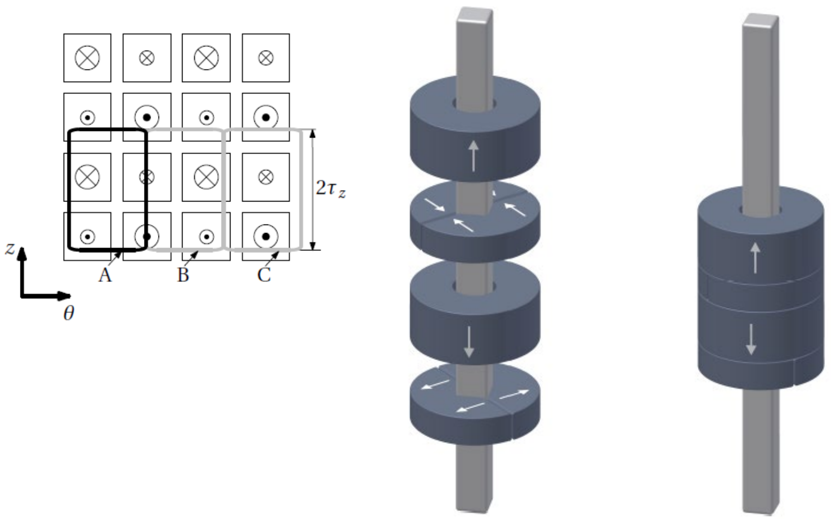

- Single set of mover permanent magnets → special arrangement to interact with rotary and linear windings
- Large air gap → low cogging force; but low machine constant

[ref] Meessen, Koen Joseph. "Electromagnetic fields and interactions in 3D cylindrical structures: Modeling and application." Dept. Electric Eng., Eindhoven Univ. Technol., the Netherlands (2012).

LiRA Example 4

- Moving coil rotary actuator & moving coil linear actuator
- Pick&Place LiRA enables rotational and translational motion for small component placement

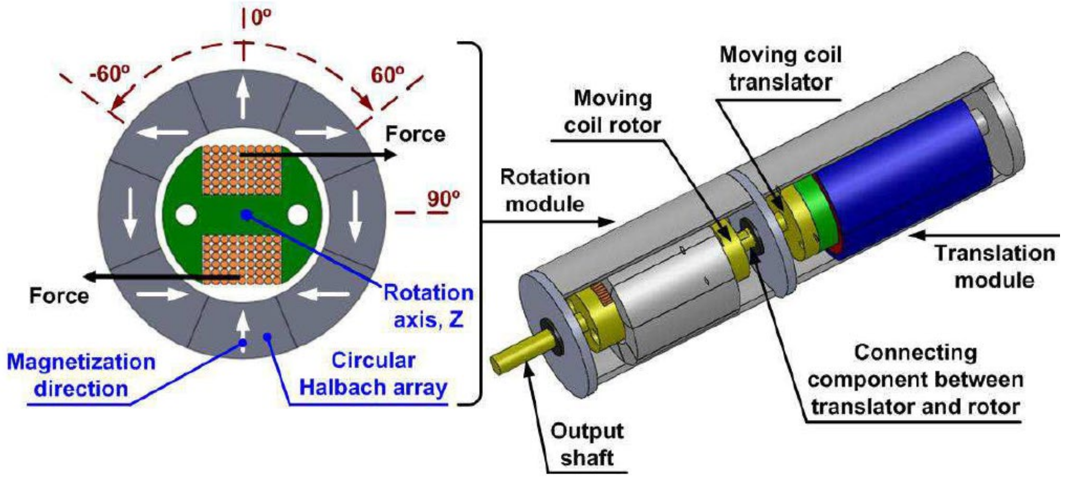

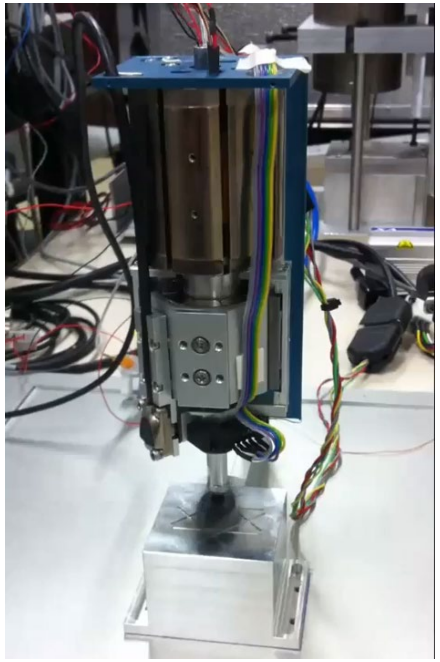

- Limited rotary stroke due to permanent magnet field arrangement → parts with no radial field
- Moving coils → moving cables limit lifetime

[ref] Teo, Tat Joo, et al. "Principle and modeling of a novel moving coil linear-rotary electromagnetic actuator." IEEE Transactions on Industrial Electronics 63.11 (2016): 6930-6940.
https://www.youtube.com/watch?v=ApWIagkbrE0
Agency for Science, Technology and Research, Singapore

LiRA Example 5

- Concentrated coils in linear and rotary direction → 'checkerboard actuator'
- Checkerboard direct drive LiRA enables rotational and translational motion

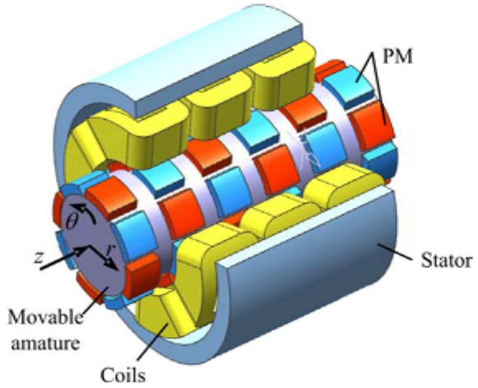

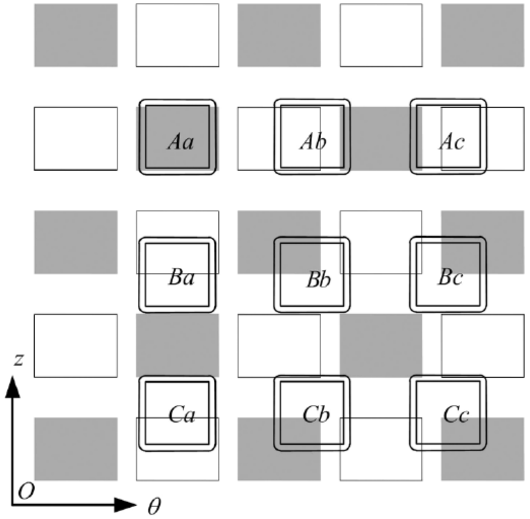

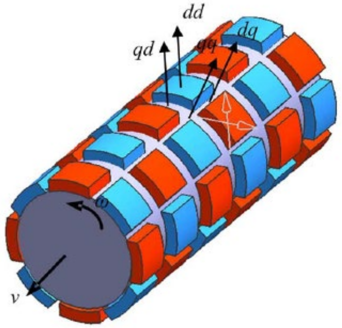

- LiRA with magnetic coupling → highest compactness, increased number of phases, increased control effort
- Ideally no end windings → end winding for the linear direction is an active part of the winding for rotary direction

[ref] Jin, Ping, et al. "3-D analytical linear force and rotary torque analysis of linear and rotary permanent magnet actuator." IEEE transactions on magnetics 49.7 (2013): 3989-3992.

LiRA Example 6

- Double stator LiRA → ‘magnetically insulated’ linear and rotary parts
- Three-phase linear and rotary machines, controlled independently

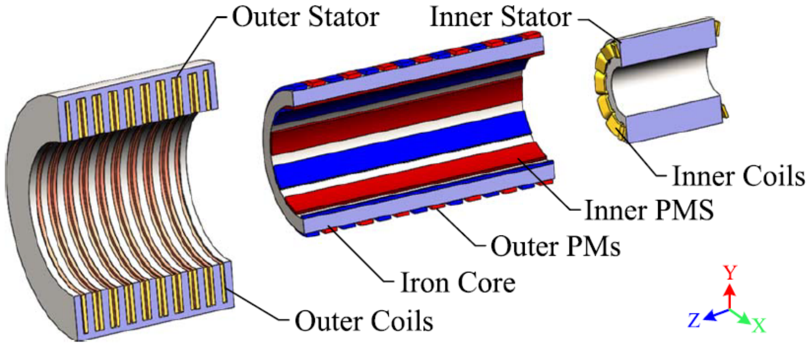

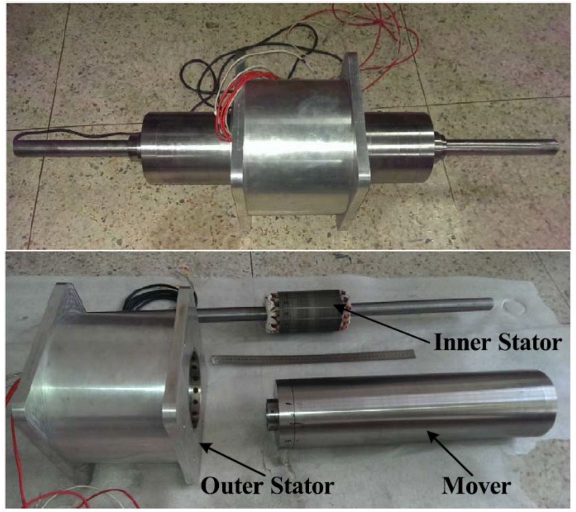

- Large force (650 N) / torque (10 Nm), dynamics limited due to the large moving mass of the mover
- Challenging design → cooling of the inner stator, mover back iron with two sets of PMs

[ref] Xu, Lei, et al. "Design and analysis of a double-stator linear–rotary permanent-magnet motor." IEEE Transactions on Applied Superconductivity 26.4 (2016): 1-4.

LiRA Example 7

- Helical winding (inner and outer) → independent thrust force and torque generation/control
- Slotless LiRA proposed usage for surgery robots in medicine

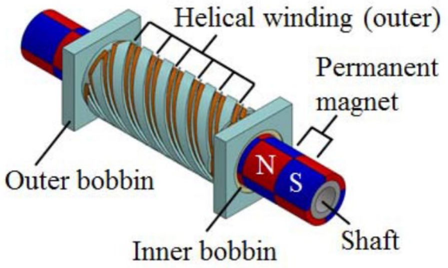

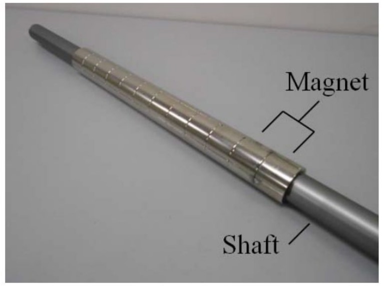

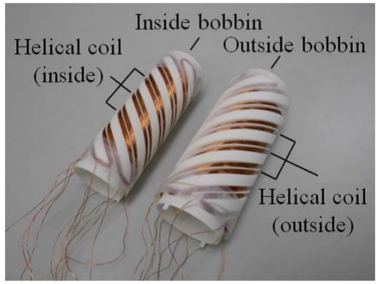

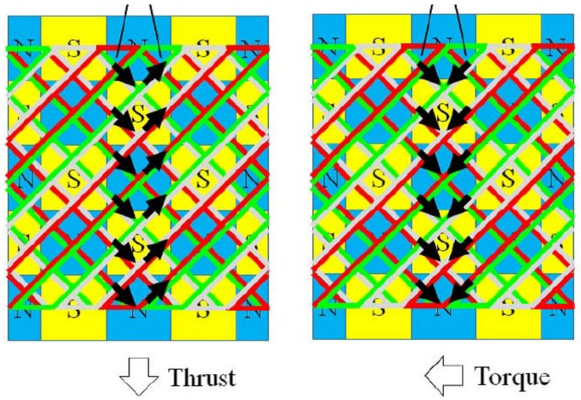

- Limited force (5 N)/torque (0.1 Nm) due to slotless winding, helical winding complicated to realize
- Mover PMs the same as for the checkerboard actuator

[ref] Tanaka, Shodai, Tomoyuki Shimono, and Yasutaka Fujimoto. "Optimal design of length factor for cross-coupled 2-DOF motor with Halbach magnet array." 2015 IEEE International Conference on Mechatronics (ICM). IEEE, 2015.

universität innsbruck

Need for Improvements

Application Requirements
Conventional Bearings
Bearingless / Self-bearing

High Precision Requirement

- High dynamics robot → reaches accelerations of $150\ ^{m}/_{s^2}$ and speeds of $5\ ^{m}/_{s}$
- Horizontal workspace of $300\ \mathrm{mm} \times 300\ \mathrm{mm}$; repeatability $< 10\ \mu\mathrm{m}$

Source: euspen

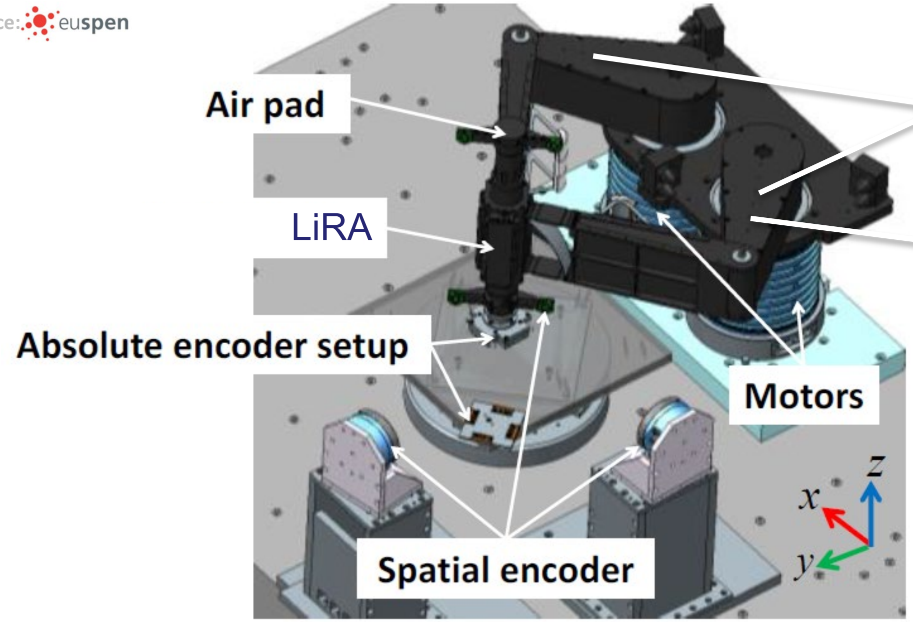

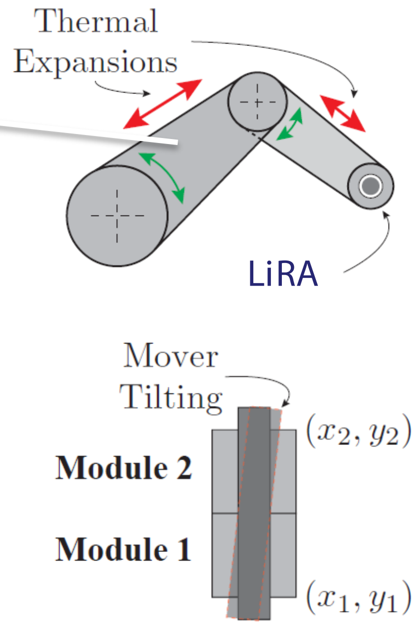

- Thermal expansions in parallel kinematics deteriorate precision → LiRA with radial position control
- Handling smaller components/dies → mover tilting necessary
- Mechanical/air bearings used in conventional LiRAs can not control radial position nor tilting

High Purity Requirement

- Applications requiring high purity → clean rooms, bioprocessing, pharmaceutical
- Mechanical bearings → limited lifetime / limited purity levels / often disassembling for cleaning

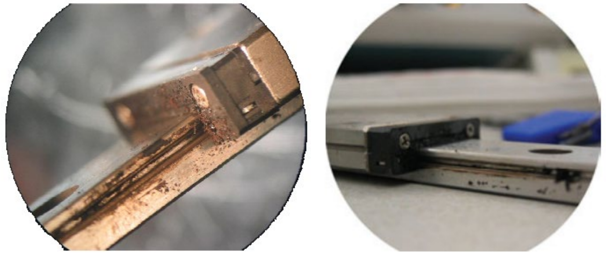

- Mechanical bearings compromise high purity

Source: LinMot®

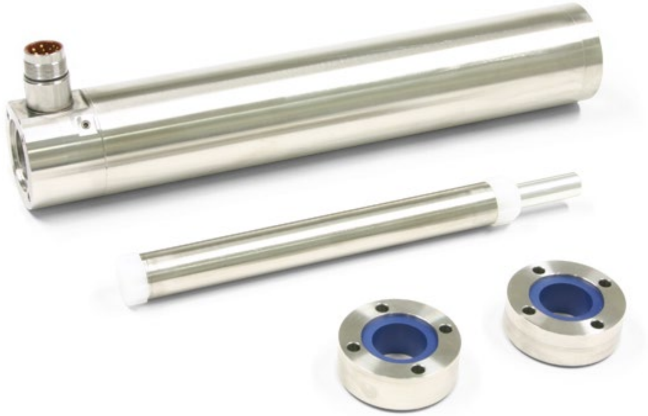

- Disassembling for regular high-pressure washdowns

- Air bearings → require air supply / prohibited operation in low-pressure environments
- High precision & high purity requirements limit usage of LiRAs with conventional bearings

[ref] Paulides, Johannes JH, Jeroen LG Janssen, and Elena A. Lomonova. "Bearing lifetime of linear PM machines." *2009 IEEE Energy Conversion Congress and Exposition*. IEEE, 2009.

Magnetic Bearings (MBs)

- Magnetic bearings → generate radial forces to keep the rotor/mover centered
- Closed loop position controller → sensor, microcontroller, power converter, MB windings

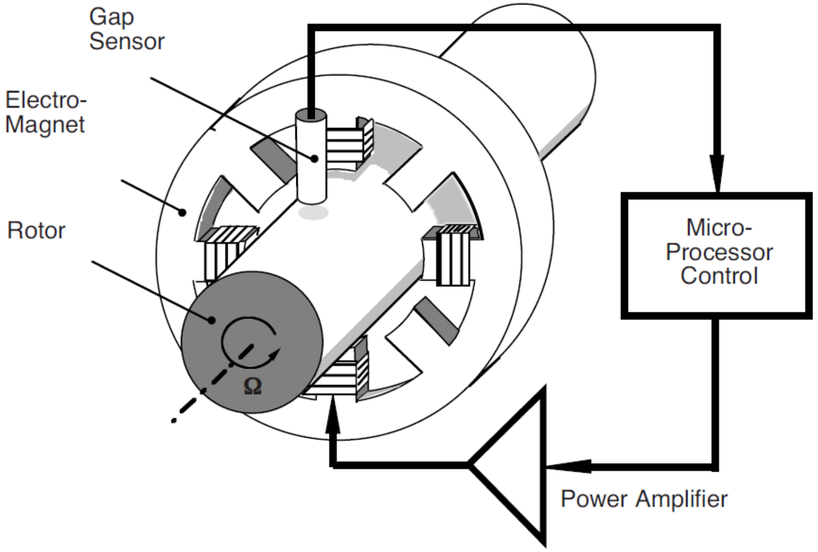

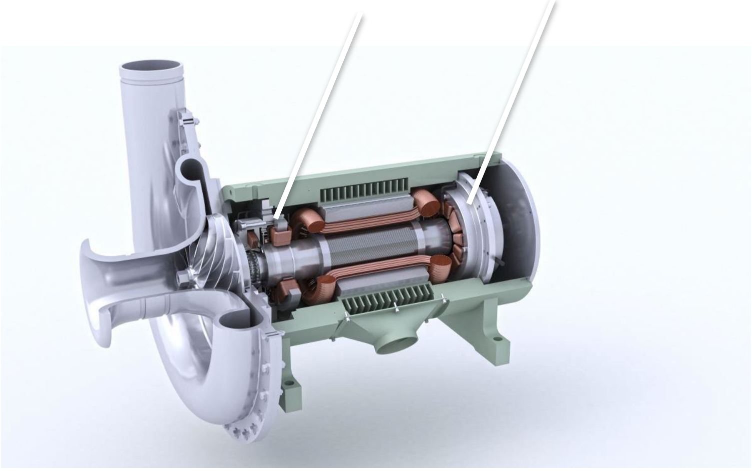

- Characteristics → free of contact, no contaminating wear, bearing stiffness control, low maintenance
- Applications → vacuum and clean room system, high-speed pumps, high-purity pumps, flywheels

[ref] Maslen, Eric H., and Gerhard Schweitzer, eds. Magnetic bearings: theory, design, and application to rotating machinery. Berlin, Heidelberg: Springer-Verlag Berlin Heidelberg, 2009.

Standalone MBs and Self-bearing/Bearingless Machines

- Self-bearing/Bearingless → integrate MBs into the existing machine structure
- Achieve self-bearing function → superimpose the main field (torque, p poles) with the $p \pm 2$ type

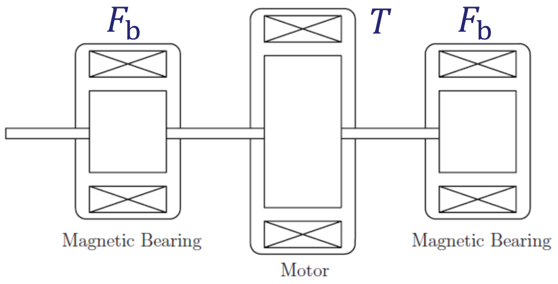

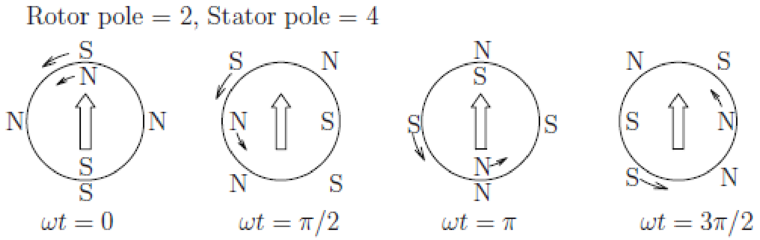

P+2

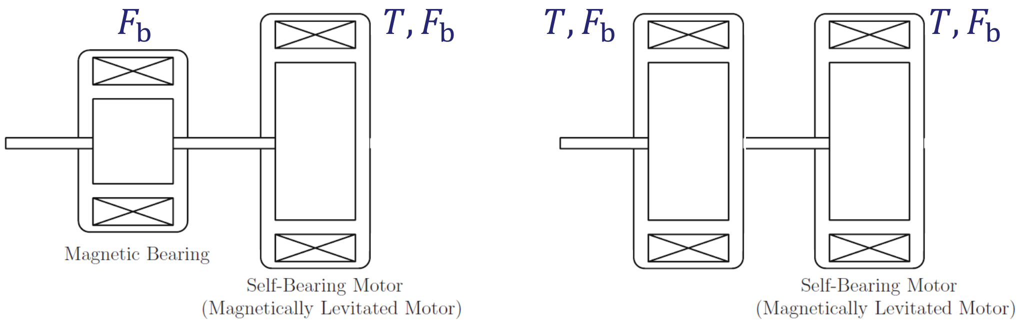

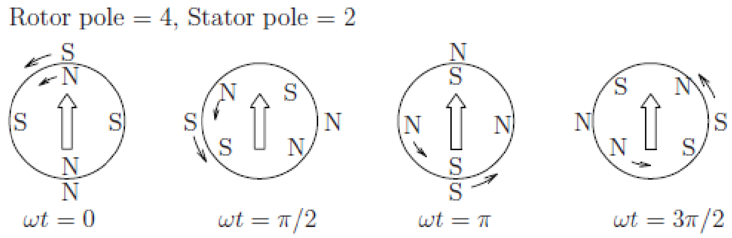

P-2

- Tilting control of the long shaft → either (F_b) & (T, F_b) or (T, F_b) & (T, F_b)
- $p \pm 2$ type is achieved by winding scheme or current distribution in the existing main windings

[ref] Maslen, Eric H., and Gerhard Schweitzer, eds. Magnetic bearings: theory, design, and application to rotating machinery. Berlin, Heidelberg: Springer-Verlag Berlin Heidelberg, 2009.

LiRA with MBs

- Integrating MBs into a LiRA → various combinations of standalone and self-bearing options are possible
- Tilting control of the mover necessary → MBs always at each axial end of a LiRA

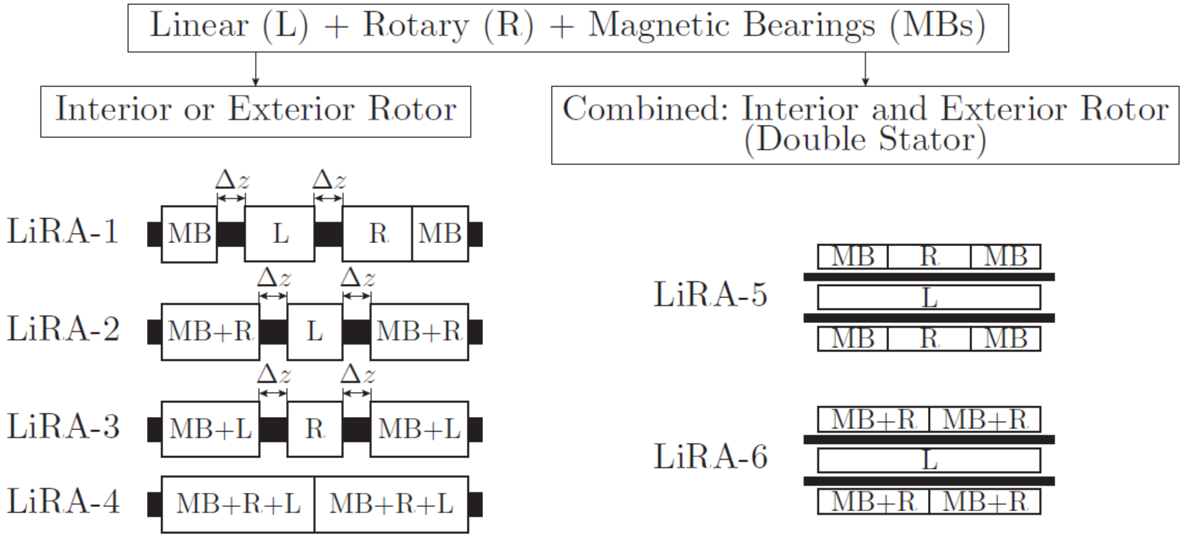

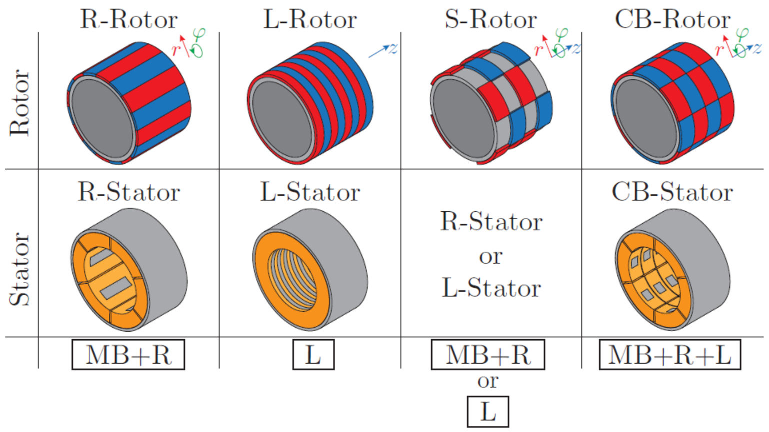

- Distance between the segments Δz = linear stroke → due to different PM arrangements in the mover
- MB + R → conventional; MB + L → interesting for further investigation!

[ref] Mirić, Spasoje, Dominik Bortis, and Johann Walter Kolar. "Design and comparison of permanent magnet self-bearing linear-rotary actuators." 2019 12th International Symposium on Linear Drives for Industry Applications (LDIA). IEEE, 2019.

universität innsbruck

Linear Actuator with Integrated MBs

Topology Derivation
Bearing Force Generation
Inverter Supply Requirements

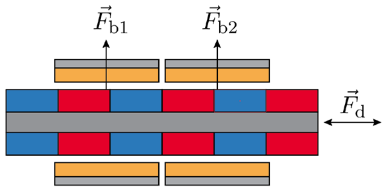

ETH zürich

International Electric Machines & Drives Conference
IEMDC 2023
San Francisco, CA May 15-18

Tubular Linear Actuator Derivation

- Derivation of TLA → tangential force for generating T in RA, generates drive F_d force in TLA
- TLA has fewer stray field compared to FLA due to the closed structure

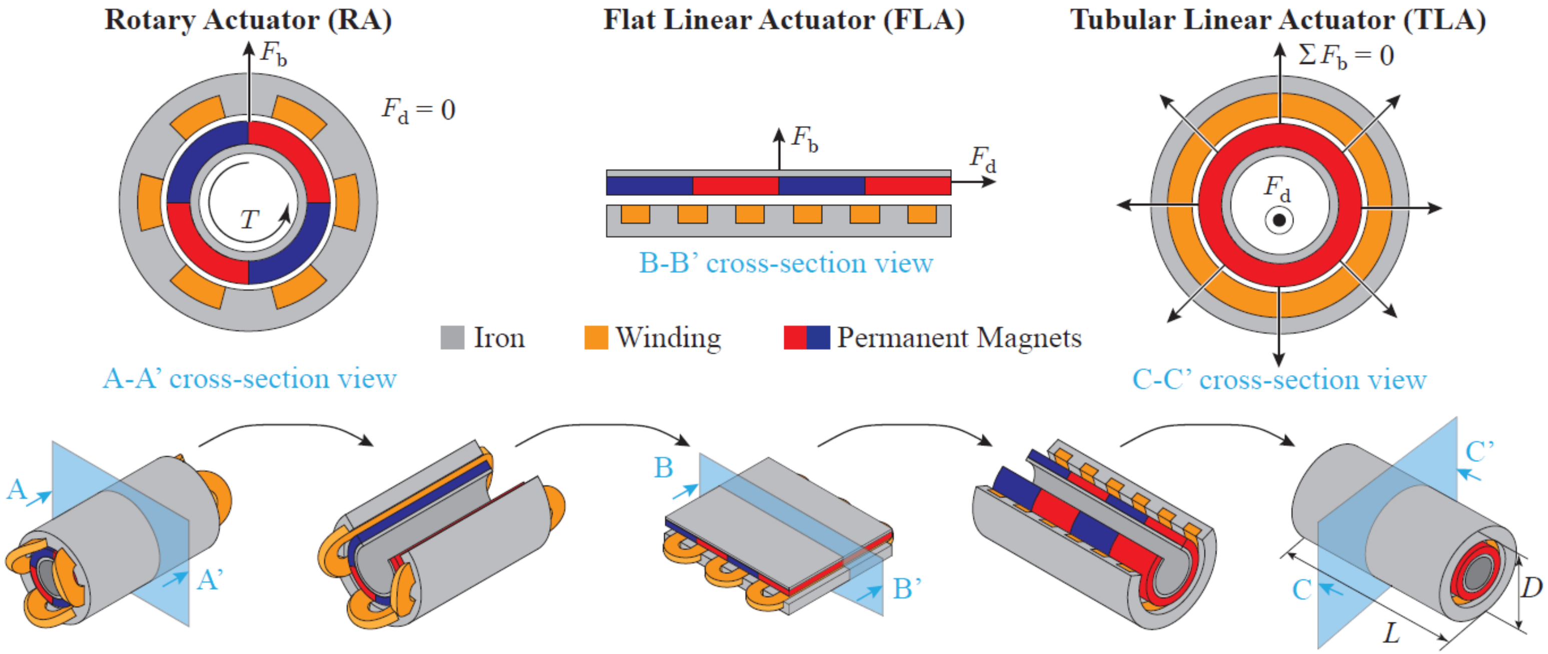

- TLA has circumferential symmetry → it can not generate bearing (radial) force, i.e., no MBs are possible
- FLA can generate bearing force F_b, but there is an attraction force between the mover PMs and the stator iron

[ref] Mirić, Spasoje, Johann W. Kolar, and Dominik Bortis. "Novel tubular linear actuator with integrated magnetic bearing." e & i Elektrotechnik und Informationstechnik 139.2 (2022): 230-242.

Tubular Linear Actuator (TLA)

- Three-phase ring windings → maximum usage of copper, no end winding
- d axis aligned with the peak flux density wave of the mover; θ is the electrical angle in a linear direction

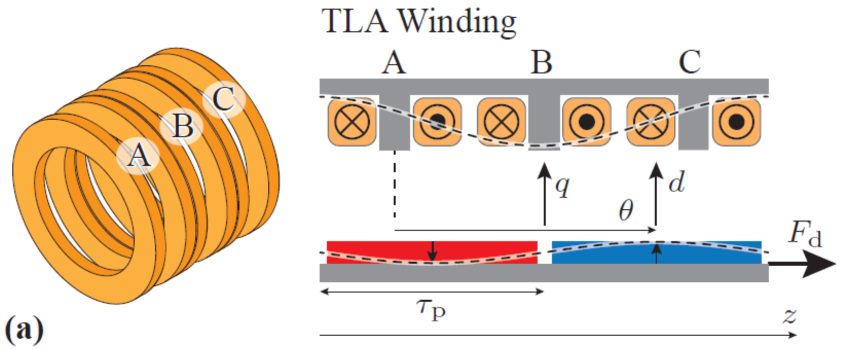

(a)

$$[x_A^d \; x_B^d \; x_C^d] = [x_d \; x_q] \cdot \begin{bmatrix} \cos(\theta+\gamma_A) & \cos(\theta+\gamma_B) & \cos(\theta+\gamma_C) \\ -\sin(\theta+\gamma_A) & -\sin(\theta+\gamma_B) & -\sin(\theta+\gamma_C) \end{bmatrix}$$

(b)

Linear Direction

$$[x_d \; x_q] = [x_A^d \; x_B^d \; x_C^d] \cdot \frac{2}{3} \begin{bmatrix} \cos(\theta+\gamma_A) & -\sin(\theta+\gamma_A) \\ \cos(\theta+\gamma_B) & -\sin(\theta+\gamma_B) \\ \cos(\theta+\gamma_C) & -\sin(\theta+\gamma_C) \end{bmatrix}$$

Linear Direction

(c)

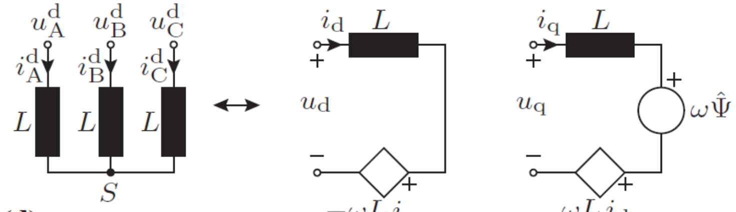

(d)

$$\gamma_A = 0, \; \gamma_B = -2\pi/3, \; \gamma_C = 2\pi/3$$

$$i_A^d = \hat{I}_d \cos(\theta + \theta_i^d + \gamma_A)$$
$$i_B^d = \hat{I}_d \cos(\theta + \theta_i^d + \gamma_B)$$
$$i_C^d = \hat{I}_d \cos(\theta + \theta_i^d + \gamma_C)$$

$$i_d^* = 0 \qquad i_q^* = \hat{I}_d = \frac{F_d^*}{K_d} \qquad K_d = \frac{3\pi}{2\tau_p}\hat{\Psi}$$

- TLA can generate linear drive force F_d; bearing force F_b is not possible to achieve with the TLA
- dq coordinated in a linear direction → stationary coordinates representation of the three-phase winding

[ref] Mirić, Spasoje, Dominik Bortis, and Johann Walter Kolar. "Design and comparison of permanent magnet self-bearing linear-rotary actuators." 2019 12th International Symposium on Linear Drives for Industry Applications (LDIA). IEEE, 2019.

xy Winding for Bearing Force Generation/Control

- A coil of the TLA split into 4 pieces, $x-$ and $y-$direction → bearing force F_b generation possible
- Bearing force generation capability → depends on the linear position of the mover/PM poles

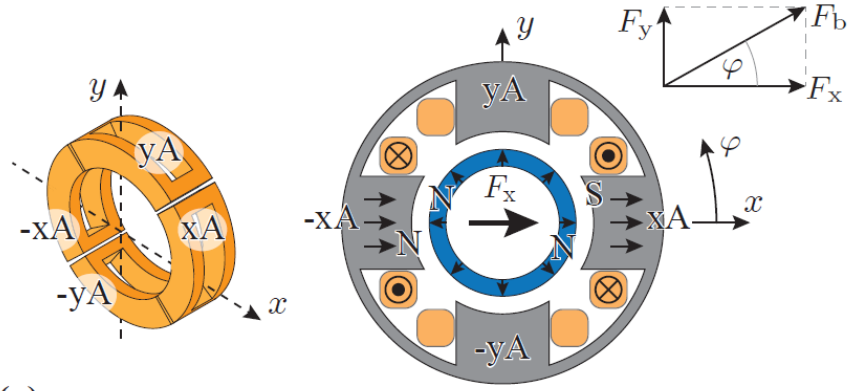

(a)

$$F_b = \sqrt{F_x^2 + F_x^2}$$
$$\varphi = \arctan 2(F_x, F_y)$$

$$i_x^* = \frac{F_x^*}{K_b} = \hat{I}_b \cos(\varphi)$$
$$i_y^* = \frac{F_y^*}{K_b} = \hat{I}_b \sin(\varphi)$$

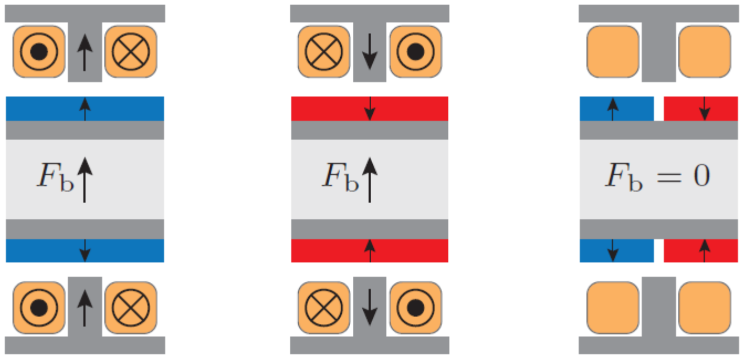

(c.i) (c.ii) (c.iii)

- $d-$ current component in a linear direction needed

- F_b generation possible if PM is facing the stator teeth → as long as there is non-zero flux linkage
- Mover/PM linear position changes in during the operation of the actuator

[ref] Mirić, Spasoje, Dominik Bortis, and Johann Walter Kolar. "Design and comparison of permanent magnet self-bearing linear-rotary actuators." 2019 12th International Symposium on Linear Drives for Industry Applications (LDIA). IEEE, 2019.

xy Winding and Three-Phase ABC Linear Winding

- Bearing force currents → 'd − component' in a linear direction, must not generate drive (linear) force
- xy – current components (circumferential) → determined by the desired force direction

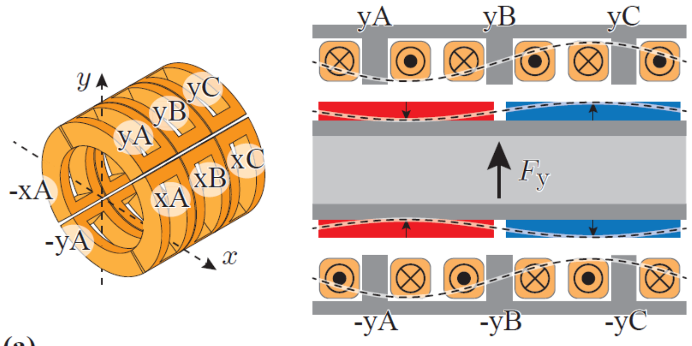

(a)

$$i^*_{xd} = i^*_x = \frac{F^*_x}{K_b} \qquad i^*_{xq} = 0$$

$$i^*_{yd} = i^*_y = \frac{F^*_y}{K_b} \qquad i^*_{yq} = 0,$$

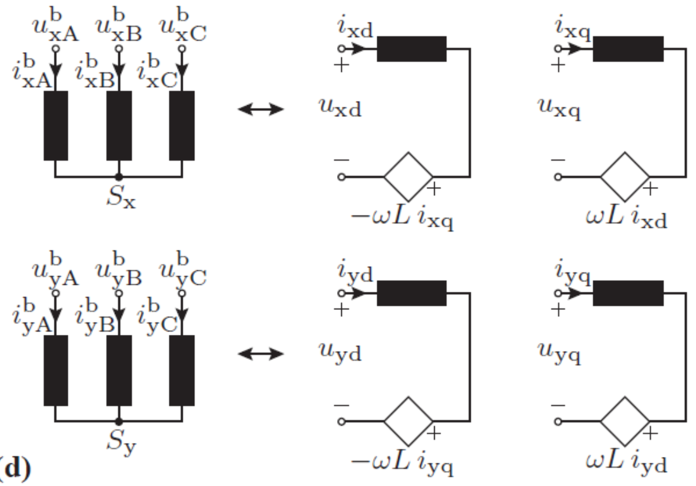

(d)

$$i^*_{x\{A,B,C\}} = i^*_{xd} \cdot \cos(\theta + \theta^b_i + \gamma_{\{A,B,C\}})$$

$$i^*_{y\{A,B,C\}} = i^*_{yd} \cdot \cos(\theta + \theta^b_i + \gamma_{\{A,B,C\}})$$

- i^*_{xd} and i^*_{yd} calculated from the force components that should act on the mover (e.g., obtained by position controller)
- θ is the electrical angle determined by the mover's axial position z → $\theta = \pi \cdot z/\tau_p$

[ref] Mirić, Spasoje, Dominik Bortis, and Johann Walter Kolar. "Design and comparison of permanent magnet self-bearing linear-rotary actuators." 2019 12th International Symposium on Linear Drives for Industry Applications (LDIA). IEEE, 2019.

xydq Transformation

- 4 stationary components → *xy* for bearing force (rotary dir.) & *dq* for drive force (linear dir.)
- Variable x can be votage v, current i or flux linkage ψ

Linear Direction

Rotary Direction

$$\underbrace{\begin{bmatrix} x_{\mathrm{xd}} & x_{\mathrm{xq}} \\ x_{\mathrm{yd}} & x_{\mathrm{yq}} \end{bmatrix}}_{\mathrm{xydq}} = \underbrace{\begin{bmatrix} x^{\mathrm{b}}_{\mathrm{xA}} & x^{\mathrm{b}}_{\mathrm{xB}} & x^{\mathrm{b}}_{\mathrm{xC}} \\ x^{\mathrm{b}}_{\mathrm{yA}} & x^{\mathrm{b}}_{\mathrm{yB}} & x^{\mathrm{b}}_{\mathrm{yC}} \end{bmatrix}}_{\mathrm{xyABC}} \times \frac{2}{3} \begin{bmatrix} \cos(\theta+\gamma_{\mathrm{A}}) & -\sin(\theta+\gamma_{\mathrm{A}}) \\ \cos(\theta+\gamma_{\mathrm{B}}) & -\sin(\theta+\gamma_{\mathrm{B}}) \\ \cos(\theta+\gamma_{\mathrm{C}}) & -\sin(\theta+\gamma_{\mathrm{C}}) \end{bmatrix}$$

Linear Direction

xydq Transformation

Linear Direction

Rotary Direction

$$\underbrace{\begin{bmatrix} x^{\mathrm{b}}_{\mathrm{xA}} & x^{\mathrm{b}}_{\mathrm{xB}} & x^{\mathrm{b}}_{\mathrm{xC}} \\ x^{\mathrm{b}}_{\mathrm{yA}} & x^{\mathrm{b}}_{\mathrm{yB}} & x^{\mathrm{b}}_{\mathrm{yC}} \end{bmatrix}}_{\mathrm{xyABC}} = \underbrace{\begin{bmatrix} x_{\mathrm{xd}} & x_{\mathrm{xq}} \\ x_{\mathrm{yd}} & x_{\mathrm{yq}} \end{bmatrix}}_{\mathrm{xydq}} \times \begin{bmatrix} \cos(\theta+\gamma_{\mathrm{A}}) & \cos(\theta+\gamma_{\mathrm{B}}) & \cos(\theta+\gamma_{\mathrm{C}}) \\ -\sin(\theta+\gamma_{\mathrm{A}}) & -\sin(\theta+\gamma_{\mathrm{B}}) & -\sin(\theta+\gamma_{\mathrm{C}}) \end{bmatrix}$$

Inverse *xydq* Transformation

- 12 phase windings, but 6 phase quantities → windings on the same axis connected in series
- Linear direction → ABC – three-phase quantities; dq – stationary coordinates quantities

[ref] Mirić, Spasoje, Dominik Bortis, and Johann Walter Kolar. "Design and comparison of permanent magnet self-bearing linear-rotary actuators." 2019 12th International Symposium on Linear Drives for Industry Applications (LDIA). IEEE, 2019.

abc Winding for Bearing and ABC Winding for Linear Motion

- Bearing force control with a three-phase winding abc → xy current components determine the $\hat{I}_b$ and φ
- φ - electrical angle for rotary direction; θ – electrical angle for linear direction

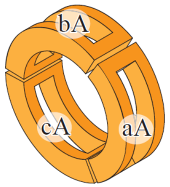

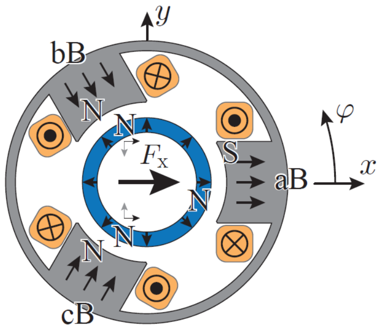

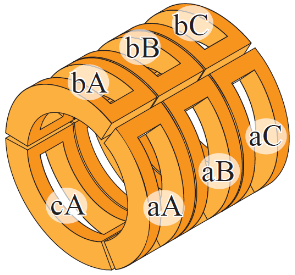

$$i^*_{xd} = i^*_x = \frac{F^*_x}{K_b} \qquad i^*_{xq} = 0$$

$$i^*_{yd} = i^*_y = \frac{F^*_y}{K_b} \qquad i^*_{yq} = 0,$$

$$\hat{I}_b = \sqrt{(i^*_{xd})^2 + (i^*_{yd})^2}$$

$$\varphi = \arctan 2(i^*_{xd}, i^*_{yd})$$

$$i^b_{a\{A,B,C\}} = \hat{I}_b \cos(\varphi + \gamma_a) \cdot \cos(\theta + \theta^b_i + \gamma_{\{A,B,C\}})$$

$$i^b_{b\{A,B,C\}} = \hat{I}_b \cos(\varphi + \gamma_b) \cdot \cos(\theta + \theta^b_i + \gamma_{\{A,B,C\}})$$

$$i^b_{c\{A,B,C\}} = \hat{I}_b \cos(\varphi + \gamma_c) \cdot \cos(\theta + \theta^b_i + \gamma_{\{A,B,C\}})$$

$$\gamma_A = 0,\ \gamma_B = -2\pi/3,\ \gamma_C = 2\pi/3$$

- Comparison between xy and abc winding type → capability for the bearing F_b and the drive F_d force generation
- Rotary direction → abc – three-phase quantities; xy – stationary coordinates quantities

[ref] Mirić, Spasoje, Dominik Bortis, and Johann Walter Kolar. "Design and comparison of permanent magnet self-bearing linear-rotary actuators." 2019 12th International Symposium on Linear Drives for Industry Applications (LDIA). IEEE, 2019.

abcdq Transformation

- 4 stationary components → xy for bearing force (rotary dir.) & dq for drive force (linear dir.)
- Variable x can be votage v, current i or flux linkage ψ

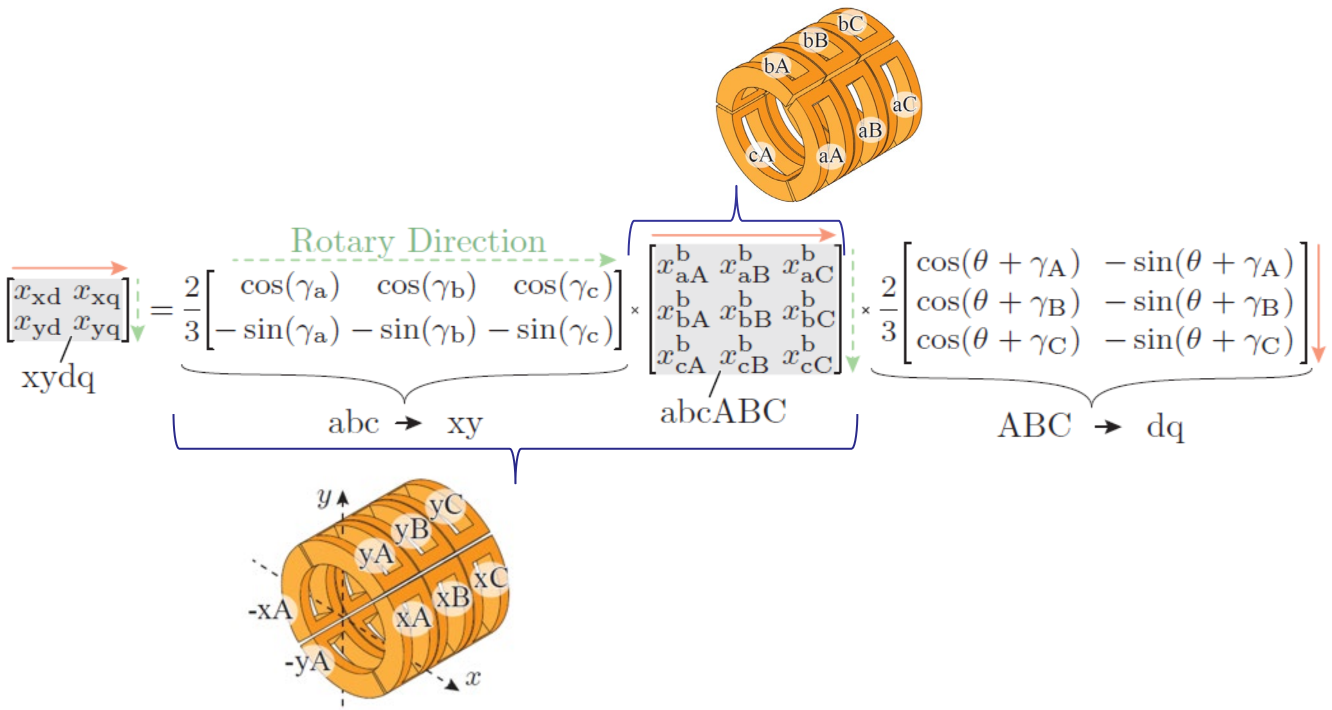

$$\begin{bmatrix} x_{xd} & x_{xq} \\ x_{yd} & x_{yq} \end{bmatrix} = \frac{2}{3}\begin{bmatrix} \cos(\gamma_a) & \cos(\gamma_b) & \cos(\gamma_c) \\ -\sin(\gamma_a) & -\sin(\gamma_b) & -\sin(\gamma_c) \end{bmatrix} \times \begin{bmatrix} x^b_{aA} & x^b_{aB} & x^b_{aC} \\ x^b_{bA} & x^b_{bB} & x^b_{bC} \\ x^b_{cA} & x^b_{cB} & x^b_{cC} \end{bmatrix} \times \frac{2}{3}\begin{bmatrix} \cos(\theta+\gamma_A) & -\sin(\theta+\gamma_A) \\ \cos(\theta+\gamma_B) & -\sin(\theta+\gamma_B) \\ \cos(\theta+\gamma_C) & -\sin(\theta+\gamma_C) \end{bmatrix}$$

abcdq Transformation

- *abcABC* winding, three-phase rotary and three-phase linear → 9 phase quantities
- Bearing current component & Drive current component → *combined* or *separated* windings

[ref] Mirić, Spasoje, Dominik Bortis, and Johann Walter Kolar. "Design and comparison of permanent magnet self-bearing linear-rotary actuators." 2019 12th International Symposium on Linear Drives for Industry Applications (LDIA). IEEE, 2019.

xyABC Winding Inverter Supply

- Bearing force and driving force function → realized with the *combined* or *separated* windings
- Combined winding → each phase winding contains the *bearing* and the *drive* current components

■ Combined winding, 12 half-bridges

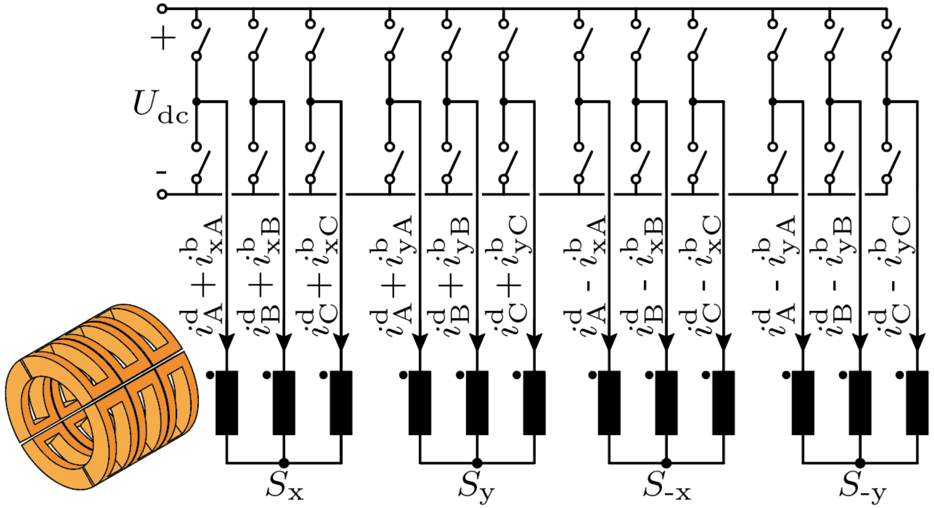

■ Separated winding, 9 half-bridges

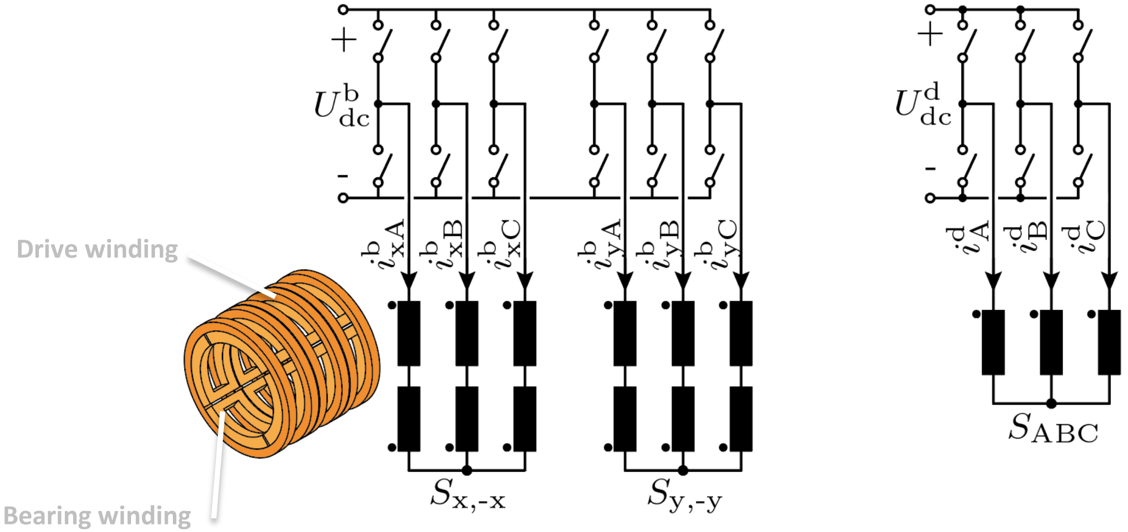

- Combined winding → each winding needs a dedicated half-bridge; star points with the linear three-phase system
- Separated winding → anti-series connection of the bearing windings, no induced back EMF

[ref] Mirić, Spasoje, Dominik Bortis, and Johann Walter Kolar. "Design and comparison of permanent magnet self-bearing linear-rotary actuators." 2019 12th International Symposium on Linear Drives for Industry Applications (LDIA). IEEE, 2019.

$abcABC$ Winding Inverter Supply

- Bearing force and driving force function → realized with the *combined* or *separated* windings
- Combined winding → each phase winding contains the *bearing* and the *drive* current components

Combined winding, 9 half-bridges

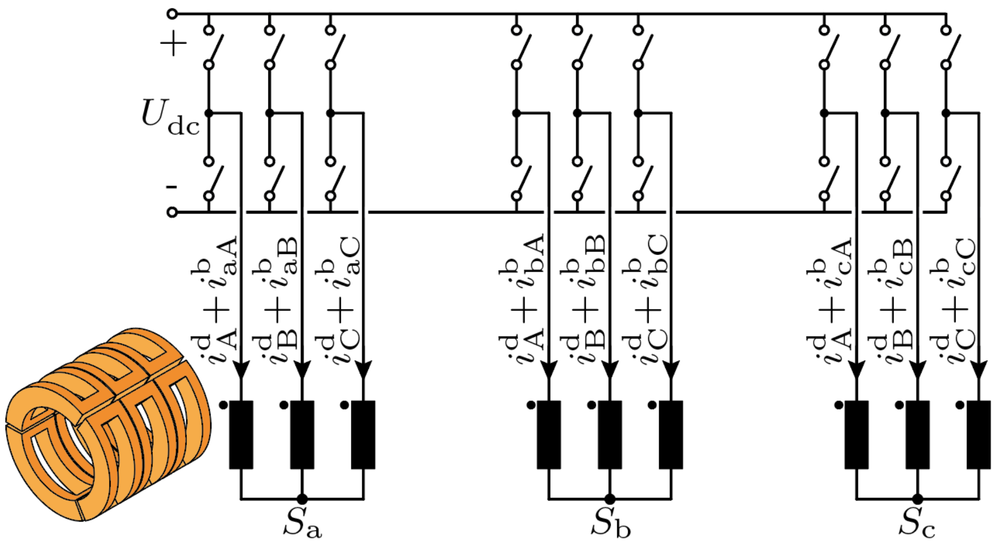

Separated winding, 12 half-bridges

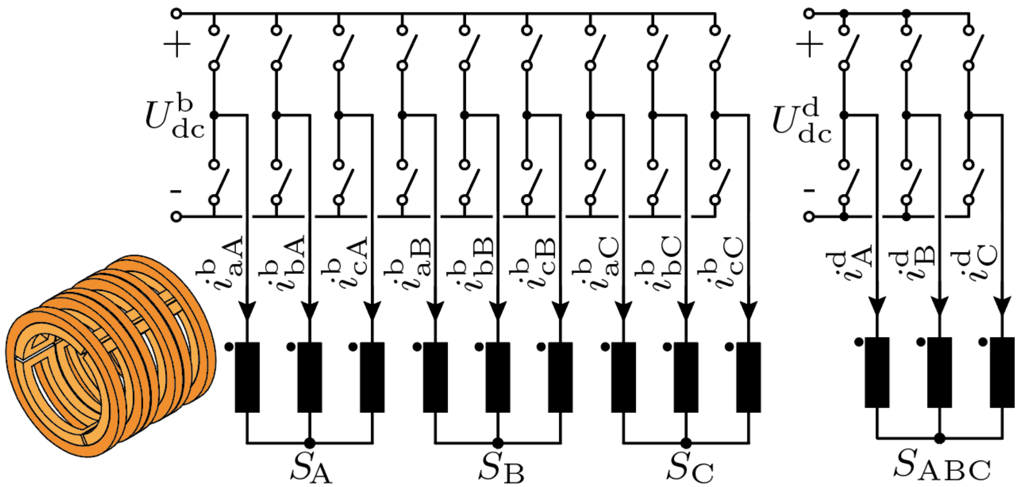

- Combined winding → each winding needs a dedicated half-bridge; star points with the linear three-phase system
- Comparison in terms of the bearing and the drive force generation capability → combined versus separated windings

[ref] Mirić, Spasoje, Dominik Bortis, and Johann Walter Kolar. "Design and comparison of permanent magnet self-bearing linear-rotary actuators." 2019 12th International Symposium on Linear Drives for Industry Applications (LDIA). IEEE, 2019.

Comparison of the Winding Types

- **Magnetically Levitated Tubular Actuator (MALTA)**
- **2 modules necessary to control the tilting of the mover**

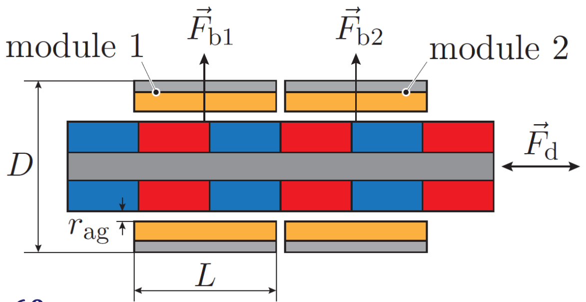

$L = 60$ mm
$D = 60$ mm
$r_{ag} = 2$ mm

- MALTA

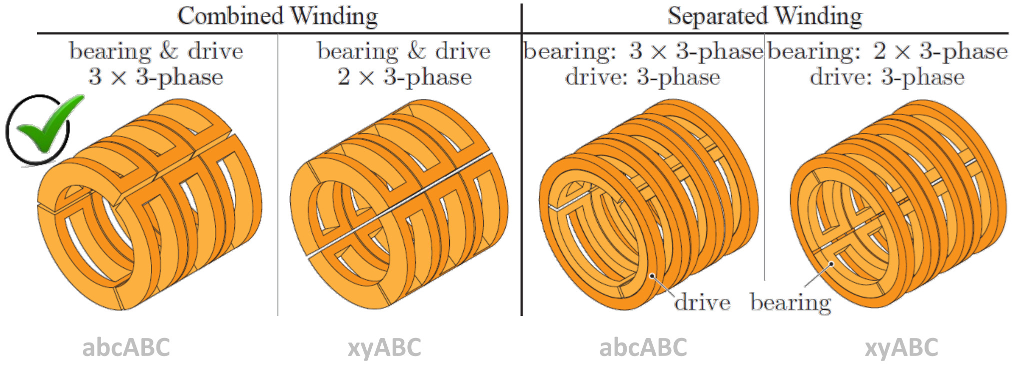

Winding Realization	Shown	Force/$F_{d,TLA}$ Drive	Force/$F_{d,TLA}$ Bearing	Number of Half-bridges
Combined				
3 × 3-phase	Fig. 4.10(a)	0.78	1.12	18
2 × 3-phase	Fig. 4.10(b)	0.76	1.1	24
Separated				
3 × 3-phase +3-phase	Fig. 4.10(c)	0.57	0.81	24
2 × 3-phase +3-phase	Fig. 4.10(d)	0.29	0.46	18

→ for 2 modules

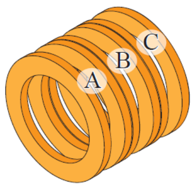

TLA Winding: benchmark for comparison

- **Comparison with respect to the driving force of the conventional TLA; 15 W of copper losses; fixed volume**
- **$abcABC$ winding or 3 × 3 phase MALTA → the largest forces; the lowest number of the inverter half-bridges**

[ref] Spasoje Miric, 'Linear-Rotary Bearingless Actuators,', PhD Thesis, ETH Zurich, 2021.

MALTA Prototype Design

Magnetic Design
18-phase Inverter Supply
Verification Measurements

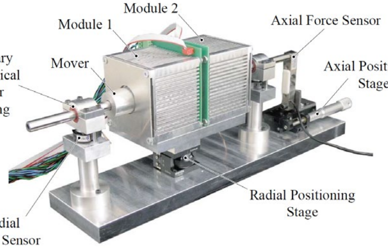

Stator Design

- Choice of the tooth width τ_t and the tooth depth r_t → considering drive, bearing, pull forces
- Scenario for the pull force calculation → the mover sitting on the touch-down bearing (start-up of the MBs)

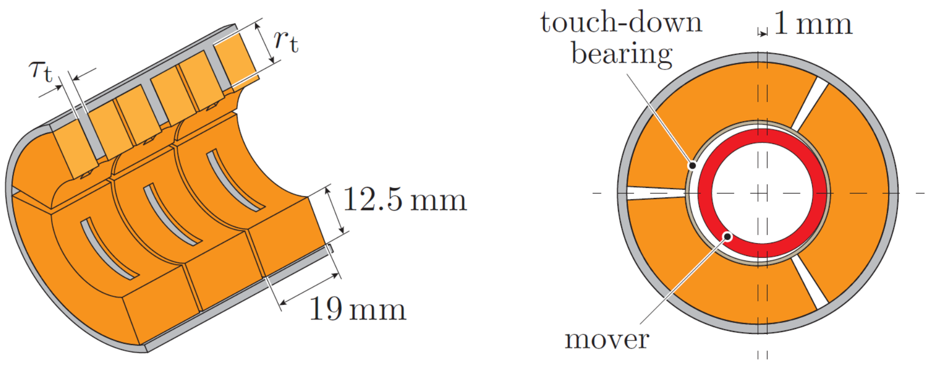

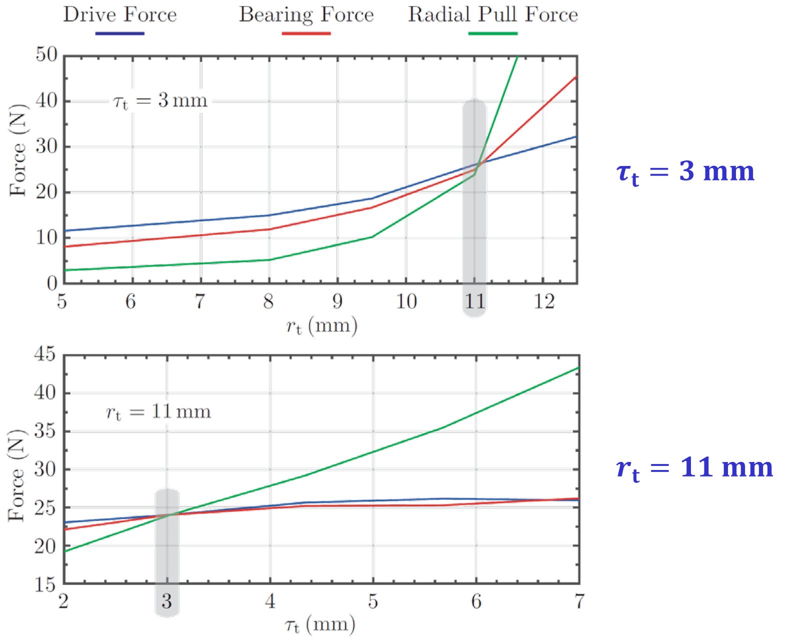

- The drive and the bearing forces → obtained for the maximally possible continuous copper losses
- Geometry parameters τ_t and r_t → chosen such that the pull force is lower than the bearing force

[ref] Mirić, Spasoje, et al. "Design and experimental analysis of a new magnetically levitated tubular linear actuator." IEEE Transactions on Industrial Electronics 66.6 (2018): 4816-4825.

Mover Design

- Two mover types considered → surface-mounted PMs (SPM) and interior PMs (IPM)
- First step → parameter range calculated using scaling laws

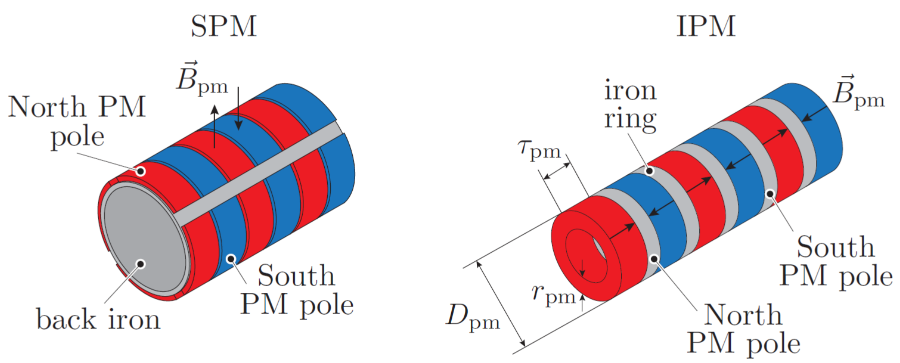

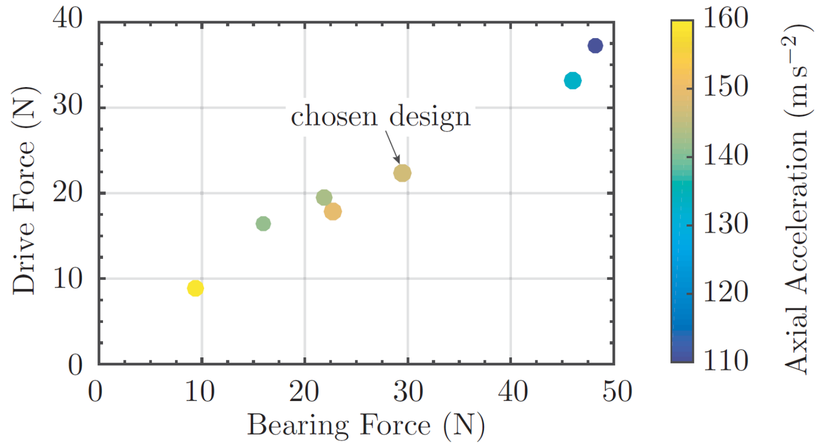

- PM geometry range from the scaling law:

$$\frac{D_{pm} + 2r_{ag}}{D - 2r_{bi}} = [0.5, 0.7] \qquad D_{pm} = (D - 2r_{bi}) \cdot [0.5, 0.7] - 2r_{ag}$$
$$= [24\ \text{mm}, 35.2\ \text{mm}]$$

- Final geometry parameters obtained by 3D-FEM:

$\tau_{pp} = 30$ mm $\quad \tau_{pm} = 10$ mm $\quad D_{pm} = 27$ mm $\quad r_{pm} = 3$ mm

- Compromize between performance parameters → drive / bearing forces and axial (linear) acceleration
- The chosen IPM design → axially magnetized PMs and iron rings allow for simplified manufacturing

[ref] Spasoje Miric, 'Linear-Rotary Bearingless Actuators,', PhD Thesis, ETH Zurich, 2021.

Eddy Current Losses

- Short stroke linear actuator → average/max. speed of the mover low to induce eddy current losses
- Solid iron used for the core design → final design check for the eddy current losses

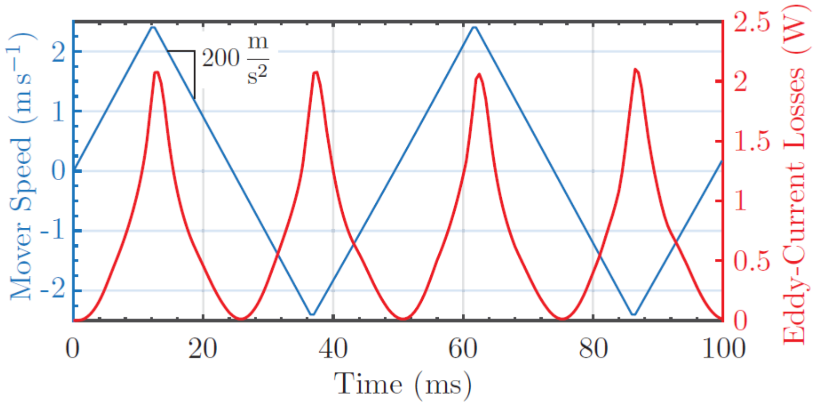

Maximum expected operation conditions:
$20g$ acceleration
30 mm stroke

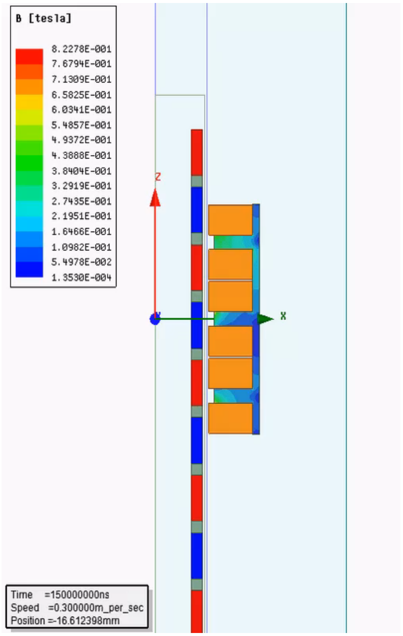

- Average eddy current losses during the operation $= 0.7$ W → 4.7% of the allowed copper losses
- Long stroke actuators that achieve higher speeds → should use low loss core, e.g., soft magnetic composite (SMC)

[ref] Mirić, Spasoje, Dominik Bortis, and Johann Walter Kolar. "Design and comparison of permanent magnet self-bearing linear-rotary actuators." 2019 12th International Symposium on Linear Drives for Industry Applications (LDIA). IEEE, 2019.
[ref] Jensen, William R., Thang Q. Pham, and Shanelle N. Foster. "Linear permanent magnet synchronous machine for high acceleration applications." 2017 IEEE International Electric Machines and Drives Conference (IEMDC). IEEE, 2017.

MALTA Hardware Prototype

- Mover's conductive sleeve → mechanical protection & eddy current position sensing
- Test bench with positioning stages and force sensors → machine constant measurements

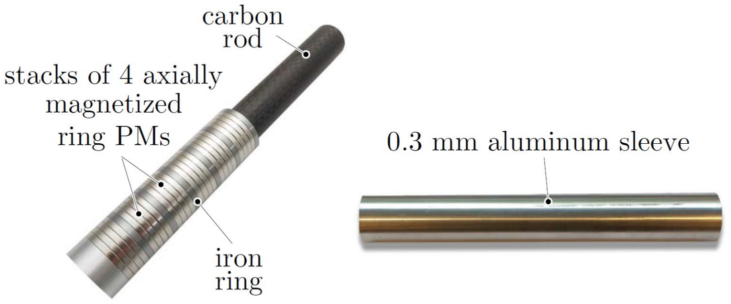

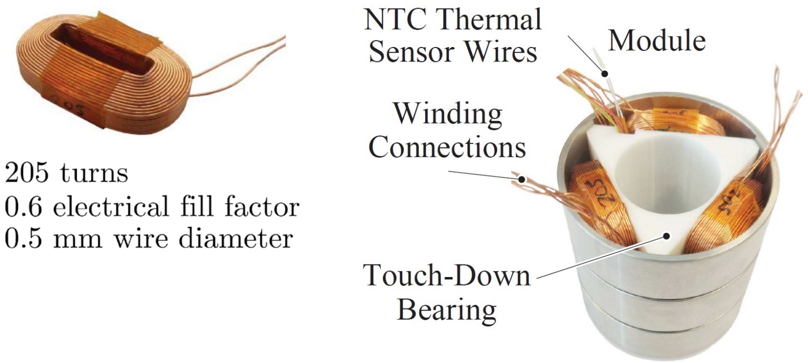

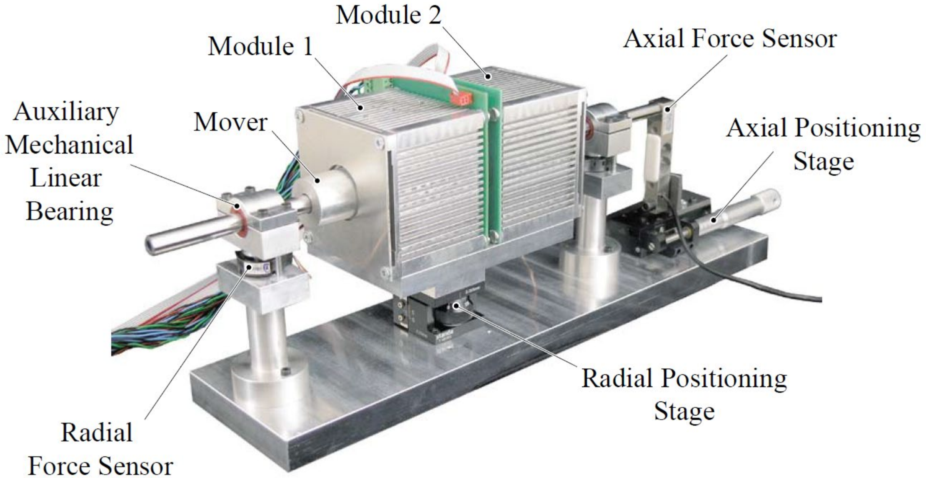

Measurements:

▼ Thermal	▼ Magnetic
$R_{th} = 1.51\ \mathrm{K/W}$	$\hat{\Psi}_M = 8.5\ \mathrm{mWb}$
$\tau_{th} \approx 30\ \mathrm{min}$	$K_D = 7.6\ \mathrm{N/A}$
	$K_B = 5.9\ \mathrm{N/A}$

MALTA Inverter Supply

- **Specifications**
  - 24 phases (8×3 phase)
  - DC link voltage: 45 V
  - DC link capacitance: 4×22 mF (buffer braking energy)
  - Power Semi.: 80 V, 10 A, 15 mΩ
  - $2 \times$ position sensor interfaces
  - Control Board: ZYNQ, Z-7020 (156 digital IOs)

Current measurement:

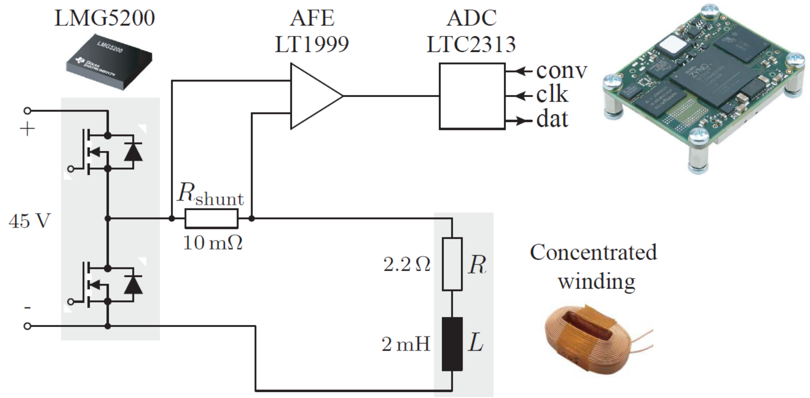

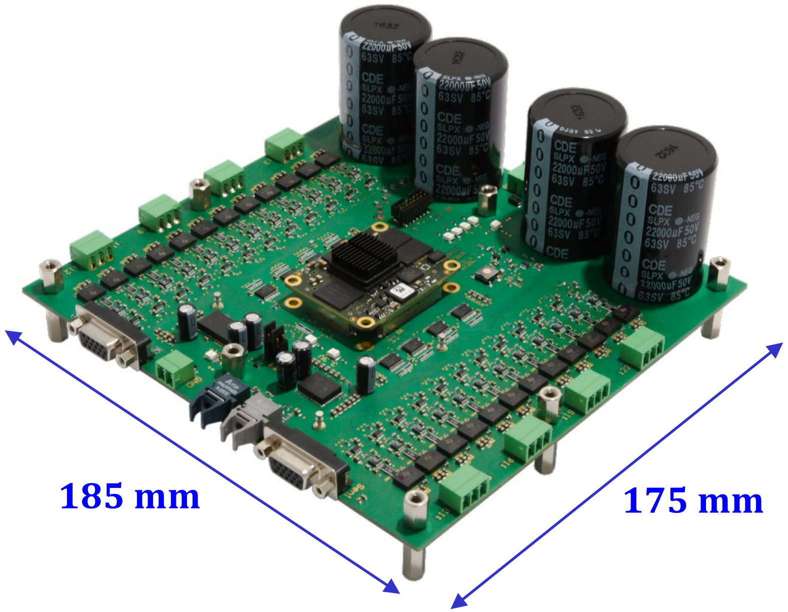

MALTA Hardware Prototype Measurements

- Measurements: flux linkage, force constants, thermal resistance → prototype characterization/model verification

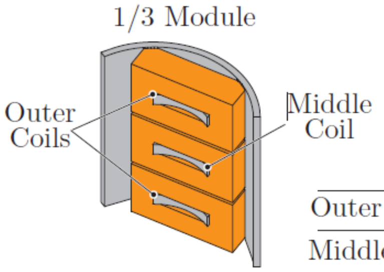

Flux Linkage

	Simulation (mWb)	Measurement (mWb)
Outer Coils:	8.3	8.35
Middle Coil:	9.0	8.85

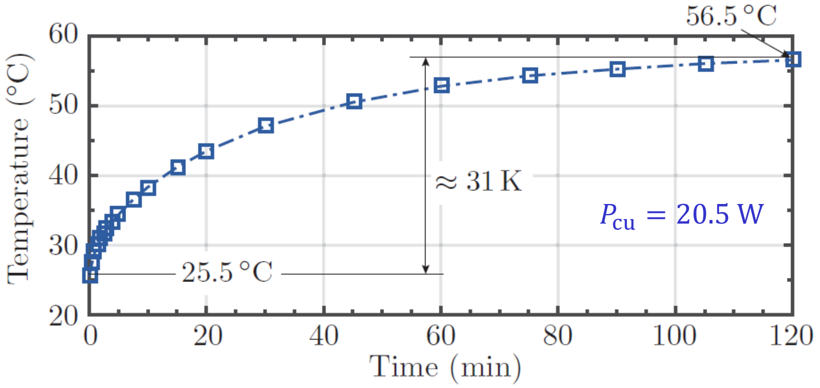

▼ Magnetic

$\hat{\Psi}_M = 8.5$ mWb

$K_D = 7.6$ N/A

$K_B = 5.9$ N/A

▼ Thermal

$R_{th} = 1.51$ K/W

$\tau_{th} \approx 30$ min

- Flux linkage measurement → measure induced back EMF and integrate to get the flux linkage
- Force constant measurement → apply known current and read the force sensor
- R_{th} measurement (winding hot spot to ambient) → apply known losses and read the built-in NTC temp. sensors

Bearing Force Constant, Decoupling of Bearing and Drive Forces

- Dependence on the rotary angle → measured and simulated with 3D-FEM (saved in a lookup table for control implem.)

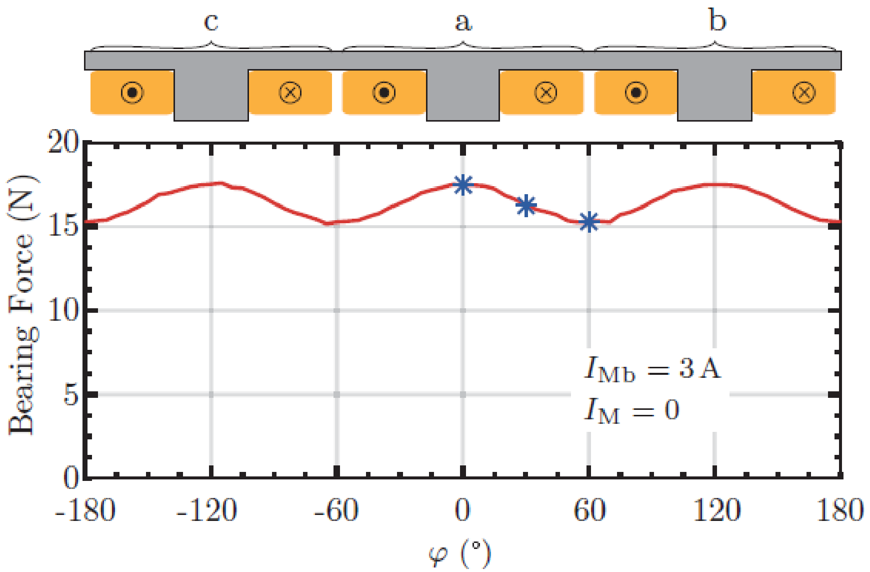

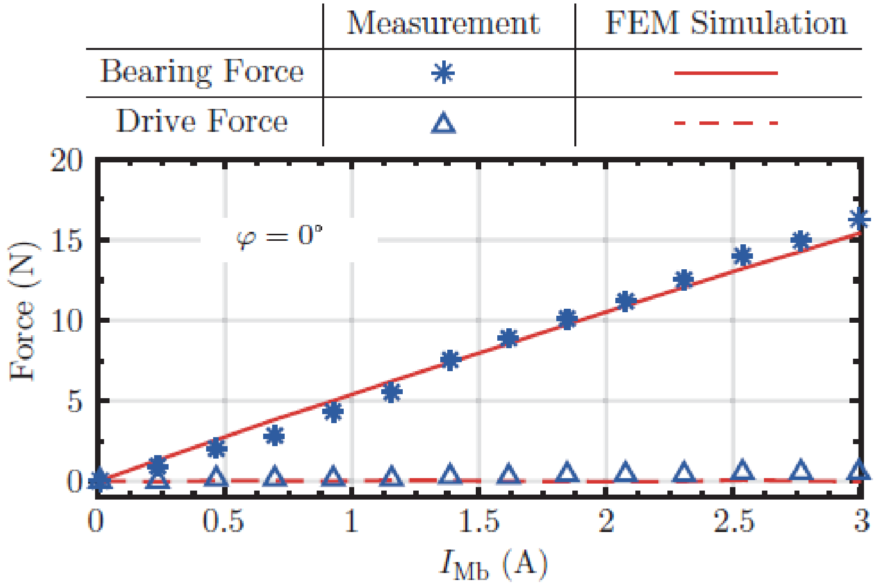

$K_B = 5.9$ N/A, measured range [5.6 N/A – 6.26 N/A]

Decoupling of the bearing and the drive force generation!

Attraction/Pull Constant K_A (Pull Force)

- Extremely important parameter for the control system design and implementation
- K_A (also K_{pull}) determines poles of the mechanical dynamic model of the mover

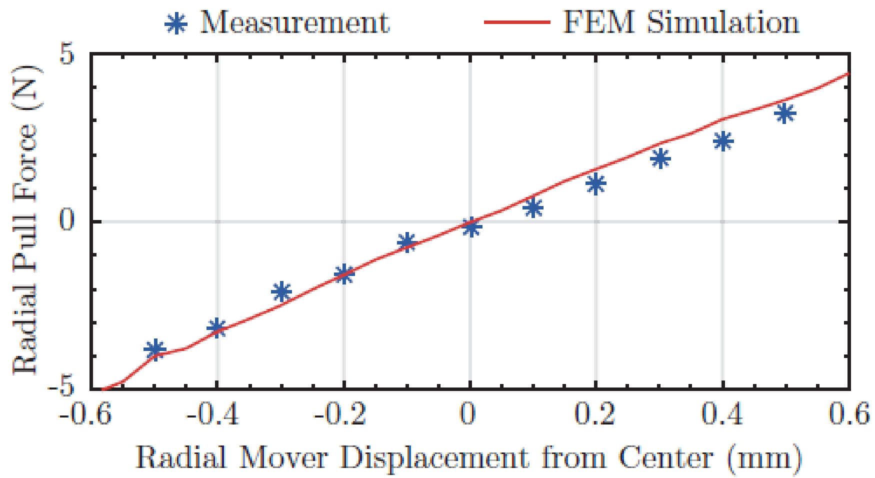

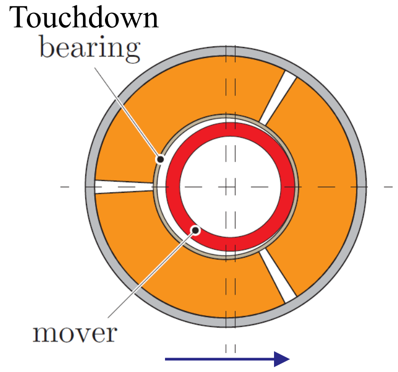

$$K_A = 8.33\ N/\mathrm{mm}$$

- K_A obtained by displacing the mover in radial direction and measuring pull force, with no currents in the winding

Position Sensor

Operating Principle
Driving Electronics
Geometry Optimization

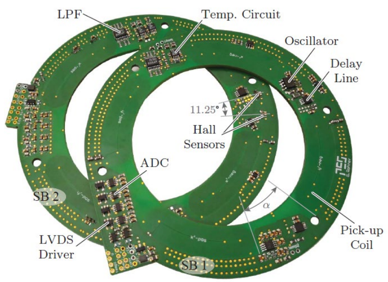

Position Sensing – Linear & Radial

- Sensing locations at the axial ends of the actuator → SP1 and SP2
- Linear position → Hall-effect-based sensors, displaced $\pi/2$ electrical

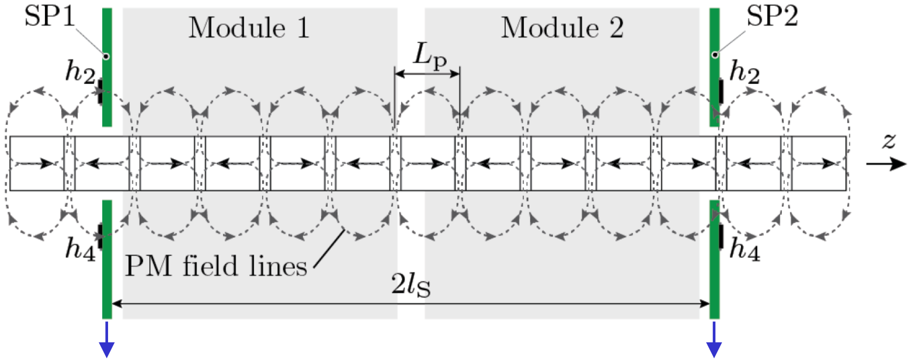

$h_{cos} = (h_1 + h_2 + h_3 + h_4)/4$

$h_{sin} = (h_1 + h_2 + h_3 + h_4)/4$

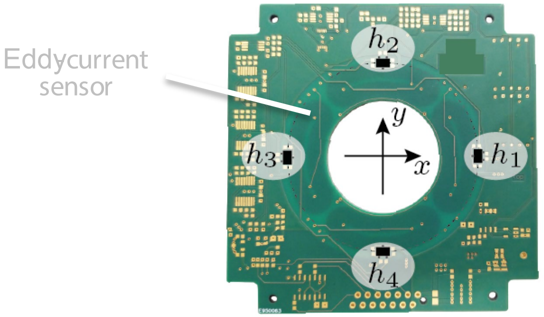

$$\theta_{el} = \mathrm{atan2}(h_{sin}, h_{cos})$$

Axial/Linear Position:

$$z = \frac{L_p}{\pi}(\theta_{el} + k \cdot 2\pi)$$

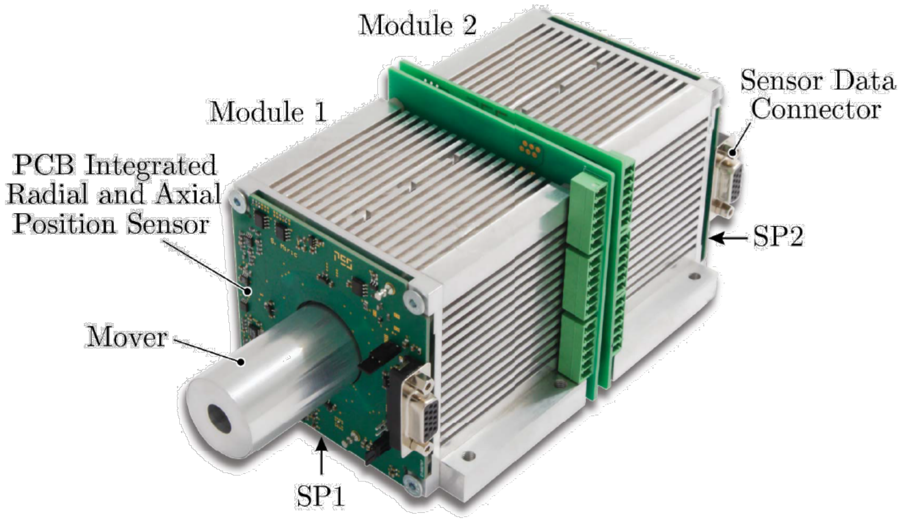

- Radial position sensor → eddy-current based; conductive mover surface is a sensing target
- Advanced eddy-current sensing techniques → later in the tutorial, blood pump part

Eddy-Current Based Position Sensor

- Injection coil carries high-frequency current → induce voltage in pick-up coils
- Upper limit for the oscillation frequency → resonant frequency of the sensor (layout/size dependent)

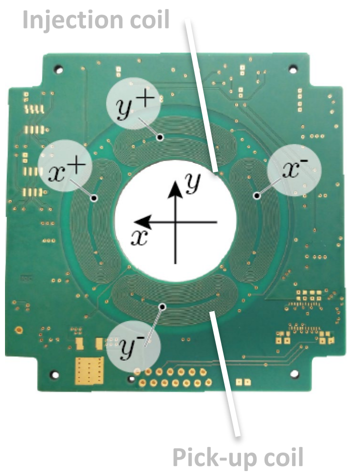

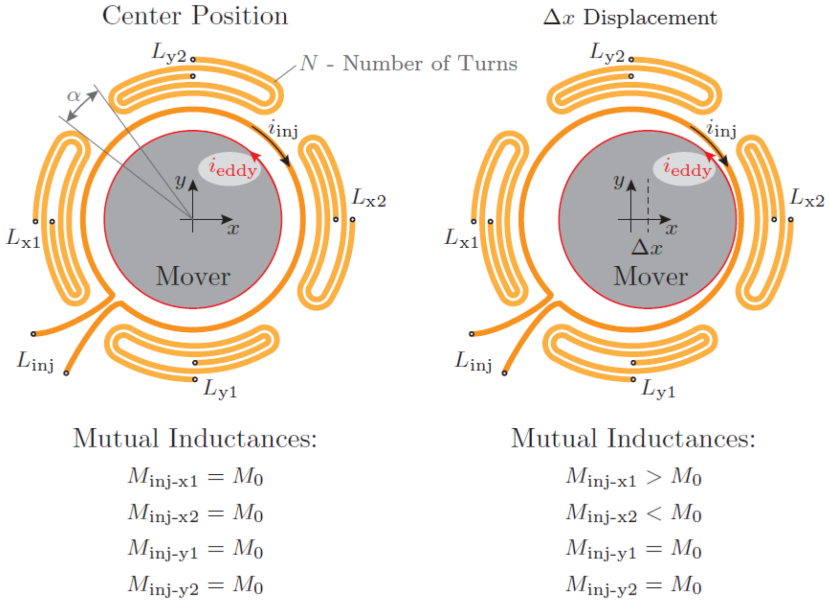

$$i_{\mathrm{inj}} = \hat{I}_{\mathrm{inj}} \sin(\omega_{\mathrm{osc}} t)$$

$$\omega_{\mathrm{osc}} \approx 3\ \mathrm{MHz},\ \hat{I}_{\mathrm{inj}} \approx 100\ \mathrm{mA}$$

$$M_{\mathrm{inj-x1}} = M_0 + \frac{\partial M_{\mathrm{inj-x1}}}{\partial x}\Delta x$$

$$M_{\mathrm{inj-x2}} = M_0 + \frac{\partial M_{\mathrm{inj-x2}}}{\partial x}\Delta x$$

$$M_{\mathrm{inj-y1}} = M_0 + \frac{\partial M_{\mathrm{inj-y1}}}{\partial y}\Delta y,$$

$$M_{\mathrm{inj-y2}} = M_0 + \frac{\partial M_{\mathrm{inj-y2}}}{\partial y}\Delta y$$

- Anti-series connection of pick-up coils of the same axis → $(L_{x1} \leftrightarrow L_{x2})$ and $(L_{y1} \leftrightarrow L_{y2})$
- At center position ind. voltage of anti-series connection is zero; it is non-zero if there is mover displacement

Eddy-Current Sensor Electronics

- x − axis example → the induced voltage Δe_x rectified and low-pass filtered results in U_x
- The same electrical circuit is employed for the y − axis

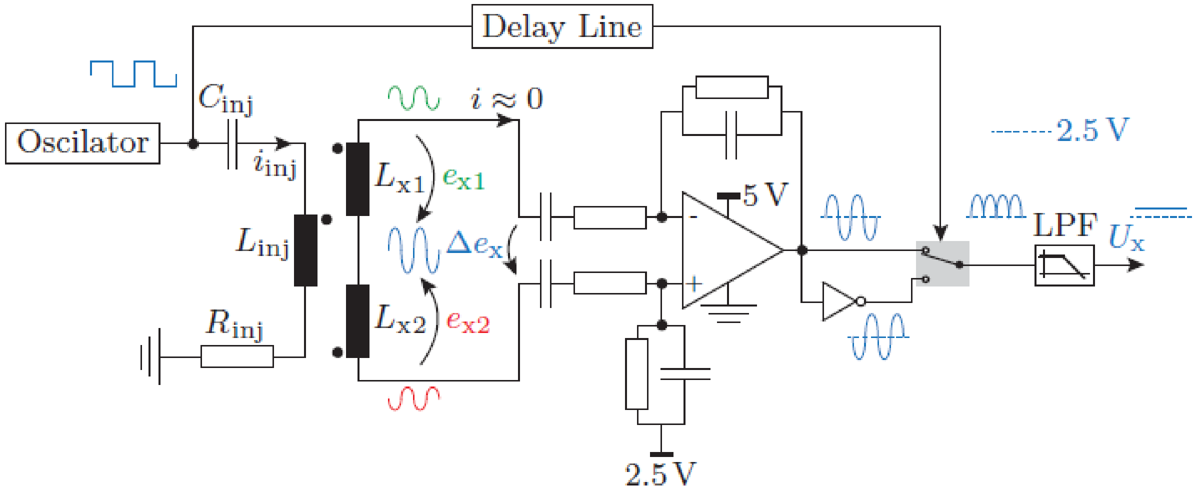

$$U_x \sim 2\omega_{osc}\,\hat{I}_{inj}\,\frac{\partial M}{\partial r}\,\Delta x.$$

$\omega_{osc} \approx$ 3 MHz, $\hat{I}_{inj} \approx$ 100 mA

- Eddy-current position sensor processing electronics

- $\partial M/\partial r$ inductance sensitivity with radial displacement → maximized by the sensor geometry optimization
- Oscillation frequency ω_{osc} limited by the resonance; injection current i_{inj} limited by the oscillator power

Eddy-Current Sensor Geometry Optimization

- Optimization parameters → angle between the pick-up coils α and the number of turns N of the pick-up coils
- Maximize sensitivity about the radial displacements of the mover → $\partial M / \partial r$

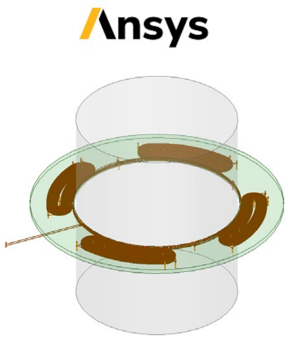

- Model in Ansys Q3D

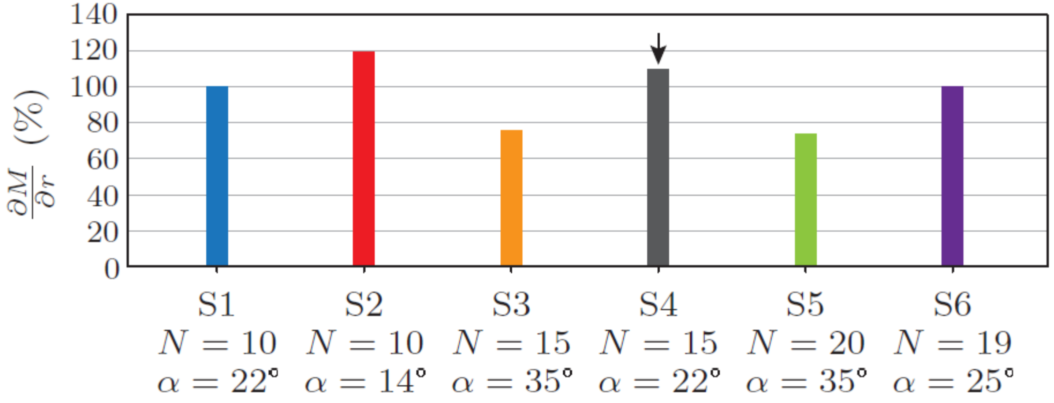

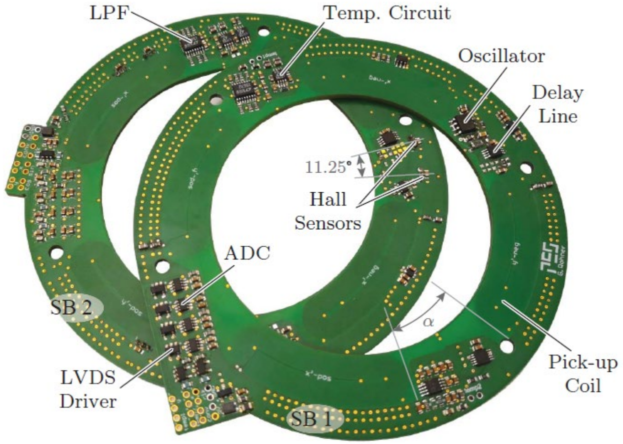

- Optimum number of turns N → larger N does means larger size of the pick-up coil
- Reasonable angle α → leave space for the signal processing electronics (analog circuits & ADCs)

universität innsbruck

Dynamic Modeling

Dynamic Model Derivation
Model Analysis
Relative Gain Array

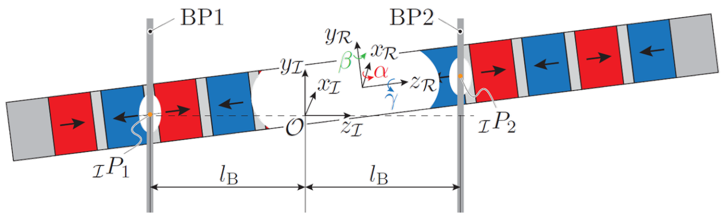

ETH zürich

International Electric Machines & Drives Conference
San Francisco, CA May 15-18
IEMDC 2023

Controller Structure

- Linear motion, radial position and tilting of the mover should be controlled
- Interaction (force action) points between the stator and the mover → middle of the stator (module)

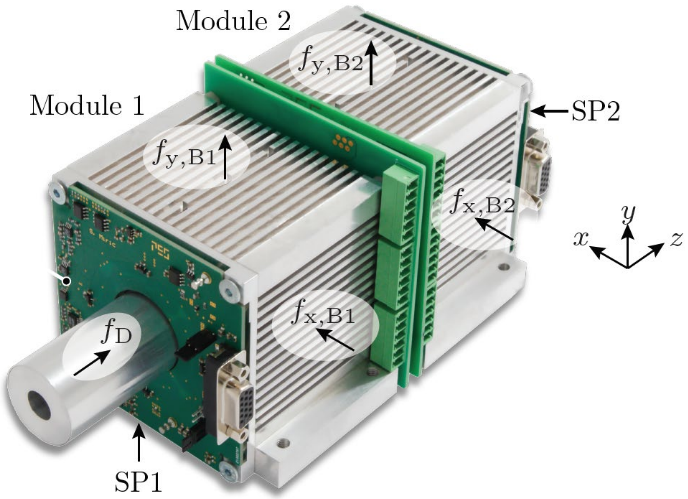

- Control plant

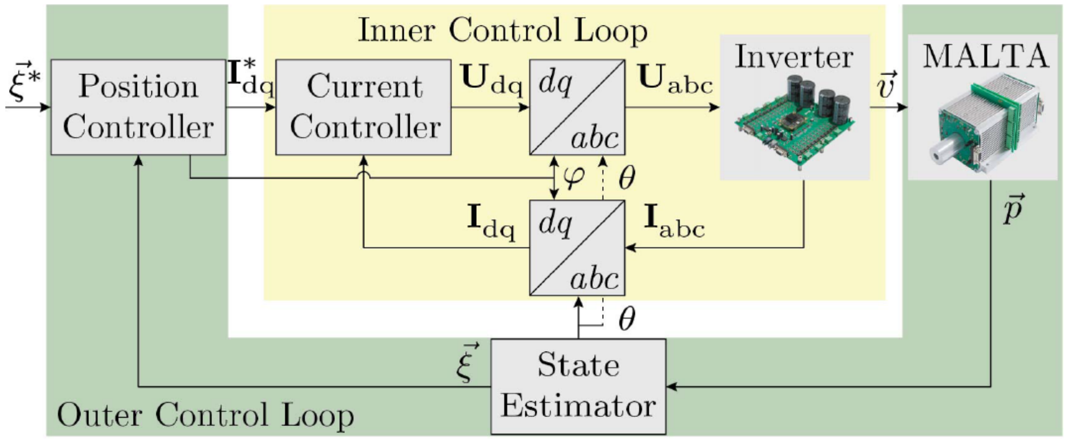

- Controller structure

- Cascaded controller structure → outer position controller (slow) and inner current control loop (fast)
- Dynamic modelling of the plant → electrical model, mechanical model, position sensor model

[ref] Mirić, Spasoje, et al. "Dynamic electromechanical model and position controller design of a new high-precision self-bearing linear actuator." IEEE Transactions on Industrial Electronics 68.1 (2020): 744-755.

Dynamic Models for Controller Design

- Dynamic models necessary for the controller design → electric, mechanical, position sensor model
- Electric model → $abcdq$ transformation of the phase quantities; dq currents control forces on the mover

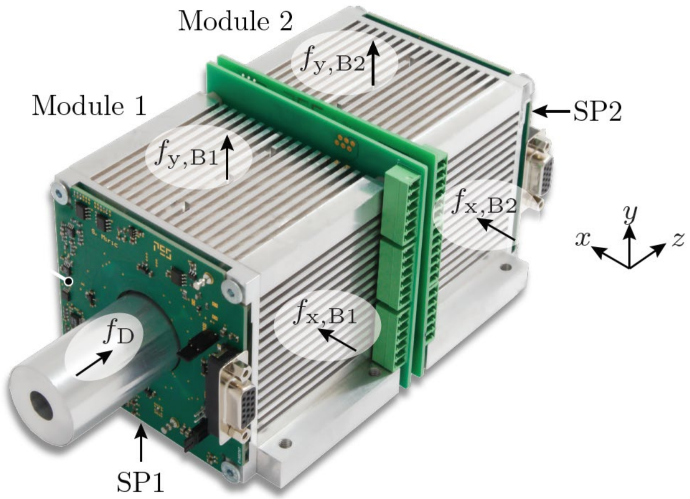

- Control plant

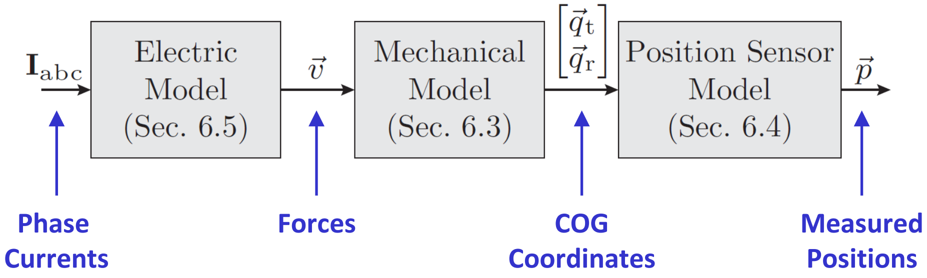

$$\mathbf{I}_{abc} = \begin{bmatrix} i_{aA} & i_{aB} & i_{aC} \\ i_{bA} & i_{bB} & i_{bC} \\ i_{cA} & i_{cB} & i_{cC} \end{bmatrix} \quad \vec{v} = \begin{bmatrix} f_{xB1} \\ f_{yB1} \\ f_{xB2} \\ f_{yB2} \\ f_{zD} \end{bmatrix} \quad \vec{q} = \begin{bmatrix} x \\ y \\ z \\ \alpha \\ \beta \\ \gamma \end{bmatrix} \begin{matrix} \} \vec{q}_t \\ \} \vec{q}_r \end{matrix} \quad \vec{p} = \begin{bmatrix} x_1 \\ y_1 \\ x_2 \\ y_2 \\ z \end{bmatrix}$$

- Overview of the dynamic models

- Mechanical model → MIMO model, coupling between the axes of motion; equations of motion must be derived
- Position sensor model → mech. model obtains COG coordinates, position sensor measures displacements

[ref] Mirić, Spasoje, et al. "Dynamic electromechanical model and position controller design of a new high-precision self-bearing linear actuator." IEEE Transactions on Industrial Electronics 68.1 (2020): 744-755.

Inertial $\mathcal{I}$ and Rotary $\mathcal{R}$ Reference Frames

- Inertial reference frame → between modules, point $\mathcal{O}$; rotary reference frame → mover's COG, point $\mathcal{O}_{COG}$
- Position of the rotary RF with respect to inertial RF determines the mover's position

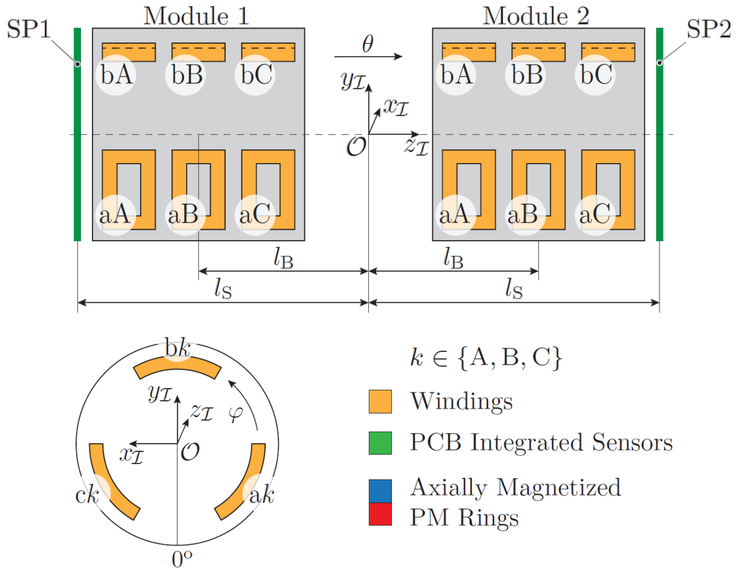

- Inertial reference frame

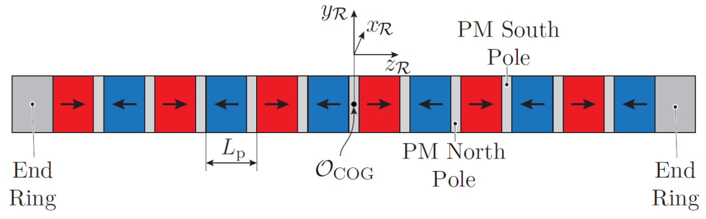

- Rotary reference frame

- l_B - the distance between the force action point and $\mathcal{O}$; l_S - the distance of the position sensors
- Electrical angles → θ – linear electrical angle; φ – rotary electrical angle (bearing force direction)

[ref] Mirić, Spasoje, et al. "Dynamic electromechanical model and position controller design of a new high-precision self-bearing linear actuator." IEEE Transactions on Industrial Electronics 68.1 (2020): 744-755.

Equations of Motion (EoM)

- Newton-Euler equations of motion → equation of motion in IRF (1) and rotation equation in RRF (2)
- Interaction points ${}_{\mathcal{I}}P_1$ and ${}_{\mathcal{I}}P_2$ → center of the stator (module)

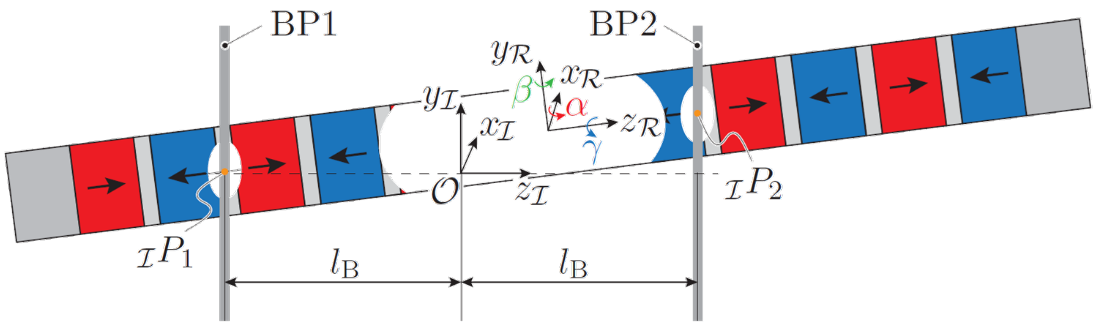

$$\vec{q}_\mathrm{t} = \begin{bmatrix} x \\ y \\ z \end{bmatrix} \qquad \vec{q}_\mathrm{r} = \begin{bmatrix} \alpha \\ \beta \\ \gamma \end{bmatrix}$$

$$m \frac{\partial^2 \vec{q}_\mathrm{t}}{\partial t^2} = {}_\mathcal{I}\vec{F}_\mathrm{tot} \quad (1)$$

$$ {}_\mathcal{R}\mathbf{I}_\mathrm{m} \cdot \frac{\partial {}_\mathcal{R}\vec{\omega}}{\partial t} + {}_\mathcal{R}\vec{\omega} \times {}_\mathcal{R}\mathbf{I}_\mathrm{m} \cdot {}_\mathcal{R}\vec{\omega} = {}_\mathcal{R}\vec{T}_\mathrm{tot}, \quad (2)$$

m - mass of the mover
${}_\mathcal{R}\mathbf{I}_\mathrm{m}$ - MoI of the mover

IRF - inertial reference frame
RRF - rotary reference frame

$$ {}_\mathcal{R}\mathbf{I}_\mathrm{m} = \begin{bmatrix} I_{xx} & 0 & 0 \\ 0 & I_{yy} & 0 \\ 0 & 0 & I_{zz} \end{bmatrix}$$

- Cardan (Euler) angles α, β, γ → mover's rotation around respective axes $x_\mathcal{I}, y_\mathcal{I}, z_\mathcal{I}$
- In total 6 equations → 3 for linear motion and 3 for rotation

[ref] Mirić, Spasoje, et al. "Dynamic electromechanical model and position controller design of a new high-precision self-bearing linear actuator." IEEE Transactions on Industrial Electronics 68.1 (2020): 744-755.

Solution of the EoM and Linearization

- Solution of the EoM is a nonlinear function → linearized to get the standard form of EoM
- Standard form of EoM → characterize the mass and the stiffness distributions within the system

$$\vec{F}_{\mathrm{EoM}}\left(\frac{\partial^2\vec{q}}{\partial t^2}, \frac{\partial\vec{q}}{\partial t}, \vec{q}, \vec{v}\right) = \begin{bmatrix} m\frac{\partial^2\vec{q}_{\mathrm{t}}}{\partial t^2} - {}_{\mathcal{I}}\vec{F}_{\mathrm{tot}} \\ {}_{\mathcal{R}}\mathbf{I}_{\mathrm{m}} \cdot \frac{\partial_{\mathcal{R}}\vec{\omega}}{\partial t} + {}_{\mathcal{R}}\vec{\omega} \times {}_{\mathcal{R}}\mathbf{I}_{\mathrm{m}} \cdot {}_{\mathcal{R}}\vec{\omega} - {}_{\mathcal{R}}\vec{T}_{\mathrm{tot}} \end{bmatrix} = \mathbf{0}_{6\times 1}$$

- Nonlinear solution of the EoM

States: $\vec{q} = \begin{bmatrix} x \\ y \\ z \\ \alpha \\ \beta \\ \gamma \end{bmatrix}$ **Inputs:** $\vec{v} = \begin{bmatrix} f_{\mathrm{xB1}} \\ f_{\mathrm{yB1}} \\ f_{\mathrm{xB2}} \\ f_{\mathrm{yB2}} \\ f_{\mathrm{D}} \end{bmatrix}$

$$\mathbf{M}\frac{\partial^2\vec{q}}{\partial t^2} + \mathbf{G}\frac{\partial\vec{q}}{\partial t} = \mathbf{S}\vec{q} + \mathbf{V}\vec{v},$$

- Linearized solution of the EoM

$$\mathrm{M}_{6\times 6} = \mathrm{J}\left(\vec{F}_{\mathrm{EoM}}, \frac{\partial^2\vec{q}}{\partial t^2}\right)\Big|_{\mathrm{at\ ss}} \qquad \mathrm{G}_{6\times 6} = \mathrm{J}\left(\vec{F}_{\mathrm{EoM}}, \frac{\partial\vec{q}}{\partial t}\right)\Big|_{\mathrm{at\ ss}}$$

$$\mathrm{S}_{6\times 6} = -\mathrm{J}\left(\vec{F}_{\mathrm{EoM}}\vec{q}\right)\Big|_{\mathrm{at\ ss}} \qquad \mathrm{V}_{6\times 5} = -\mathrm{J}\left(\vec{F}_{\mathrm{EoM}}, \vec{v}\right)\Big|_{\mathrm{at\ ss}}$$

- Linearization

- EoM matrices → M – mass matrix; G – gyroscopic matrix; S – stiffness matrix;
- Second-order differential equations (DE) → reduction the first order DE, i.e., the state space

[ref] Mirić, Spasoje, et al. "Dynamic electromechanical model and position controller design of a new high-precision self-bearing linear actuator." IEEE Transactions on Industrial Electronics 68.1 (2020): 744-755.

EoM to State-Space Equations

- Transform second order EoM to the first order state-space → double the number of states
- Controller design standardized for state-space equations

$\vec{q}$ → Positions

$\frac{\partial \vec{q}}{\partial t}$ → Speeds

$$\vec{\xi} = \begin{bmatrix} \vec{q} \\ \frac{\partial \vec{q}}{\partial t} \end{bmatrix}_{[12 \times 1]}$$

- Extension of the states

$$\mathbf{A} = \mathbf{E}^{-1}\begin{bmatrix} \mathbf{0} & \mathbf{I} \\ \mathbf{S} & \mathbf{0} \end{bmatrix} \qquad \mathbf{B} = \mathbf{E}^{-1}\begin{bmatrix} \mathbf{0} \\ \mathbf{V} \end{bmatrix} \qquad \mathbf{C} = \begin{bmatrix} \mathbf{P} & \mathbf{0} \end{bmatrix},$$

- Calculation of state space matrices

$$\frac{\partial \vec{\xi}}{\partial t} = \mathbf{A}\vec{\xi} + \mathbf{B}\vec{v},$$
$$\vec{p} = \mathbf{C}\vec{\xi},$$

- State space equations

$$\mathbf{P}\ (z) = \begin{bmatrix} 1 & 0 & 0 & 0 & -(l_S+z) & 0 \\ 0 & 1 & 0 & (l_S+z) & 0 & 0 \\ 1 & 0 & 0 & 0 & (l_S-z) & 0 \\ 0 & 1 & 0 & -(l_S-z) & 0 & 0 \\ 0 & 0 & 1 & 0 & 0 & 0 \end{bmatrix}$$

Sensor measurements

$$\vec{p} = \begin{bmatrix} x_1 \\ y_1 \\ x_2 \\ y_2 \\ z \end{bmatrix}$$

COG coordinates (states)

$$\vec{p} = \mathbf{P}\ (z) \begin{bmatrix} \vec{q}_t \\ \vec{q}_r \end{bmatrix}$$

- Position sensor model

- Position sensor model → relates sensor measurements with COG coordinates (states) of the mechanical model
- Different quantities in the model (positions, angles, forces) → normalization

[ref] Mirić, Spasoje, et al. "Dynamic electromechanical model and position controller design of a new high-precision self-bearing linear actuator." IEEE Transactions on Industrial Electronics 68.1 (2020): 744-755.

Normalization

- Normalization is important for the implementation & debugging → values get to the similar level, [-1,1]
- Absolute values before normalization → different nature (electrical, mechanical) and value range

$$\vec{\xi}_{\mathrm{pu}} = \mathbf{D}_{\xi}^{-1}\vec{\xi} \in \mathbb{R}^{10}, \quad \vec{v}_{\mathrm{pu}} = \mathbf{D}_{v}^{-1}\vec{v} \in \mathbb{R}^{5}, \quad \vec{p}_{\mathrm{pu}} = \mathbf{D}_{p}^{-1}\vec{p} \in \mathbb{R}^{5},$$

- MIMO normalization

$$\alpha_{\max} = \operatorname{atan}\left(\frac{x_{\max}}{l_{\mathrm{B}}}\right)$$

Given by the mechanical air gap

Base angle value

Base force value, given by the max winding current

$$\dot{\alpha}_{\max} = \sqrt{\frac{4 l_{\mathrm{B}}\, f_{\mathrm{Bmax}}\, \alpha_{\max}}{I_{\mathrm{xx}}}}$$

Base rotation value

$$\dot{x}_{\max} = \sqrt{\frac{4 f_{\mathrm{Bmax}}\, x_{\max}}{m}}$$

Base speed value

$$\frac{\partial \vec{\xi}_{\mathrm{pu}}}{\partial t} = \mathbf{A}_{\mathrm{pu}}\vec{\xi}_{\mathrm{pu}} + \mathbf{B}_{\mathrm{pu}}\vec{v}_{\mathrm{pu}},$$
$$\vec{p}_{\mathrm{pu}} = \mathbf{C}_{\mathrm{pu}}\vec{\xi}_{\mathrm{pu}}$$

$$\mathbf{D}_{\xi} = \begin{bmatrix} \mathbf{D}_q & \mathbf{0} \\ \mathbf{0} & \mathbf{D}_{\dot{q}} \end{bmatrix},$$
$$\mathbf{D}_q = \operatorname{diag}\left(x_{\max} \quad y_{\max} \quad z_{\max} \quad \alpha_{\max} \quad \beta_{\max}\right),$$
$$\mathbf{D}_{\dot{q}} = \operatorname{diag}\left(\dot{x}_{\max} \quad \dot{y}_{\max} \quad \dot{z}_{\max} \quad \dot{\alpha}_{\max} \quad \dot{\beta}_{\max}\right),$$
$$\mathbf{D}_{v} = \operatorname{diag}\left(f_{\mathrm{Bmax}} \quad f_{\mathrm{Bmax}} \quad f_{\mathrm{Bmax}} \quad f_{\mathrm{Bmax}} \quad 2 f_{\mathrm{Dmax}}\right),$$
$$\mathbf{D}_{p} = \operatorname{diag}\left(x_{\max} \quad y_{\max} \quad x_{\max} \quad y_{\max} \quad z_{\max}\right).$$

- Normalized state-space equations
- Normalization matrices diagonal
- Choice of normalization values

- Choice of the normalization (base) values → based on physical limits of the actuator
- Normalized state-space equations used for the system analysis and the controller design

[ref] Mirić, Spasoje, et al. "Dynamic electromechanical model and position controller design of a new high-precision self-bearing linear actuator." IEEE Transactions on Industrial Electronics 68.1 (2020): 744-755.

Position Control Bandwidth, SISO or MIMO Controller

- Eigenvalues of the matrix A → determine the dynamics of the systems and the minimum required bandwidth
- Closed-loop position controller bandwidth → should be at least twice the maximum unstable pole

Symbol	Mode	Eigenvalue
$\lambda_{1,2}$	x	$\pm 218.92\,\mathrm{rad\,s^{-1}}$
$\lambda_{3,4}$	y	$\pm 218.92\,\mathrm{rad\,s^{-1}}$
$\lambda_{5,6}$	z	$\pm 0.9893\,\mathrm{rad\,s^{-1}}$
$\lambda_{7,8}$	α	$\pm 157.53\,\mathrm{rad\,s^{-1}}$
$\lambda_{9,10}$	β	$\pm 157.53\,\mathrm{rad\,s^{-1}}$

- Eigenvalues of the matrix A

$$G_{ij}(s) = \mathbf{C}_i \cdot (s\mathbf{I} - \mathbf{A})^{-1} \cdot \mathbf{B}_j$$

$$\Lambda(G(s)) \mathrel{\hat{=}} G(s) \times \left(G(s)^{-1}\right)^{\top}$$

$$\text{RGA-number}(G(s)) = \|\Lambda(G(s)) - I_{Pair}\|_{Sum}$$

$$\begin{aligned}\omega_c &= 2 \times \max\left(|\lambda_{\{1,2,3,4,5,6,7,8,9,10\}}|\right)\\ &= 2 \times 218.92\,\mathrm{rad\,s^{-1}}\\ &= 436\,\mathrm{rad\,s^{-1}}.\end{aligned}$$

- Minimum closed-loop bandwidth of the position controller

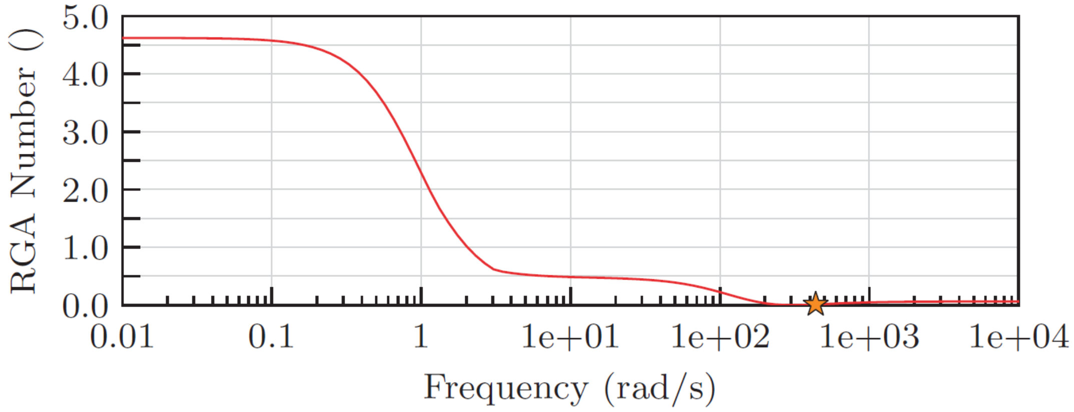

- RGA number

- RGA number → helps to identify the level of coupling between the input and outputs of the system
- Low RGA number → low coupling and SISO control possible

[ref] Mirić, Spasoje, et al. "Dynamic electromechanical model and position controller design of a new high-precision self-bearing linear actuator." IEEE Transactions on Industrial Electronics 68.1 (2020): 744-755.

Simple Bandwidth Requirement Assessment

- Closed-loop bandwidth requirement → can be imposed by the disturbances
- Disturbance parameters of the LiRA with MBs → m – mass; K_{pull} - attraction/pull constant

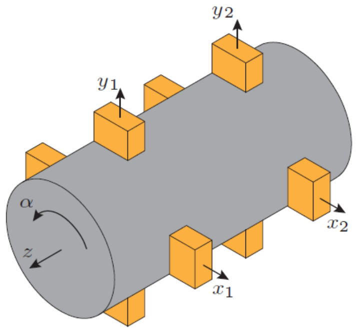

$$F_{\text{pull,x}} = x\,K_{\text{pull}}, \quad F_{\text{pull,y}} = y\,K_{\text{pull}}$$

$$K_{\text{pull}} = 8330\,\text{N/m}$$
$$m = 0.360\,\text{kg}$$

$$\omega_{\text{BW}} > \omega_{\text{D}}, \quad \omega_{\text{D}} \text{ such that } \left\| G_{\text{D}}^{\text{pu}}(j\omega_{\text{D}}) \right\| = 1$$

$$a_x = \frac{2}{m} F_x, \quad a_y = \frac{2}{m} F_y$$

$$G_{\text{OL}}(s) = \frac{\{x(s), y(s)\}}{F_{\{x,y\}}(s)} = \frac{2}{m\,s^2}$$

$$G_{\text{D}}^{\text{pu}}(s) = \frac{x(s)/\hat{x}}{F_x(s)\,/\hat{F}_x} = \frac{2\;K_{\text{pull}}}{m\,s^2}$$

$$\omega_{\text{D}} = \sqrt{\frac{2K_{\text{pull}}}{m}} \;\Rightarrow\; \omega_{\text{BW}} > \sqrt{\frac{2\,K_{\text{pull}}}{m}} \approx 220\,\text{rad/s}$$

- Simplified equation of motion
- Bandwidth imposed by disturbance

- Position controller $\omega_{BW} = 2\omega_D \approx 440$ rad/s → current controller bandwidth $> 5 \cdot 440 = 2200$ rad/s
- Current controller bandwidth → determines the stiffness capability of the MBs

[ref] Mirić, Spasoje M., et al. "Enhanced complex space vector modeling and control system design of multiphase magnetically levitated rotary–linear machines." IEEE Journal of Emerging and Selected Topics in Power Electronics 8.2 (2019): 1833-1849.

Controller Design

MIMO and SISO Controllers
Measurement Results
Tilting Control Example

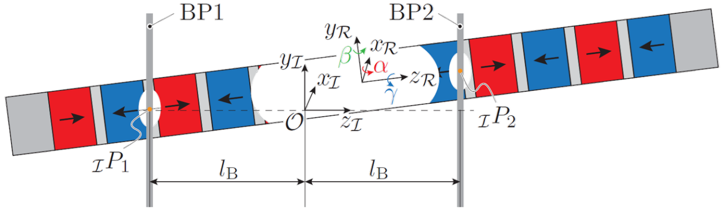

MIMO Controller

■ Cascaded Control Structure

- Outer Loop: Position Control (BW: 60 Hz)
- Inner Loop: Current Control (BW: 470 Hz)

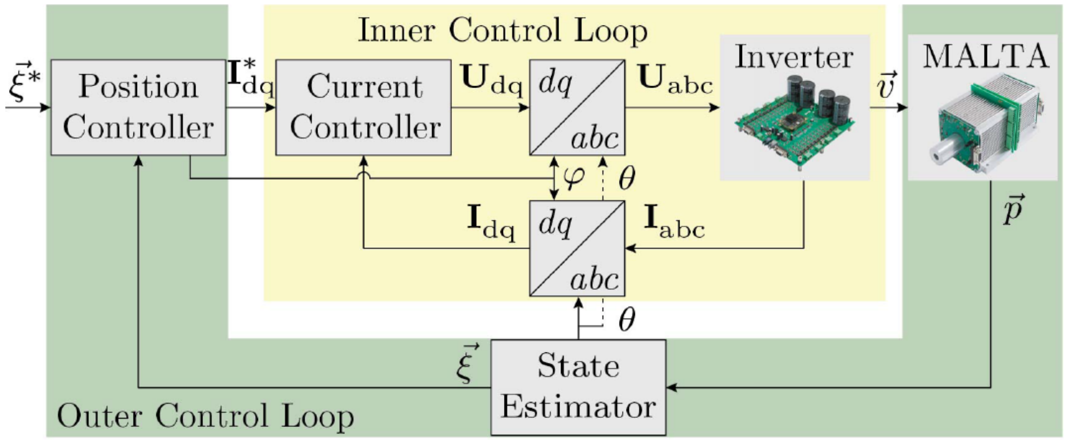

- Position Controller Tuning: LQG
- (MALTA – Magnetically Levitated Tubular Actuator)

■ Position Controller Structure ($\vec{\xi}_{\text{aug,pu}} \in \mathbb{R}^{15}$)

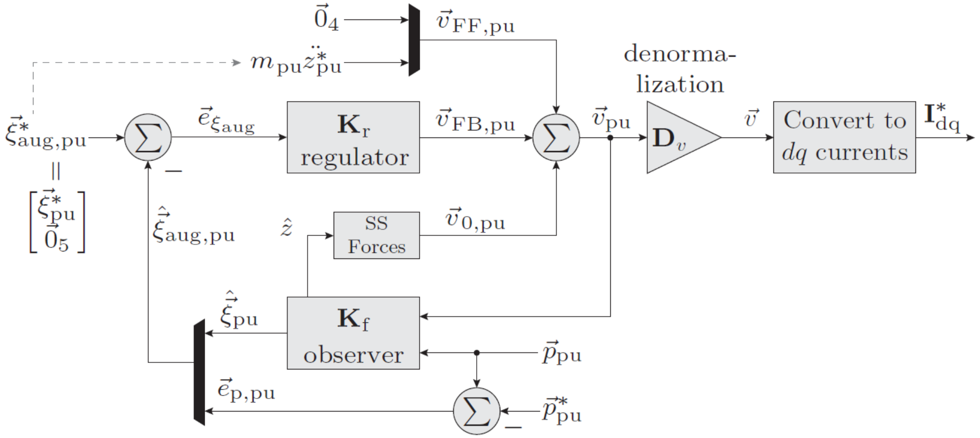

■ Current Controller Structure ($\mathbf{I}_{\text{dq}} \in \mathbb{R}^{4\times4}$)

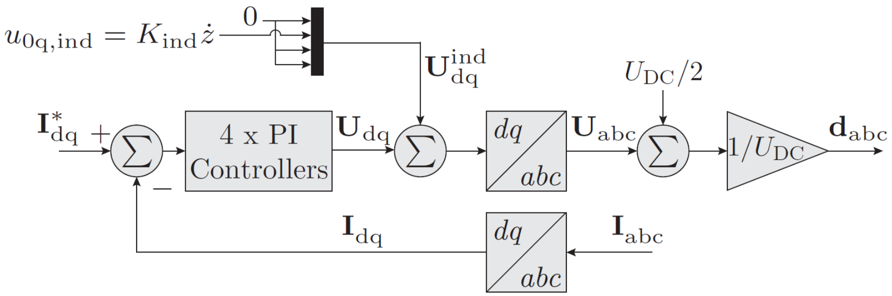

[ref] Mirić, Spasoje, et al. "Dynamic electromechanical model and position controller design of a new high-precision self-bearing linear actuator." IEEE Transactions on Industrial Electronics 68.1 (2020): 744-755.

SISO Controller (1)

- Separated winding example
- xy bearing winding

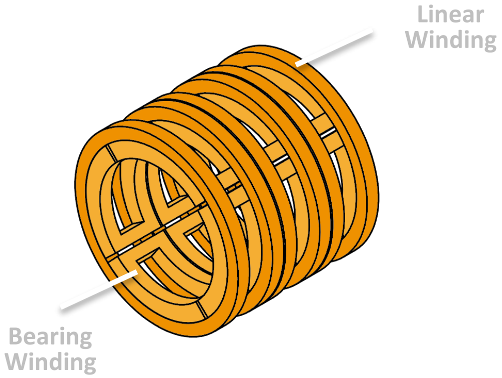

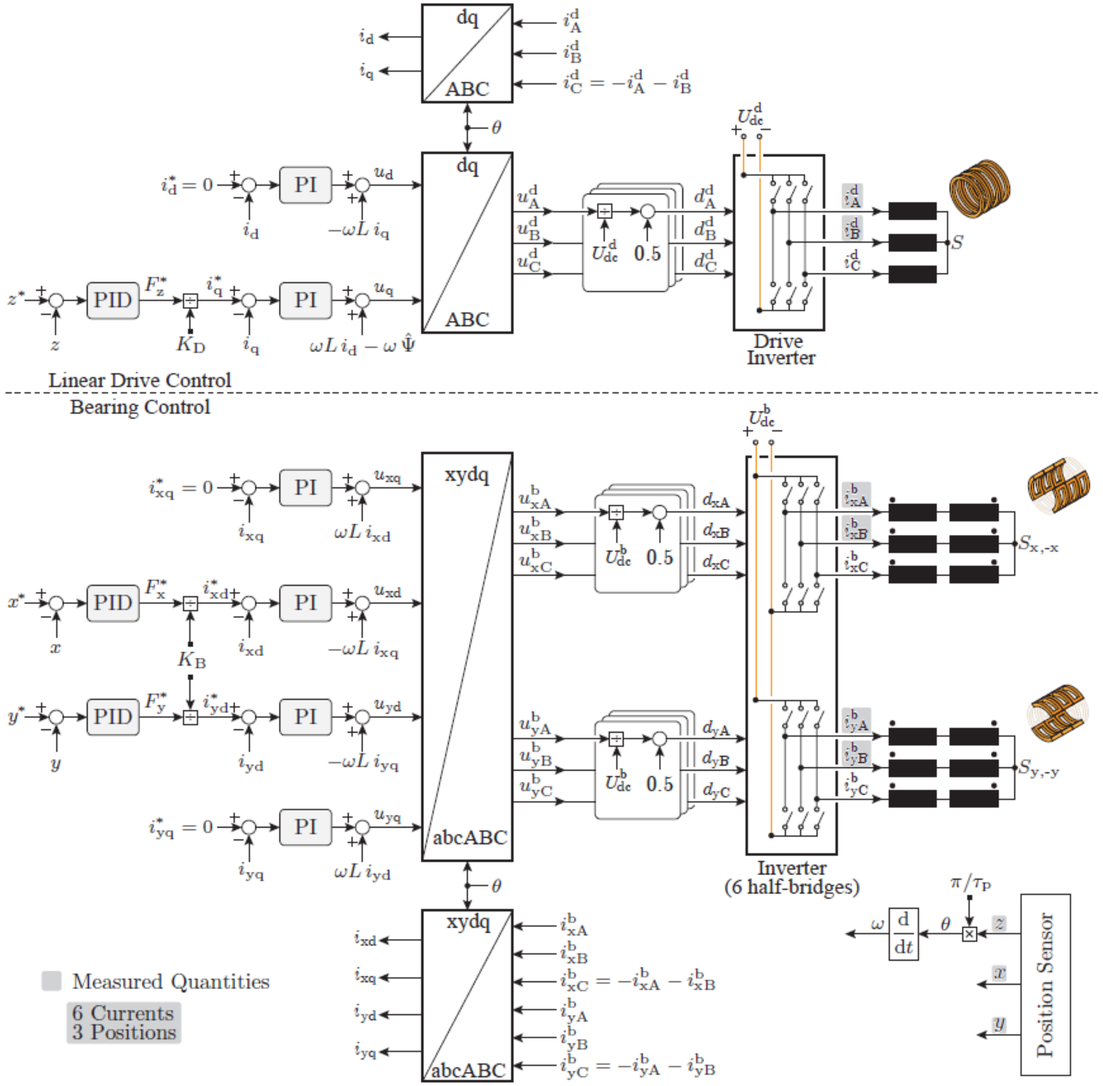

- Linear & bearing controller separated
- Bearing windings in anti-series conn.

[ref] Mirić, Spasoje, Dominik Bortis, and Johann Walter Kolar. "Design and comparison of permanent magnet self-bearing linear-rotary actuators." 2019 12th International Symposium on Linear Drives for Industry Applications (LDIA). IEEE, 2019.

SISO Controller (2)

- Combined winding example
- $abcABC$ winding

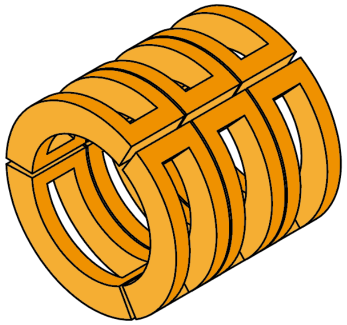

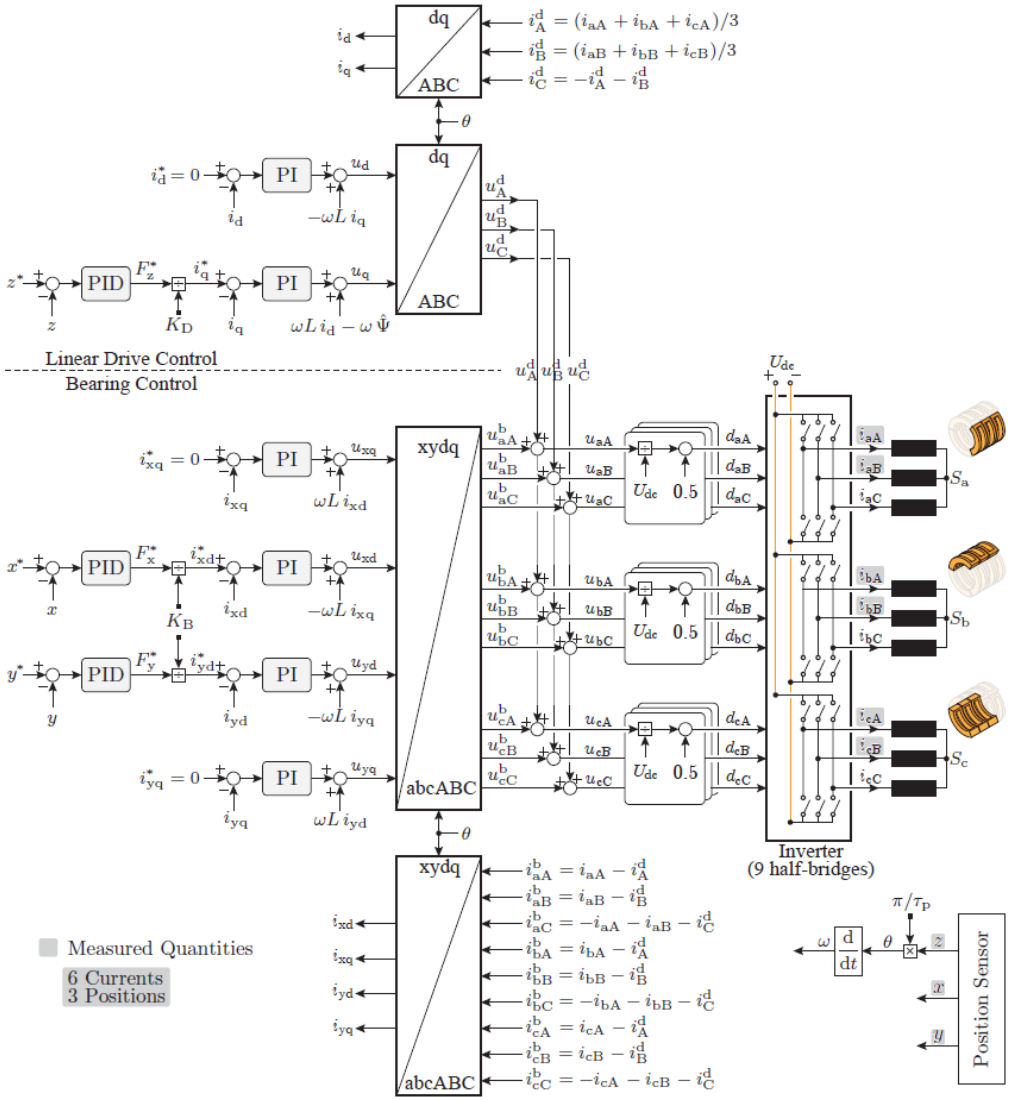

- Superimpose control signals
- 3 three-phase systems in linear dir.

[ref] Mirić, Spasoje, Dominik Bortis, and Johann Walter Kolar. "Design and comparison of permanent magnet self-bearing linear-rotary actuators." 2019 12th International Symposium on Linear Drives for Industry Applications (LDIA). IEEE, 2019.

MIMO – Measurement Results

■ **Axial Reference Tracking**

- **Axial Position and Force**

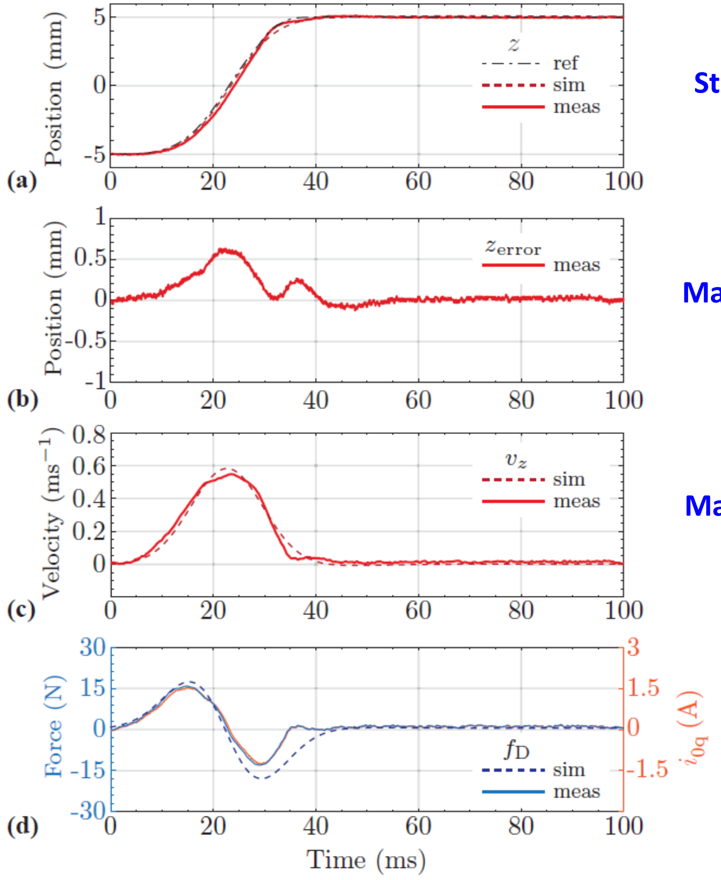

Stroke: 10 mm

Max. Pos. Error: 0.5 mm

Max. Speed: 0.6 m/s

Axial Force: ±15 N

- **Radial Position and Force**

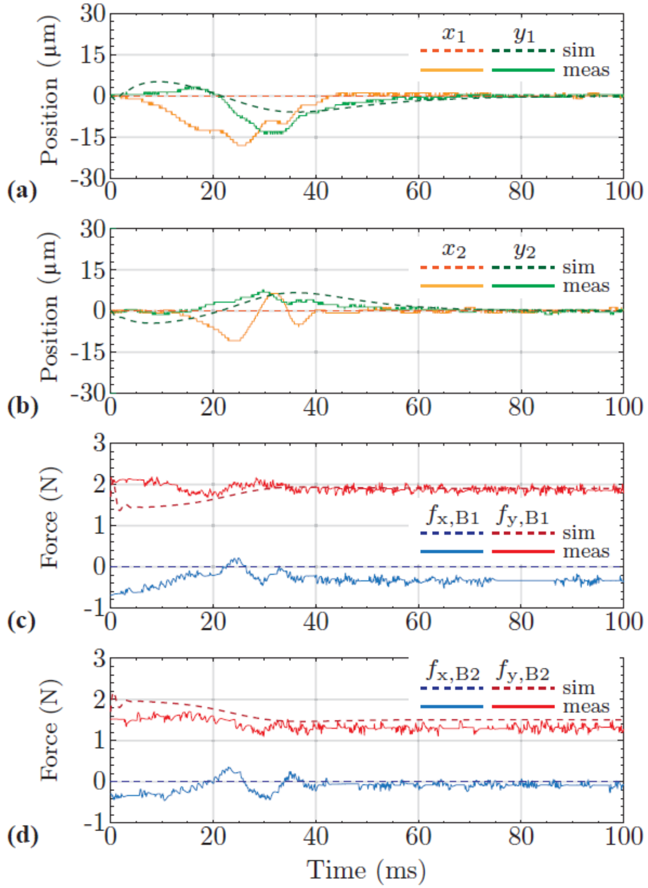

Max. Radial Position Oscillation (1.5%): ±15 µm

Mechanical Air Gap ±1000 µm

Y-direction Compensates Gravity Force: 3.25 N

MIMO – Measurement Results

Steady-State Positioning

- Sensor Resolution ~1 µm
- Number of Measured Samples: 2000

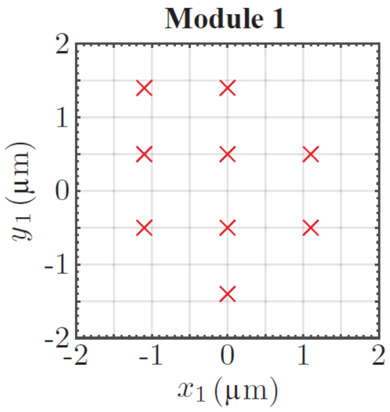

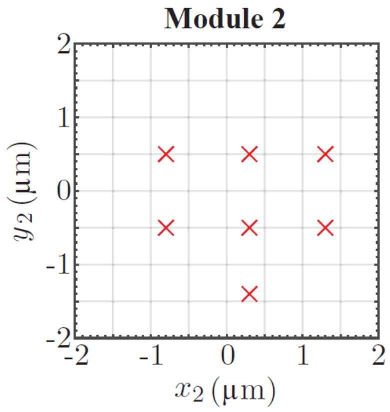

Mean
$\text{mean}(x_1) = 0.0335\ \mu m$
$\text{mean}(y_1) = -0.0212\ \mu m$

STD
$\text{std}(x_1) = 0.3883\ \mu m$
$\text{std}(x_1) = 0.5579\ \mu m$

Mean
$\text{mean}(x_2) = 0.0579\ \mu m$
$\text{mean}(y_2) = -0.0735\ \mu m$

STD
$\text{std}(x_2) = 0.4827\ \mu m$
$\text{std}(x_2) = 0.4956\ \mu m$

Mover Tilting Control

- High Precision Applications (e.g. Pick-And-Place)
- Thermal Expansions of Parallel Kinematics

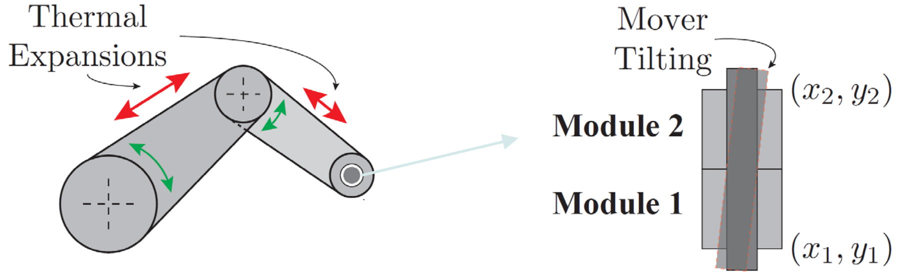

- Tilting Experimental Verification:

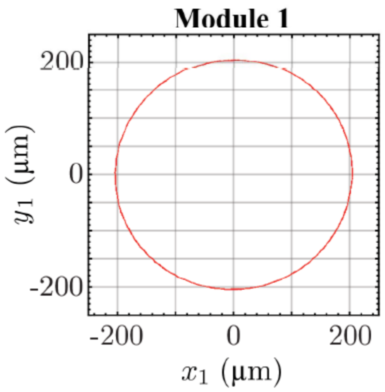

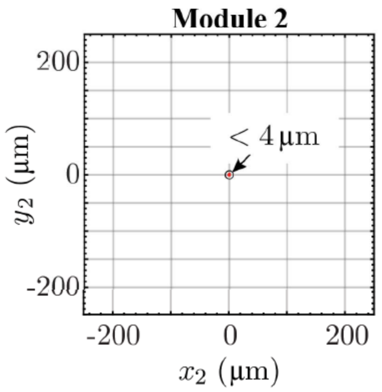

SISO – Measurement Results

■ Oscillatory Operation

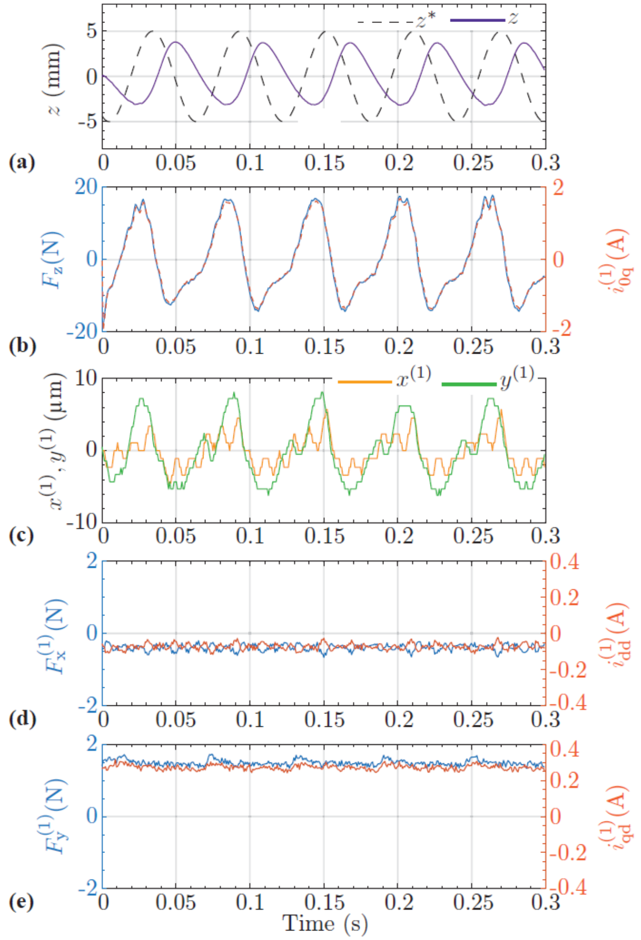

Stroke: 10 mm
Frequency: 17 Hz

Force: $< |\pm 20|$ N

Radial Position:
$< |\pm 10|$ µm

■ Axial Sub-plant Bode Plot

- **Blue: Analytically Derived Transfer Function**
- **Red: Experimentally Verified Points: $f_z = \{1, 3, 5, \ldots, 19, 21\}$ Hz**

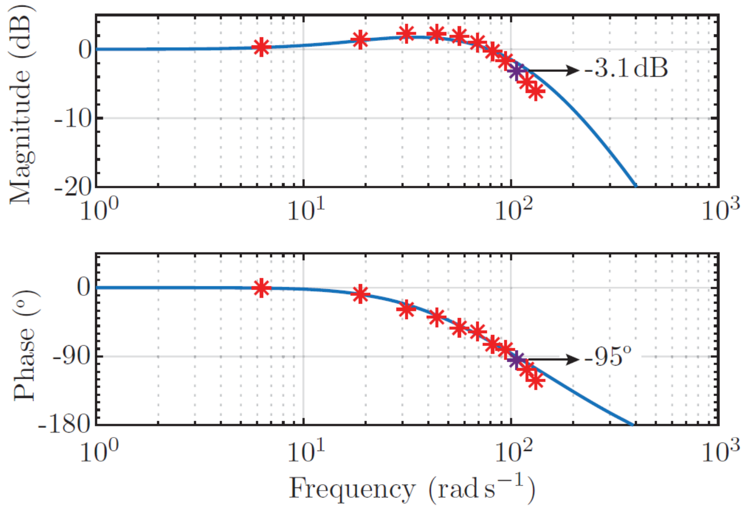

- **Demonstration of the Real Life Operation →**

Linear Bearingless Actuator

- Video (10 Hz, 1 Hz)

Generalized Complex Space Vector Modelling

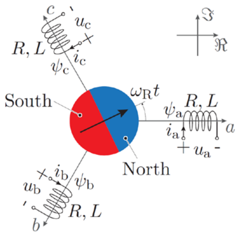

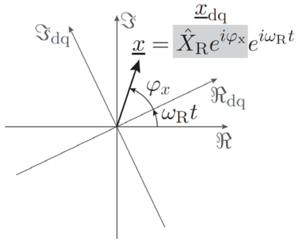

Generic Complex Space Vector Modeling (1)

Three-Phase (a,b,c) → Two-Phase (d,q)

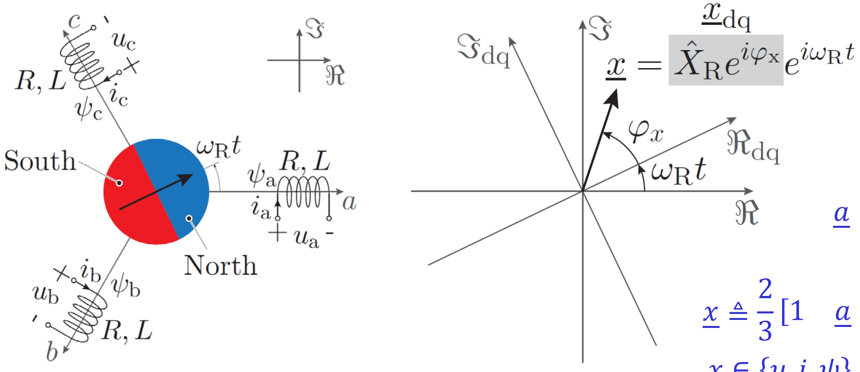

$\underline{a} = e^{i(2\pi/3)}$

$$\underline{x} \triangleq \frac{2}{3}\begin{bmatrix}1 & \underline{a} & \underline{a}^2\end{bmatrix}\begin{bmatrix}x_a \\ x_b \\ x_c\end{bmatrix}$$

$x \in \{u, i, \psi\}$

Rotary Machine: Torque

▼ Stator: 6 concentrated coils

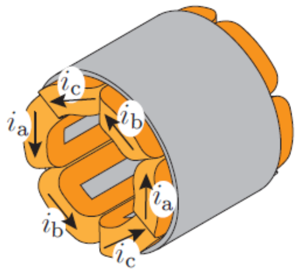

▼ PM Rotor: $N_{pp,R} = 4$

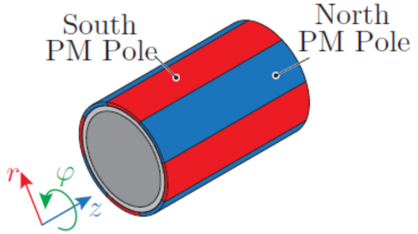

$\underline{\psi}_{dq} = \hat{\Psi}_R$

$$\boldsymbol{T_z} = \frac{3}{2}\boldsymbol{N_{pp,R}} \cdot \boldsymbol{\hat{\Psi}_R} \cdot \boldsymbol{i_q}$$

Example: Current Space Vector

▼ Three-phase currents

$$i_a = \hat{I}_R \cdot \cos(\omega_R t + \varphi_i)$$
$$i_b = \hat{I}_R \cdot \cos(\omega_R t + \varphi_i - 2\pi/3)$$
$$i_c = \hat{I}_R \cdot \cos(\omega_R t + \varphi_i + 2\pi/3)$$

▼ Space vector

$$\underline{i} = \underbrace{\hat{I}_R \cdot e^{i\cdot\varphi_i}}\cdot e^{i\cdot\omega_R t}$$

$$\underline{i}_{dq} = \hat{I}_R \cdot e^{i\cdot\varphi_i} = i_d + i \cdot i_q$$

Linear Machine: Thrust Force

▼ Stator: 3 concentrated coils

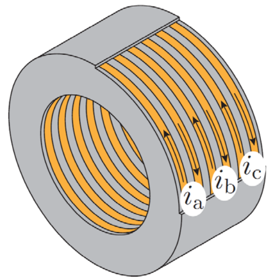

▼ PM Rotor: 4 poles

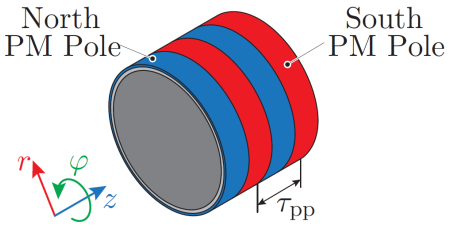

$\underline{\psi}_{dq} = \hat{\Psi}_L$

$$\omega_L = \frac{2\pi}{\tau_{pp}} \cdot v_z$$

$$\boldsymbol{F_z} = \frac{\boldsymbol{3\pi}}{\boldsymbol{\tau_{pp}}} \cdot \boldsymbol{\hat{\Psi}_L} \cdot \boldsymbol{i_q}$$

Generic Complex Space Vector Modeling (2)

- **Rotary Machine: Bearing Force**

▼ Torque Generation

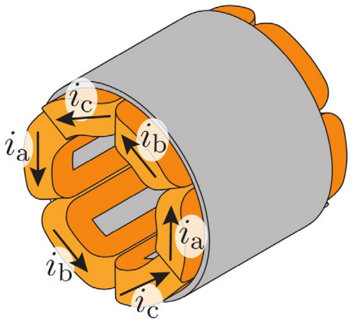

▼ Bearing Force Generation

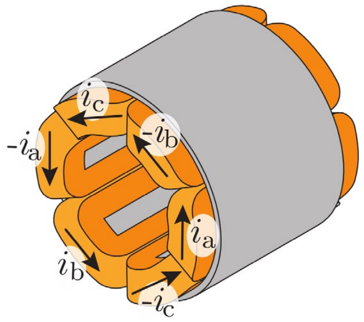

- **Rotor in Center → No Flux Linkage**
  - Model: two coils in anti-series connection

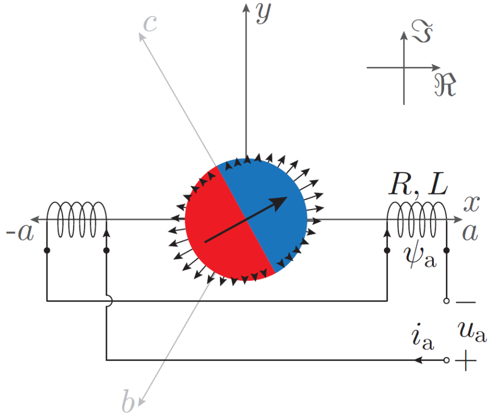

- **Displaced Rotor → $\frac{\mathrm{d}\hat{\Psi}_R}{\mathrm{d}x} = \frac{\mathrm{d}\hat{\Psi}_R}{\mathrm{d}y} = \chi_{pm,R}$**
  - Flux linkage radial sensitivity

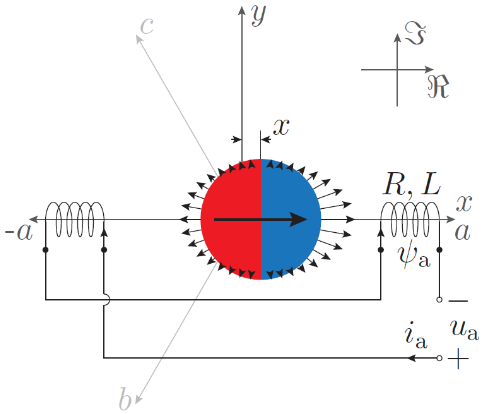

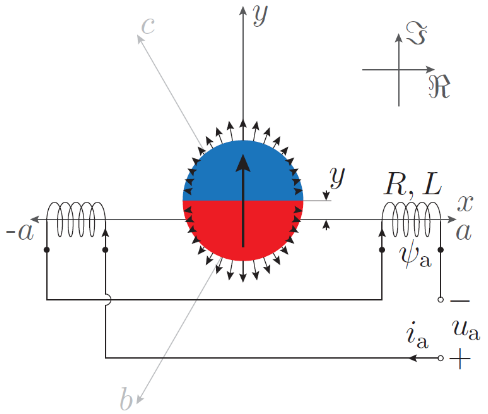

▼ Three Phase Flux Linkage

$$\psi_a = \chi_{pm,R} \cdot [x \cdot \cos(\omega_R t + \varphi_\psi) - y \cdot \sin(\omega_R t + \varphi_\psi)]$$
$$\psi_b = \chi_{pm,R} \cdot [x \cdot \cos(\omega_R t + \varphi_\psi - 2\pi/3) - y \cdot \sin(\omega_R t + \varphi_\psi - 2\pi/3)]$$
$$\psi_c = \chi_{pm,R} \cdot [x \cdot \cos(\omega_R t + \varphi_\psi + 2\pi/3) - y \cdot \sin(\omega_R t + \varphi_\psi + 2\pi/3)]$$

▼ Space Vector

$$\underline{\psi} = \underbrace{\chi_{pm,R} \cdot (x + i \cdot y) \cdot e^{i \cdot \varphi_\psi}} \cdot e^{i \cdot \omega_R t}$$

$$\underline{\psi}_{dq} = \chi_{pm,R} \cdot (x + i \cdot y) \cdot e^{i \cdot \varphi_\psi}$$

$$\boldsymbol{F_x = \frac{3}{2} \cdot \chi_{pm,R} \cdot i_d} \qquad \boldsymbol{F_y = \frac{3}{2} \cdot \chi_{pm,R} \cdot i_q}$$

Generic Complex Space Vector Modeling (3)

■ Linear-Rotary Machine

▼ Stator: 18 concentrated coils

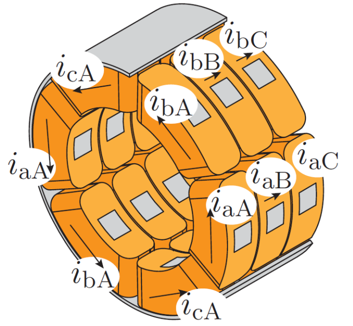

▼ PM Rotor: $N_{pp,R} = 4$

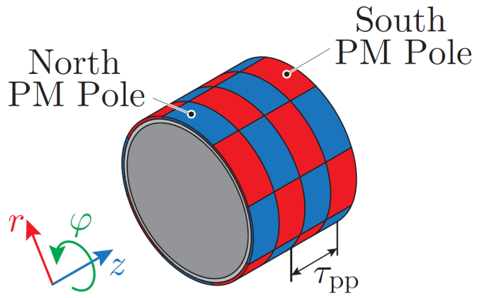

▼ Phase quantity

$$x_{aA} = \hat{X}_{RL} \cdot \cos(\omega_R t + \varphi_x) \cdot \cos(\omega_L t + \theta_x) \qquad \hat{X}_{RL} \in \{\hat{U}_{RL}, \hat{I}_{RL}, \hat{\Psi}_{RL}\}$$

▼ Double space vector transformation

$$\underline{\underline{x}} \triangleq \frac{4}{9}\begin{bmatrix}1 & \underline{a} & \underline{a}^2\end{bmatrix}\begin{bmatrix}x_{aA} & x_{aB} & x_{aC} \\ x_{bA} & x_{bB} & x_{bC} \\ x_{cA} & x_{cB} & x_{cC}\end{bmatrix}\begin{bmatrix}1 \\ \underline{b} \\ \underline{b}^2\end{bmatrix} \qquad \underline{\underline{x}} \in \{\underline{\underline{u}}, \underline{\underline{i}}, \underline{\underline{\psi}}\}$$

$$\underline{a} = e^{i(2\pi/3)} \qquad \underline{b} = e^{j(2\pi/3)}$$

▲ Rotary i complex plane ▲ Linear j complex plane

■ Double Complex Space Vector

$$\underline{\underline{x}} = \underbrace{\hat{X}_{RL} \cdot e^{i\cdot\varphi_x} \cdot e^{j\cdot\theta_x}} \cdot e^{i\cdot\omega_R t} \cdot e^{i\cdot\omega_L t}$$

$$\underline{\underline{x}}_{dq} = \hat{X}_{RL} \cdot e^{i\cdot\varphi_x} \cdot e^{j\cdot\theta_x} = x_{dd} + i \cdot x_{qd} + j \cdot x_{dq} + i \cdot j \cdot x_{qq}$$

▼ Flux linkage ($\varphi_\psi = 0$ and $\theta_\psi = 0$)

$$\underline{\underline{\psi}}_{dq} = \psi_{dd} = \hat{\Psi}_{RL}$$

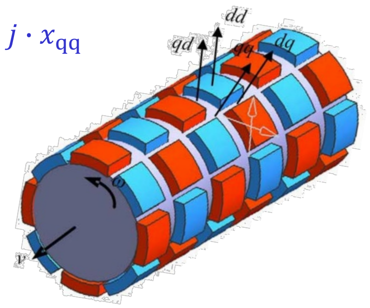

Source: Jin et al., 2012

■ Torque and Linear Force

$$\boldsymbol{T}_z = \frac{9}{4} \boldsymbol{N}_{pp,R} \cdot \hat{\boldsymbol{\Psi}}_{RL} \cdot \boldsymbol{i}_{qd} \qquad \boldsymbol{F}_z = \frac{9\pi}{2\tau_{pp}} \cdot \hat{\boldsymbol{\Psi}}_{RL} \cdot \boldsymbol{i}_{dq}$$

■ Bearing Force

- Rotary phase rescheduling needed

$$\boldsymbol{F}_x = \frac{9}{4} \cdot \chi_{pm,RL} \cdot \boldsymbol{i}_{dd} \qquad \boldsymbol{F}_y = \frac{9}{4} \cdot \chi_{pm,RL} \cdot \boldsymbol{i}_{qd}$$

Generic Complex Space Vector Modeling (4)

Linear Force Generation

- Simpler than full linear-rotary machine

▼ Stator: 9 concentrated coils

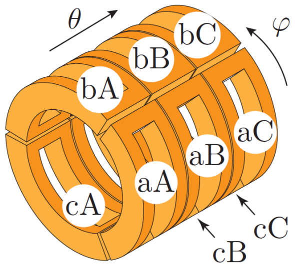

$\underline{\psi}_{\mathrm{dq}} = \hat{\Psi}_{\mathrm{M}}$

▼ PM Mover

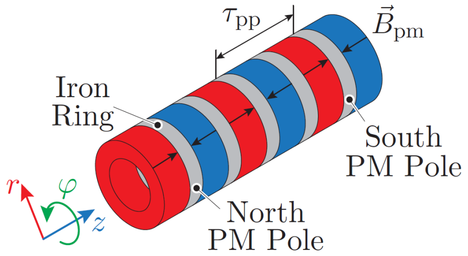

$\boldsymbol{F}_{\mathrm{z}} = \frac{9\pi}{\tau_{\mathrm{pp}}} \cdot \hat{\Psi}_{\mathrm{M}} \cdot i_{\mathrm{q}}$

Bearing Force Generation

- Linear-rotary machine with $\omega_{\mathrm{R}} = 0$

▼ Flux linkage

$$\underline{\underline{\psi}} = \underbrace{\chi_{\mathrm{pm,M}} \cdot (x + i \cdot y) \cdot e^{i \cdot \varphi_\psi} \cdot e^{j \cdot \theta_\psi}}_{} \cdot e^{j \cdot \omega_{\mathrm{L}}}$$

$$\chi_{\mathrm{pm,M}} = \frac{\mathrm{d}\hat{\Psi}_{\mathrm{M}}}{\mathrm{d}x} = \frac{\mathrm{d}\hat{\Psi}_{\mathrm{M}}}{\mathrm{d}y}$$

$$\underline{\underline{\psi}}_{\mathrm{dq}} = \chi_{\mathrm{pm,M}} \cdot (x + i \cdot y) \cdot e^{i \cdot \varphi_\psi} \cdot e^{j \cdot \theta_\psi}$$

$$\boldsymbol{F}_{\mathrm{x}} = \frac{9}{4} \cdot \chi_{\mathrm{pm,M}} \cdot i_{\mathrm{dd}} \qquad \boldsymbol{F}_{\mathrm{y}} = \frac{9}{4} \cdot \chi_{\mathrm{pm,M}} \cdot i_{\mathrm{qd}}$$

Double Stator LiRA

Stator Arrangement
Cooling of Inner Stator
Geometry Optimization

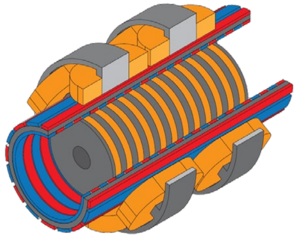

Double Stator (DS) LiRA Realization Options

Stator Arrangement

- Outer → Linear, Inner → Rotary

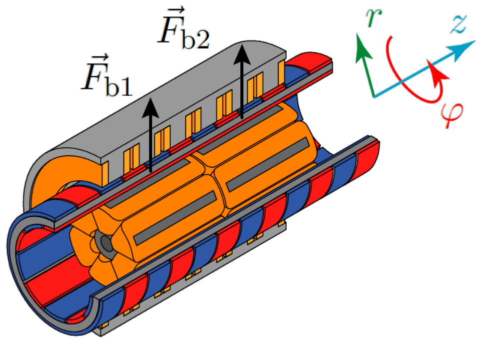

- Outer → Rotary, Inner → Linear

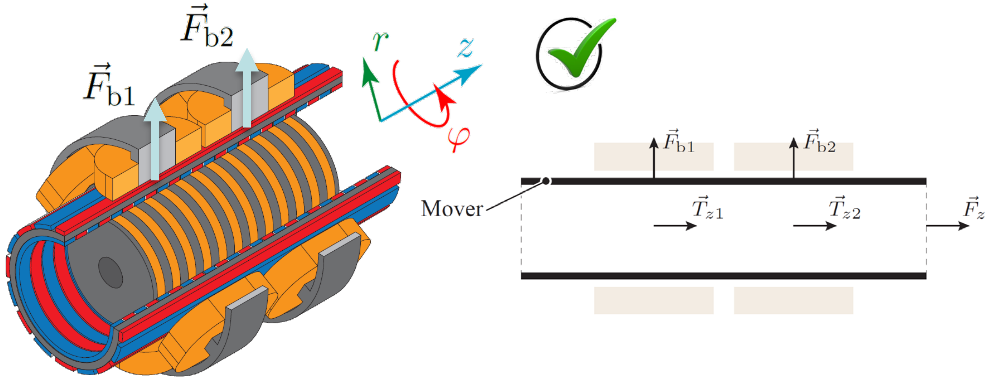

Mover Types

- With and Without Back Iron

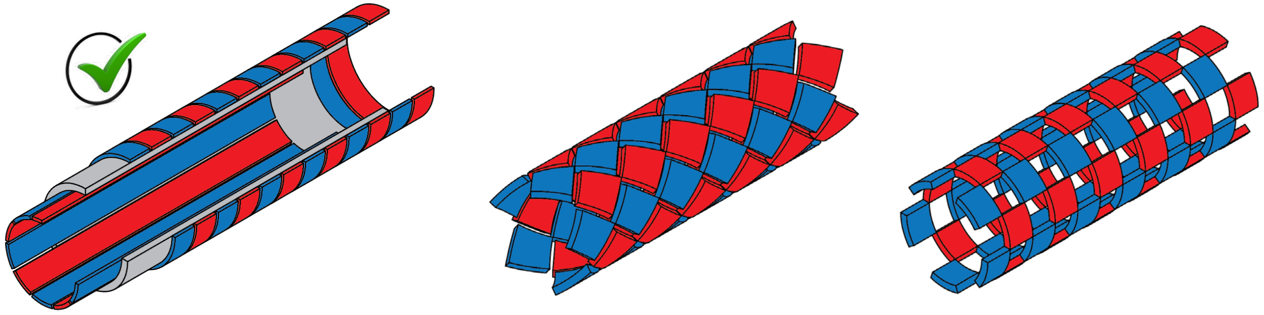

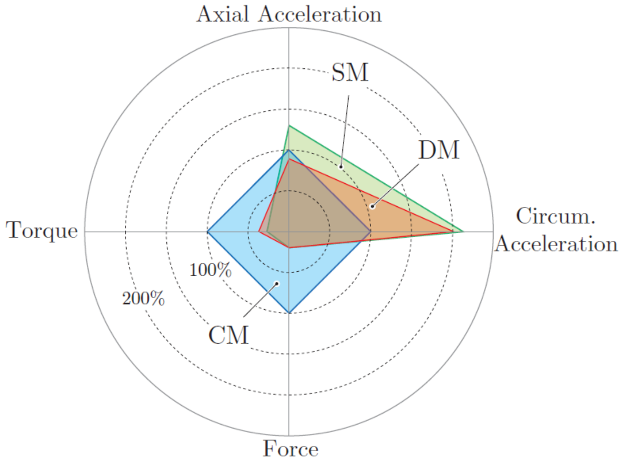

Cooling of the Inner Stator

Heat Flow Conduction Paths

- Outer Stator: Radial Heat Flow
- Inner Stator: Axial Heat Flow

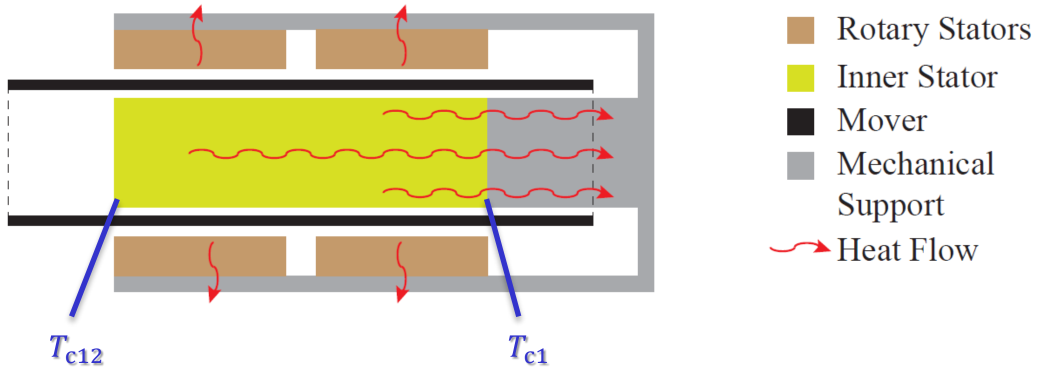

- Winding Temperature: $T_{c12} > T_{c1}$
- Unequal Temperature Distribution due to Axial Heat Flow and Thermal Resistance

Reduction of Axial Thermal Conductivity

- Iron Core Thermal Conductivity: $\sim 20\ \mathrm{W/(mK)}$
- Copper Pipe Thermal Conductivity: $\sim 400\ \mathrm{W/(mK)}$

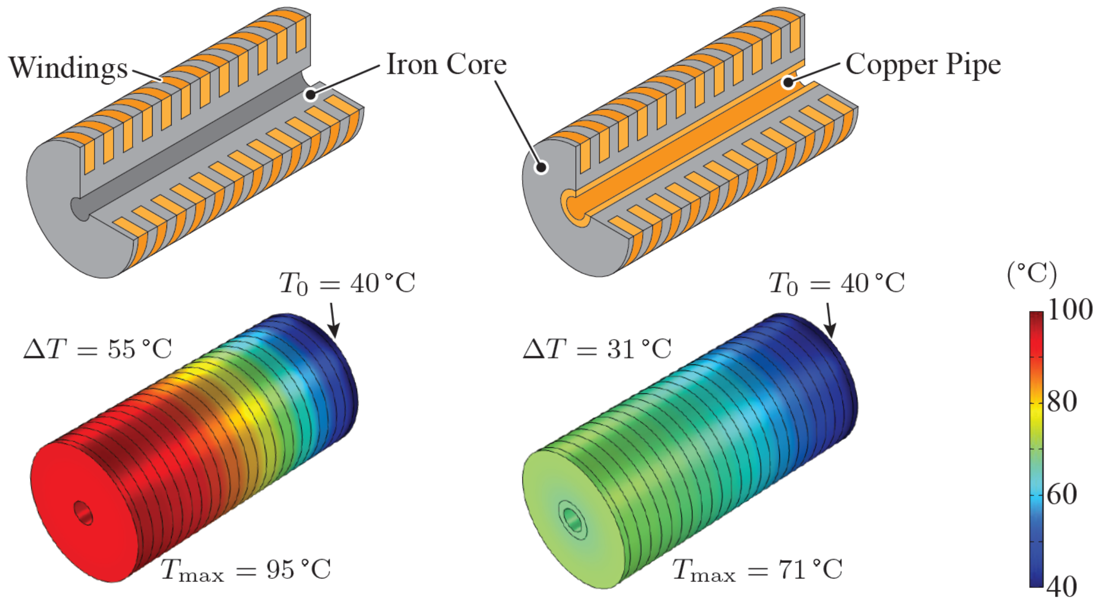

- Optimization Between 'Magnetic' and 'Thermal' Material

Analytic Thermal Model

- **Inner Linear Stator**
  - **Hot Spot Temperature: $T_{c12} < 120$℃**

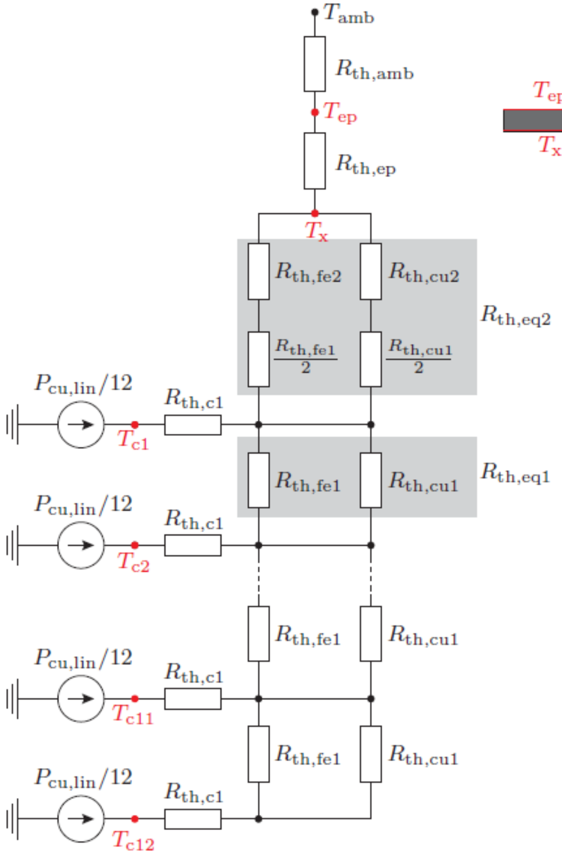

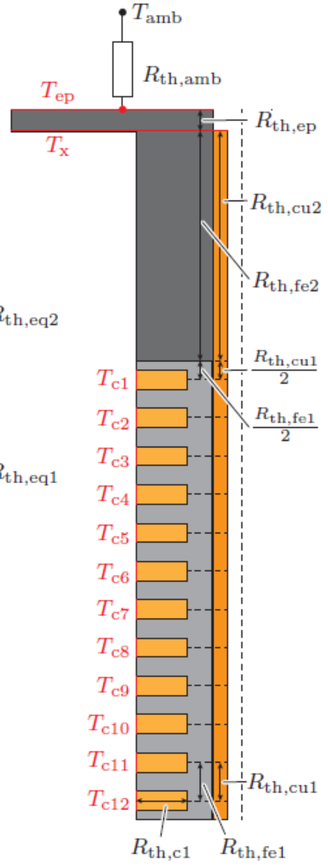

- **Outer Rotary Stators**
  - **Hot Spot Temperature: $T_{w1-6} < 120$℃**

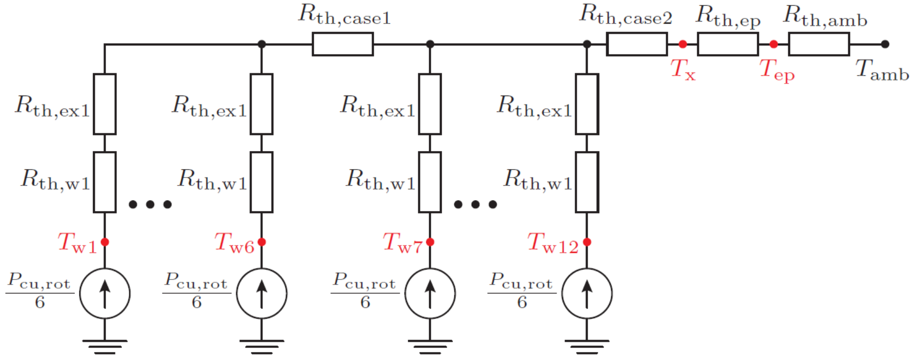

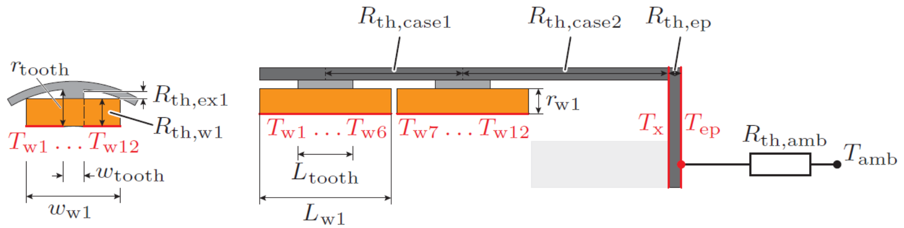

- **Thermal Model Equivalent Circuit**

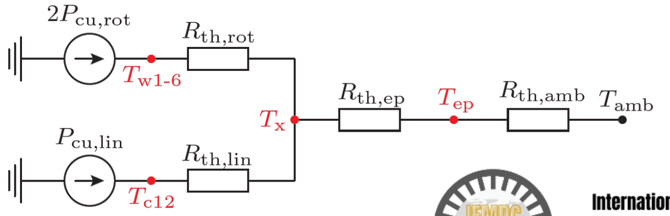

DS LiRA Geometry Optimization

- **Parametrize Geometry**
  - Outer Dimensions Fixed: $L = 100$ mm, $D = 100$ mm
  - Air Gaps: $r_{ag} = 0.7$ mm
  - Copper Pipe Hole: $D_{hole} = 8$ mm (Sensor Cables)
  - Max. Winding Temp.: 120℃

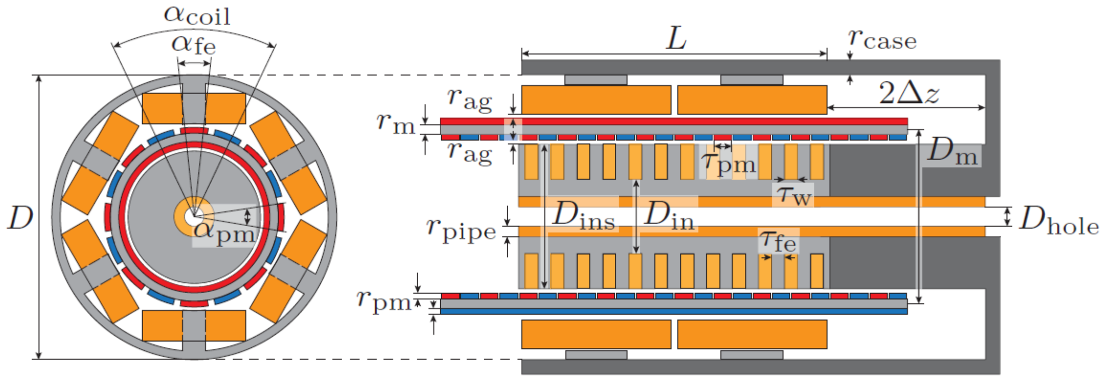

- Models:
  -Magnetic: 2D-FEM
  -Thermal: Analytic Lumped Parameter Circuit Network →

- **Automatized Optimization Procedure**
  - Discrete Design Space

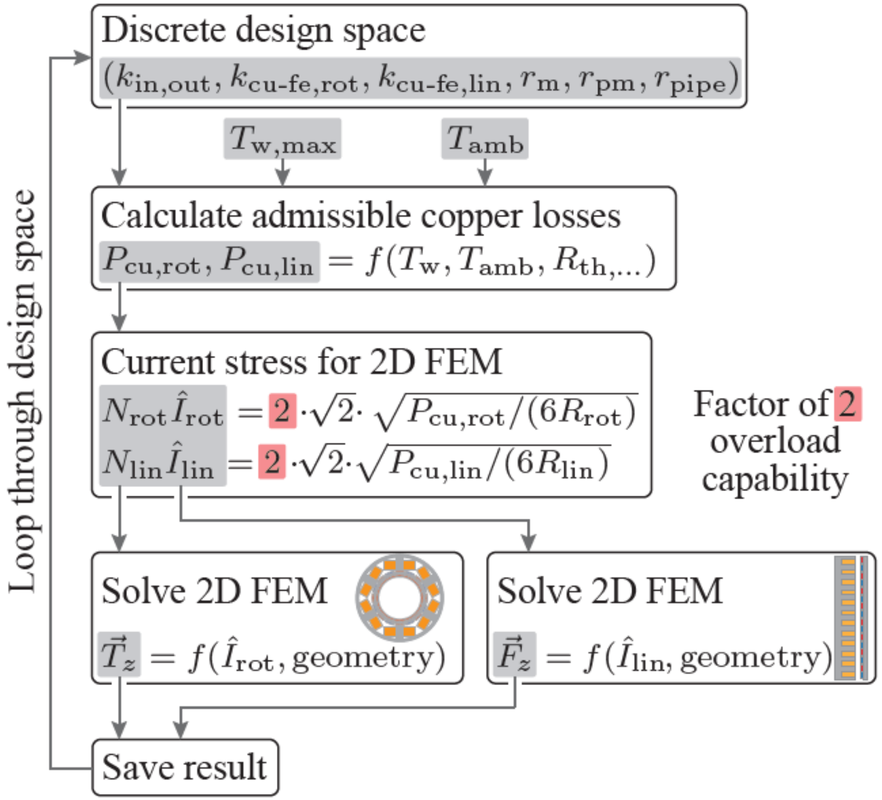

Optimization Results

Torque vs. Linear Force Pareto Plots

- Compromise Between Torque/Force and Acceleration

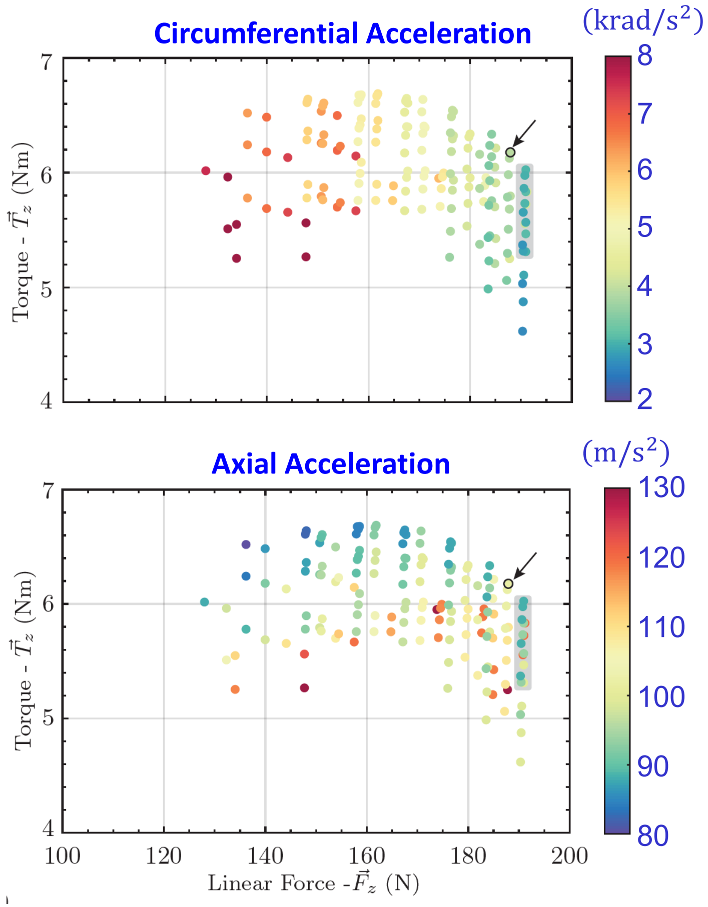

Chosen Design:
$5.3\ \mathrm{krad}/s^2$
$123.5\ \mathrm{m}/s^2$
$6.24\ \mathrm{Nm}$
$181.5\ \mathrm{N}$

3D FEM Flux Density Distribution in the Chosen Design

- Flux Density Evaluated for Double the Continues Current
- Outer stator: < 2.1 T, Inner Stator: < 1.4 T, Mover: < 2.1 T

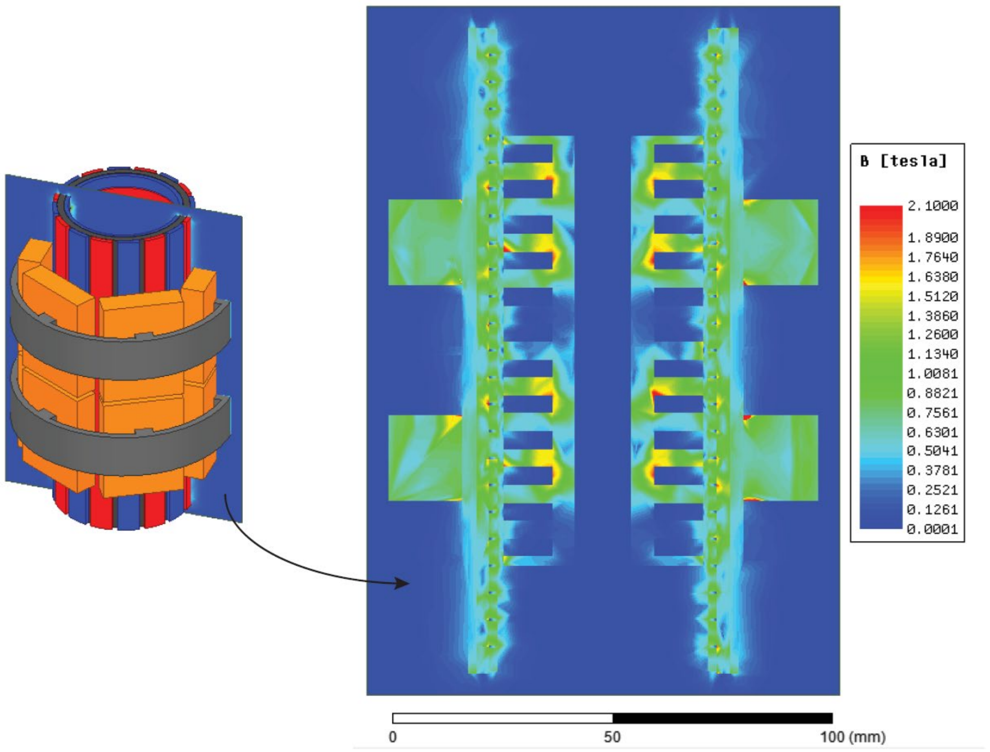

- Hardware Prototype →

DS LiRA Prototype

■ 3D CAD Model

- ‘Exploded View’ of the Outer Rotary and Inner Linear Stator

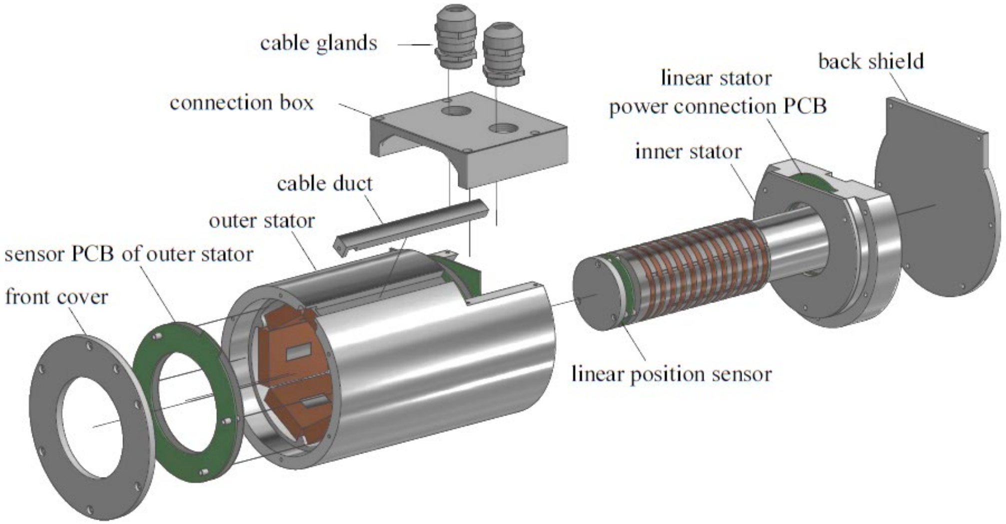

- Inner Stator: 12 × Coil Windings,
  1 × Lin. Pos. Sensor PCB,
  1 × Power Connection PCB
- Outer Stator: 12 × Concentrated Windings,
  2 × Rotary/Radial Pos. Sensor PCBs,
  1 × Power Connection PCB

■ Prototype Realization

- Outer Rotary Stator

- Inner Stator

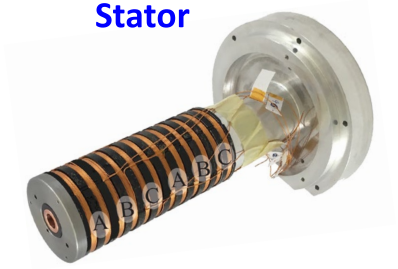

- DS LiRA

- Mover

18-Phase Inverter Supply

Schematic

- LC Output Filter with Parallel RC Damping

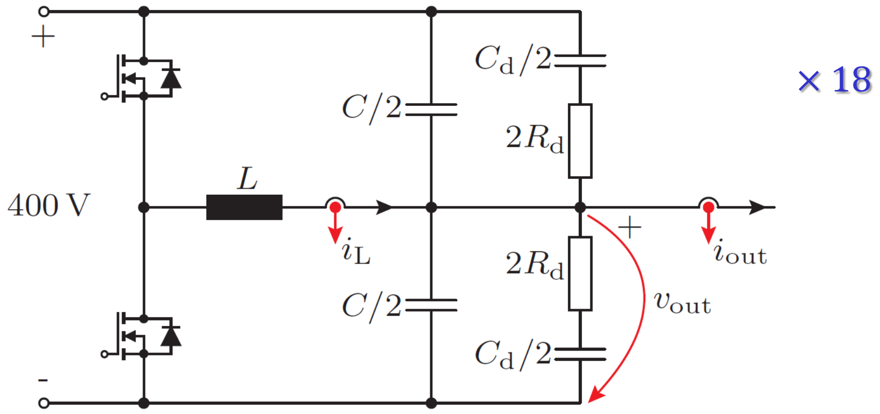

- Power Semiconductors: $600\ \mathrm{V}, 70\ \mathrm{m\Omega}, \mathrm{CoolGaN-MOSFET}$
- Inductor: $L = 80\mu\mathrm{H}, \mathrm{N87}, \mathrm{RM12}, 23\ \mathrm{Turns}, 71\mu\mathrm{m\ Strand}$
- Capacitance: $C = 4.8\mu\mathrm{F}$ for $THD_{vout} = 1\%$
- Heatsink Design: $CSPI = 12\ \mathrm{W/(Kdm^3)}$

Hardware Realization

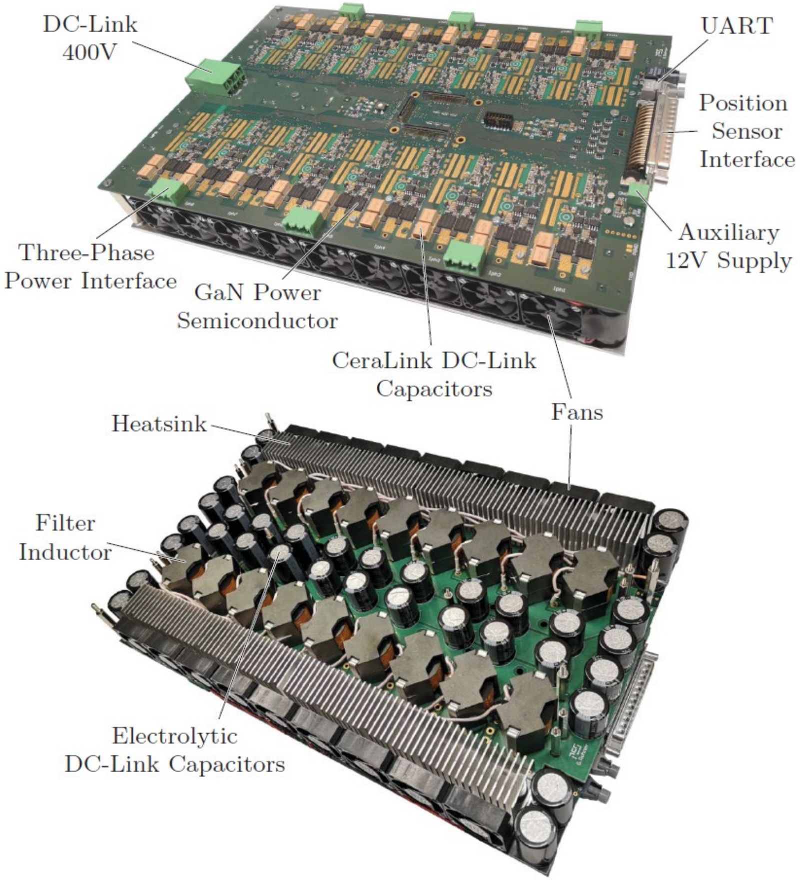

Current & Position Controller

Current Control Structure

- Input: i_{out} References → From the Position Controller

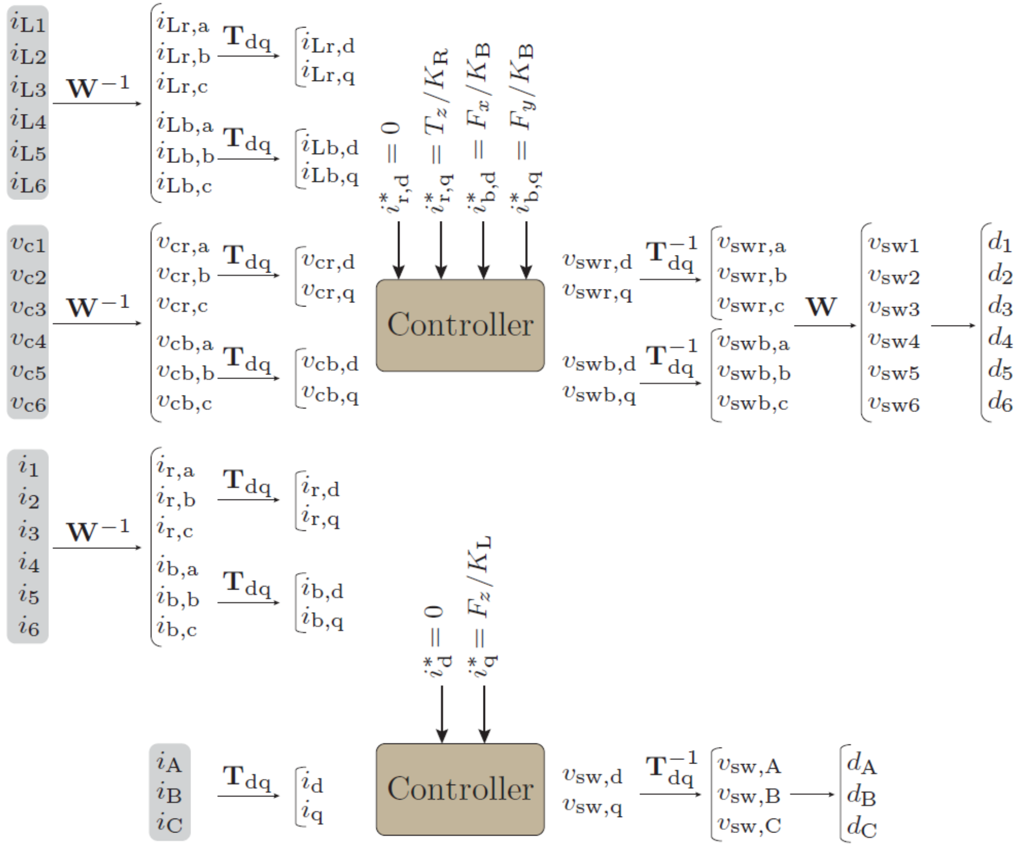

'Decentralized' Position Control

- Dedicated PID Controller for Each Motion Mode

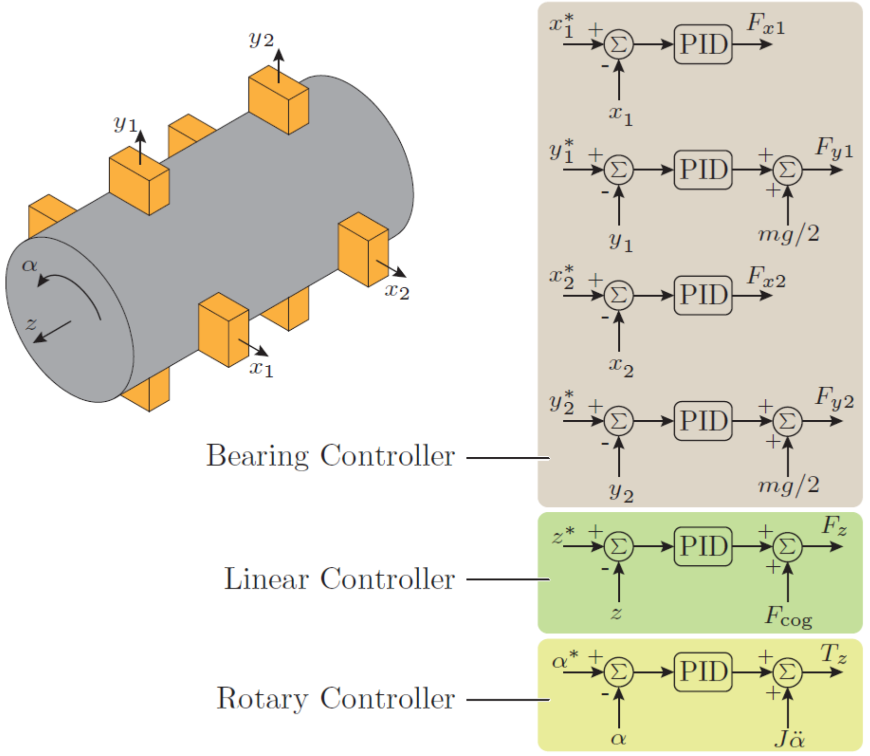

DS LiRA Measurement Results

■ Rotary Step

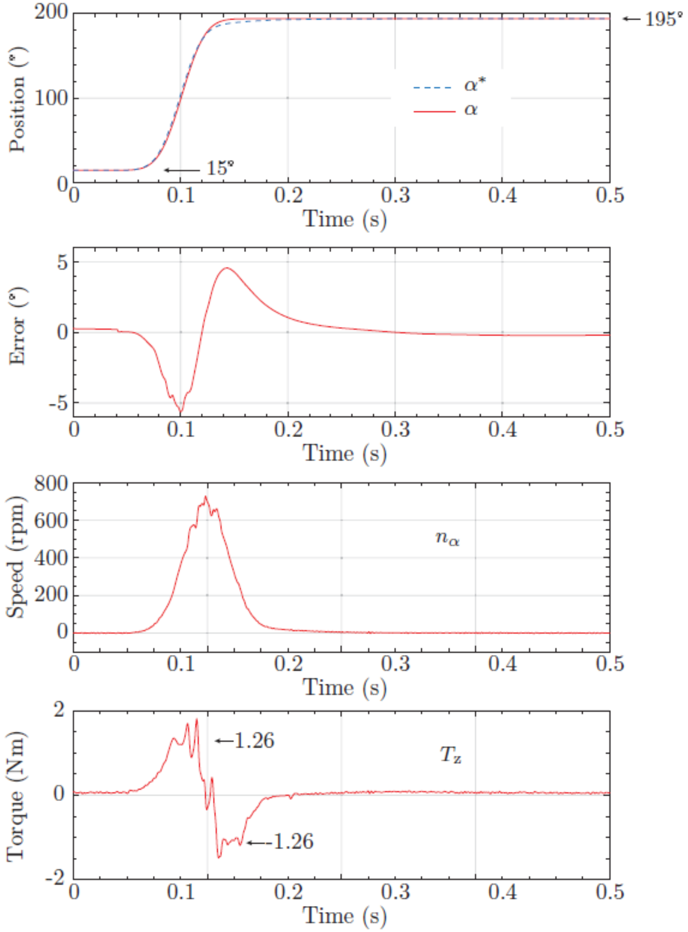

Stroke: **180** °

Error: < |±5| °

Max. Speed: **~700 rpm**

Torque Limit: ± 1.26 **Nm**

■ Rotary Step: Radial Positions

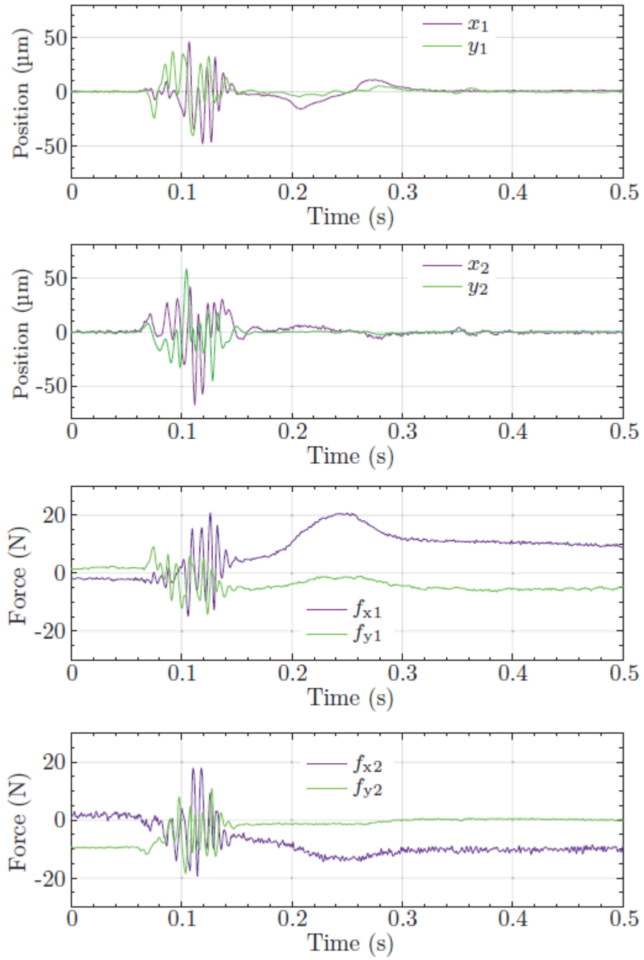

References:

$x_1^* = 0$

$y_1^* = 0$

$x_2^* = 0$

$y_2^* = 0$

Deviations: ± 50 **µm**

DS LiRA Measurement Results

- Video

Part 1 Summary

- Linear Bearingless Actuator

  - Integration of Magnetic Bearings into a Linear Actuator
  - Radial Position and Tilting Control in Micro Meter Range
  - High-Precision/Purity/Dynamic Linear Motor Applications

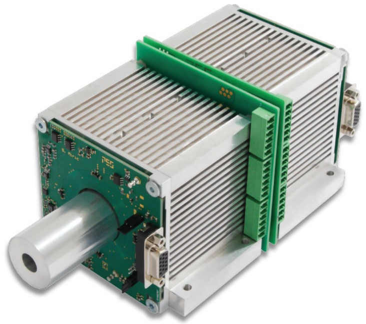

- Linear-Rotary Bearingless Actuator

  - Coupling of Rotation, Linear Motion, Magnetic Bearings
  - Automatized Semi-Numerical Optimization Procedure
  - High-Precision/Purity Applications

Part 2

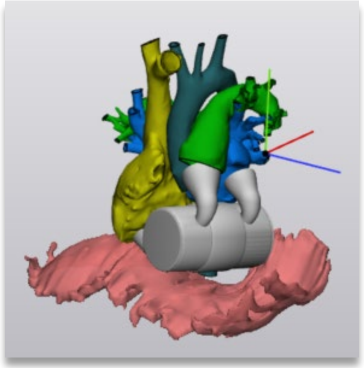

Outline

Part 1

- *Introduction*
- *LiRA Examples / Applications*
- *Linear Actuator with Integrated MBs*
- *Position Sensors*
- *Dynamic Modeling, Controller Design*
- *Generalized Complex Space Vector*
- *Double Stator LiRA*
- *Outlook*

Part 2

- *Introduction*
- *Application: Blood Pumps*
- *Sensors for SB-LiRAs*
- *Design Example: the ShuttlePump*
- *Outlook*

Part 3

- *Introduction*
- *WPT to Linear Actuators*
- *Orthogonal and Parallel Field Concept*
- *Supplying Multiple Receivers*
  Voltage & Current Impressed WPT
- *Outlook*

universität innsbruck

Blood Pumps

Motivation
Types and Applications
Existing Systems

Heart Failure

- > 26 million people worldwide, expected to increase with aging of population
- Congenital heart defects: ≈ 1% of newborns → complications

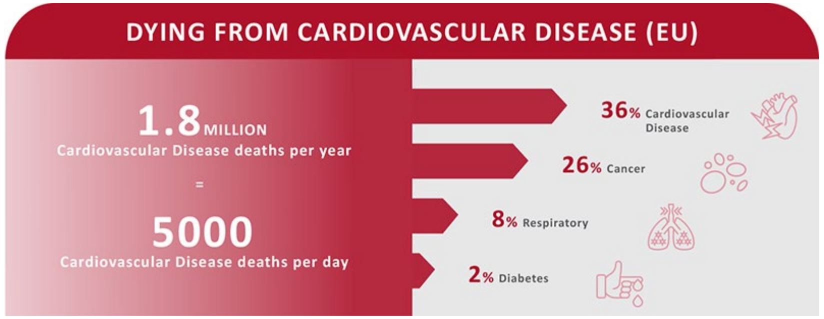

Source: ehnheart.com

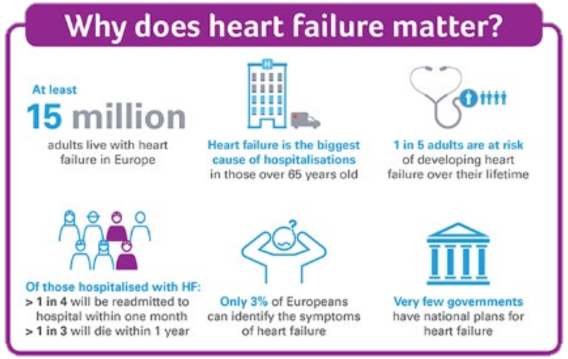

Source: hfpolicynetwork.org

Source: ox.ac.uk

- Heart transplantation: not enough donors → ≈ 20% of patients dies on the waiting list
- Urgent need for short- and long-term solutions → Mechanical Circulatory Supports (MCSs)

Heart Failure – Mechanical Circulatory Support (MCS)

- Short-term (acute) → e.g. Extra-Corporeal Membrane Oxygenation (ECMO)
- Long-term (chronic) → e.g. Ventricular Assist Devices (VADs) or Total Artificial Hearts (TAH)

ECMO

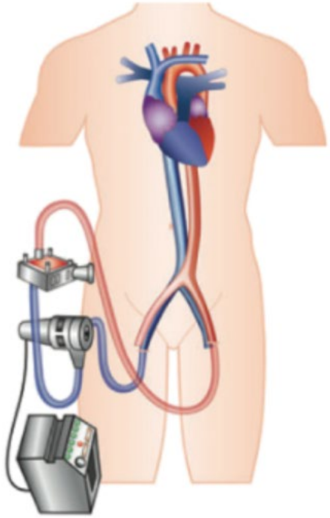

TandemHeart

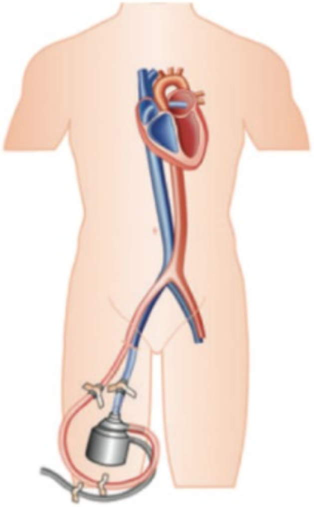

Source: Werdan et al., 2014

LVAD

TAH

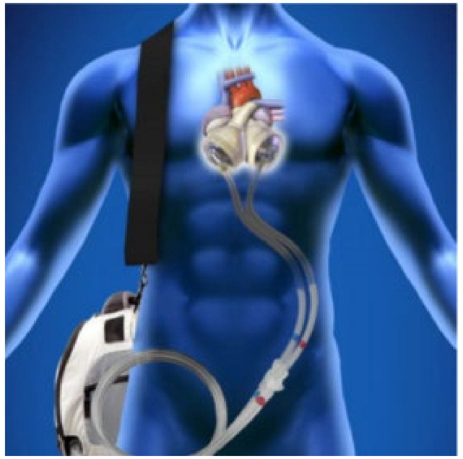

Source: jacobmedicaladvisors.com

- Either case: keep blood circulating → Mechanical Circulatory Support (MCS), i.e. a blood pump

Blood Pumps – A Taxonomy

Pulsatile / Continuous Flow | Axial Flow / Centrifugal | Extra-Corporeal / Implantable

- Common requirements: gentle blood handling (low hemolysis) | small volume

Blood Pumps – Pulsatile vs Continuous Flow

- Pulsatile / "1st gen" / Positive displacement → Physiological, pneumatically or electrically driven
- Example: BerlinHeart EXCOR® | VAD (L/R/Bi), Paracorporeal

Berlin Heart®

- Larger / heavier / valves needed / external driving units

Blood Pumps – Pulsatile vs Continuous Flow

- Continuous / "2nd gen" / Rotary Blood Pumps (RBPs) → electrically driven | efficient | compact
- Example: Abbott HeartMate II | LVAD, Implantable

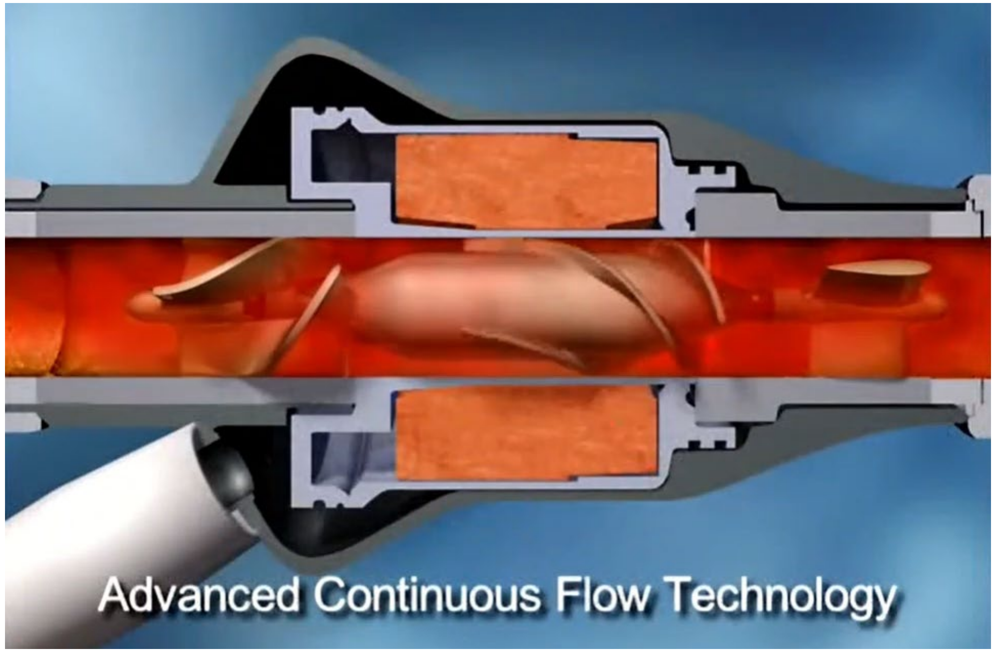

THORATEC CORPORATION now part of Abbott

- Can be realized with just one moving part / no need for valves → reliability, durability

Blood Pumps – Axial Flow vs Centrifugal Flow

- Continuous Flow Rotary Blood Pumps: two options
- Centrifugal flow → can integrate non-contact bearing options

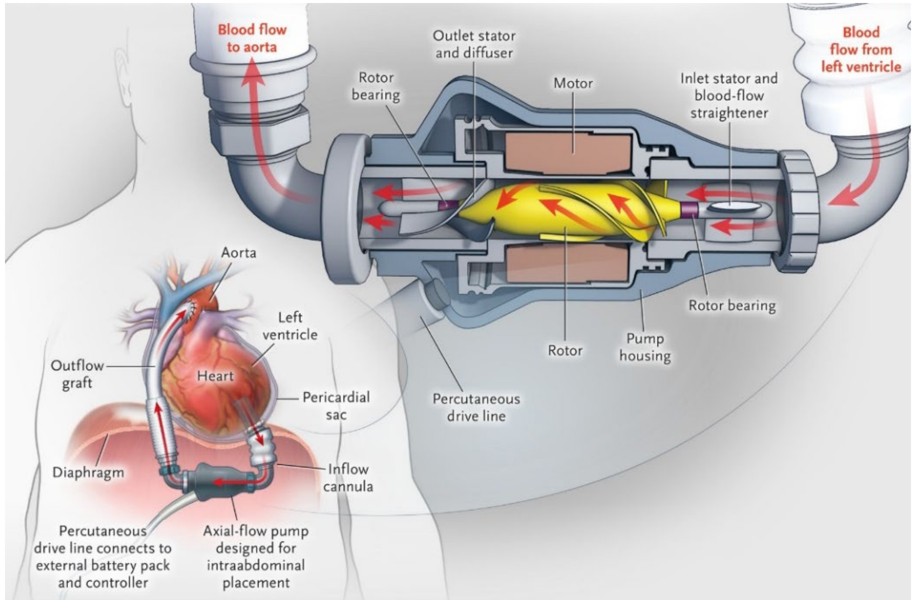

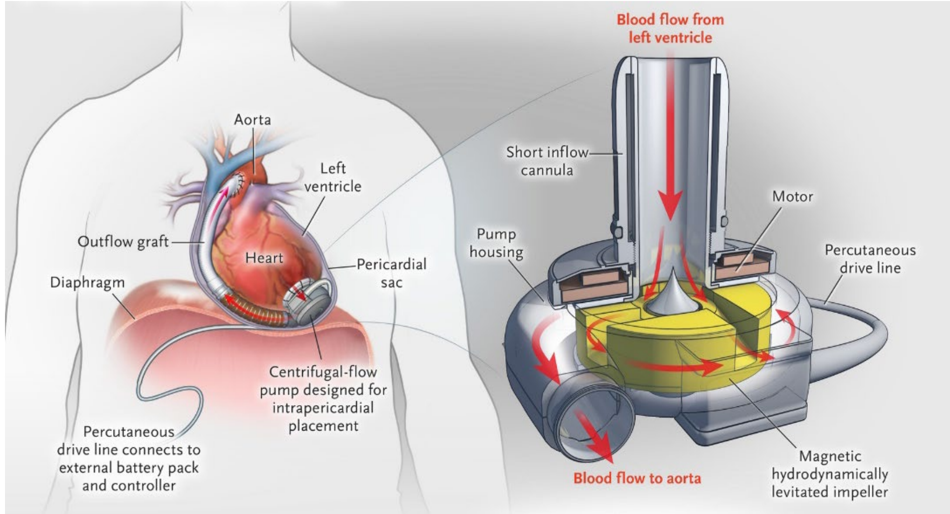

Source: Rogers et al, 2017

Blood Pumps – Axial Flow vs Centrifugal Flow

- Centrifugal flow / “2nd gen” / Rotary Blood Pumps (RBPs)
- Example: Medtronic HeartWare HVAD | LVAD, Implantable

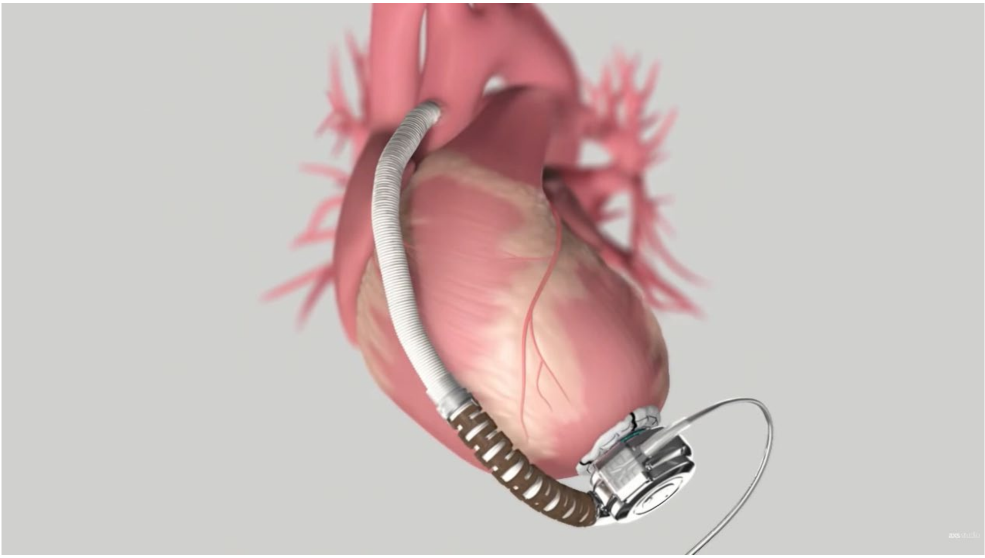

HeartWare
Medtronic

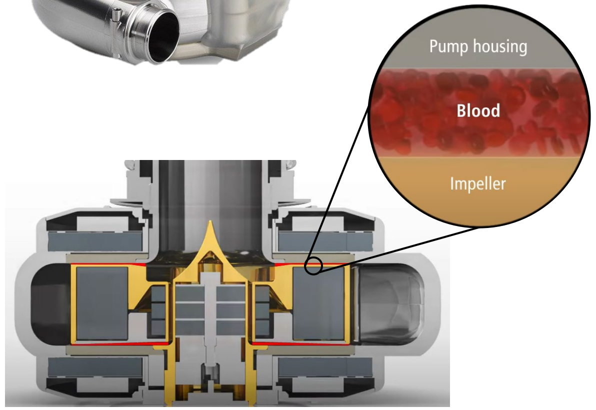

- Hybrid passive magnetic + hydrodynamic bearing

Blood Pumps – Magnetically Levitated

- Centrifugal flow / "3nd gen" / Rotary Blood Pumps (RBPs) with Magnetic Bearings
- Example: Abbott HeartMate 3 | LVAD, Implantable

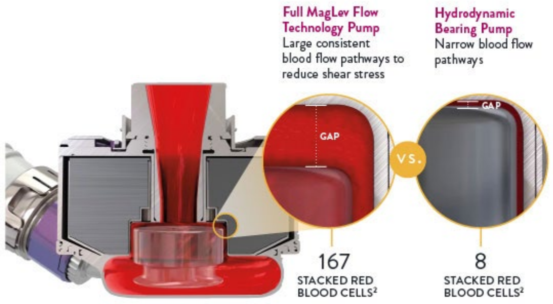

Source:
cardiovascular.abbott

- Most advanced LVAD → direction for future systems

Total Artificial Hearts (TAH)

- Bi-ventricular failure → more compact wrt 2 x VADs
- Same pump types as for LVADs | Not as mature, research and development needed

Pulsatile pumps

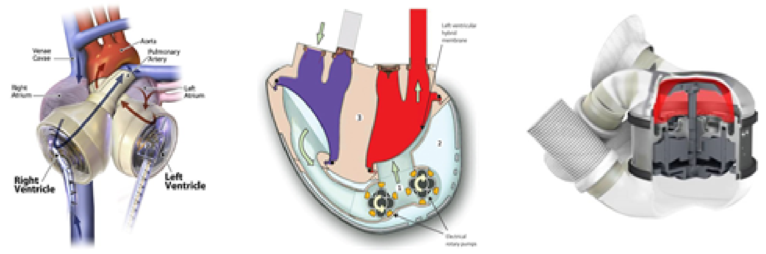

SynCardia (FDA appr.) | Carmat | ReinHeart

Rotary pumps

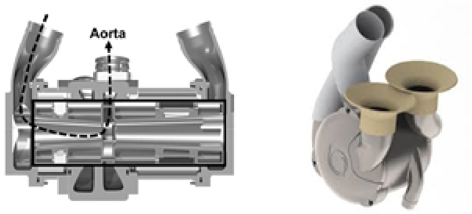

OregonHeart | BiVACOR

\+ Physiological, pulsatile flow

\- Valves can promote thrombus formation
\- Flexible membranes and valves can be risk prone to device failure
\- SynCardia has excorporal pneumatic driving unit (not fully implantable)

\+ High durability: one moving part, no valves
\- High shear stresses because of spinning rotor
\- No or limited pulsatile flow

Source: BIH Innovations The Technology Transfer Office of BIH and Charité

Total Artificial Hearts (TAH)

- Other research directions: entirely-soft 3D-printed TAH (silicone) | Developed @ ETH Zurich
- Only lasts for ≈ 3000 beats (45 mins) → feasibility / more research needed

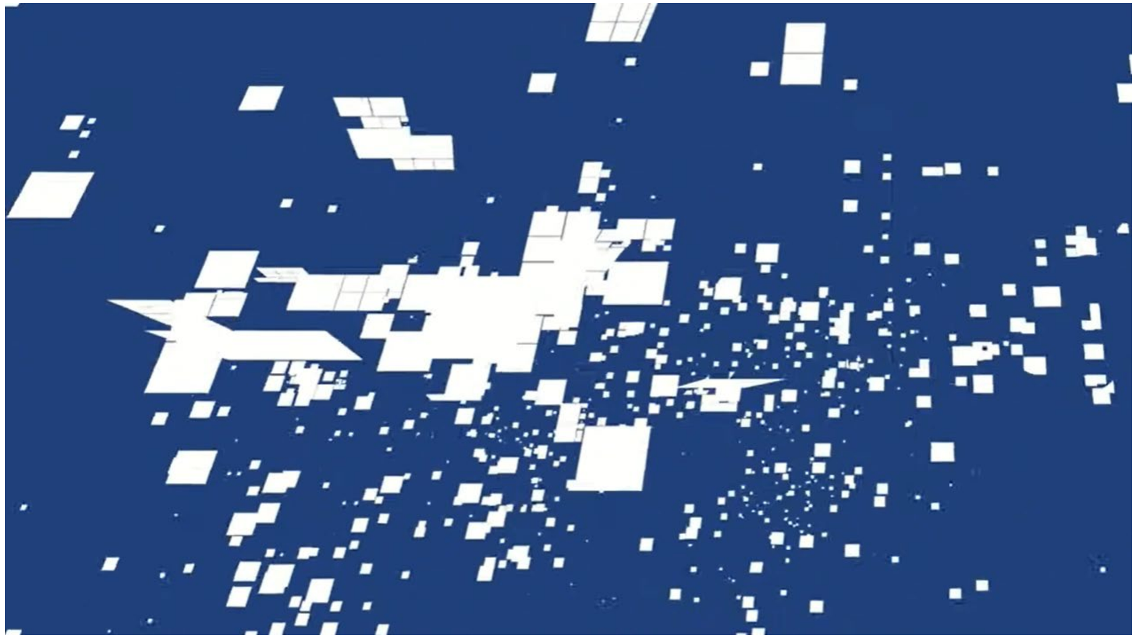

Universität Zürich[UZH] | ETH zürich

USZ Universitäts Spital Zürich | Balgrist Universitätsklinik | Universitäts-Kinderspital Zürich | Psychiatrische Universitätsklinik Zürich

Extra-Corporeal Blood Pumps

- Short-term treatment: extra-corporeal circulation | bridging strategy | e.g. COVID patients
- Example: Abbott CentriMag ECMO | Rotary / Continuous Flow / Centrifugal

Source: cardiovascular.abbott

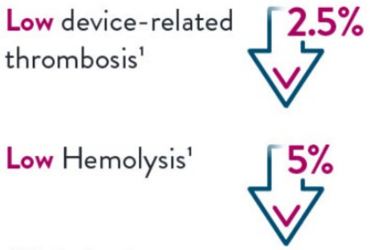

Abbott

universität innsbruck

Sensor Systems for SB-LiRAs

Sensor Types
Non-contact Sensors
Use in SB-LiRAs

ETH zürich

International Electric Machines & Drives Conference
San Francisco, CA May 15-18
IEMDC 2023

Sensors for SB-LiRAs, what to measure?

- High precision requirements → Feedback control → Need precise measurements
- Linear, Rotary, Radial position/displacement sensors

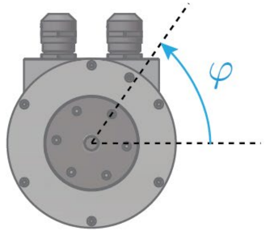

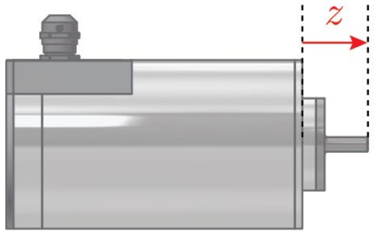

Source: linmot.com

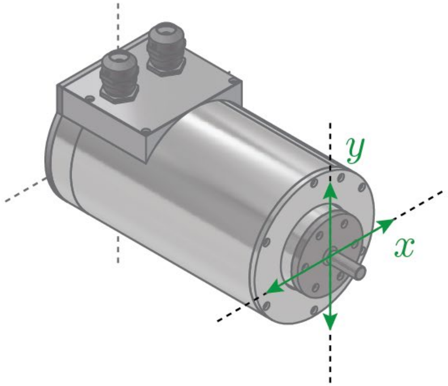

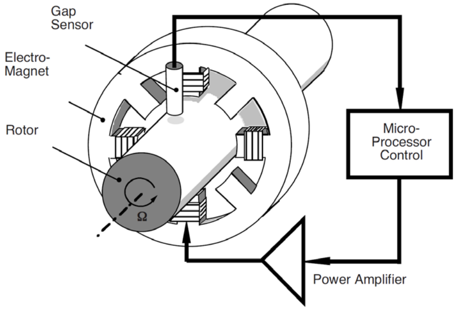

Source: Schweitzer, 2009

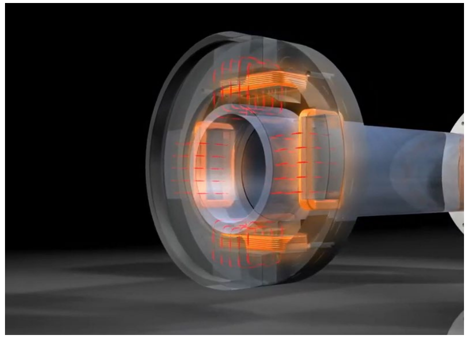

Source: keba.com

- Especially important / demanding to enable MBs!

Position/Displacement Sensors – Non-contact

- MBs → Non-contact sensors / large bandwidth (up to 1 kHz) / high precision (sub-µm range)
- Different options / operating principles

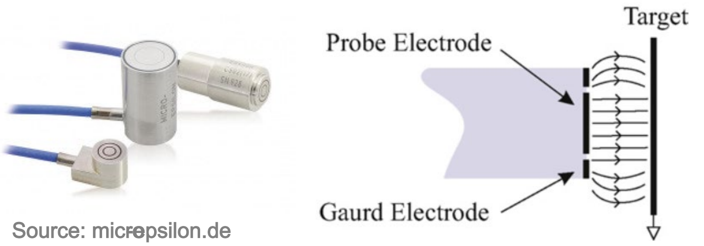

Source: micro-epsilon.de

Source: Fleming et al, 2013

Capacitive

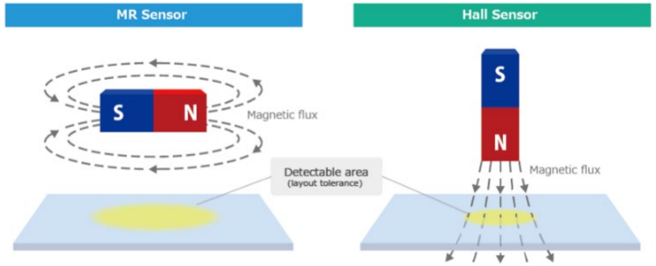

Magnetic

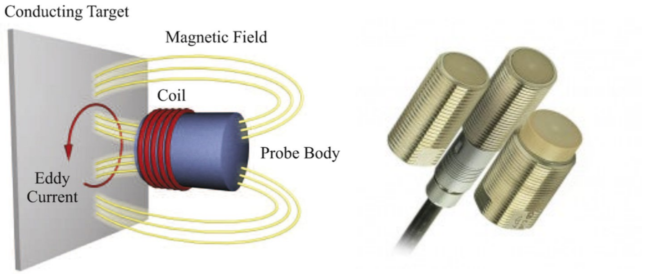

Eddy Current

Source: micro-epsilon.de

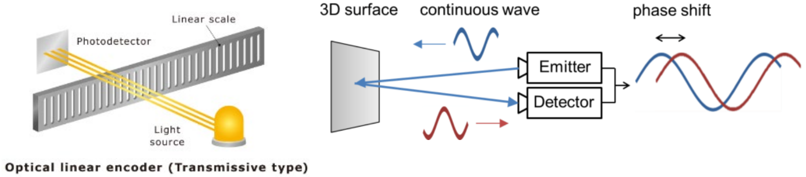

Optical

- Capacitive: grounded target | Optical: no objects between sensor and target
  → Mostly suited: Magnetic and Eddy Current

Hall-Effect Sensors

- Magnetic sensors, based on Hall effect | Hall element + conditioning circuit → DC output
- Conveniently packaged as a single IC | Multiple elements (axes) possible in the same package

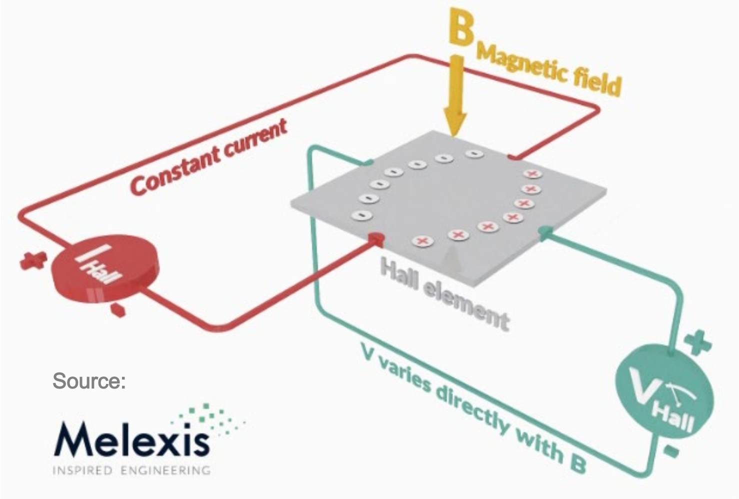

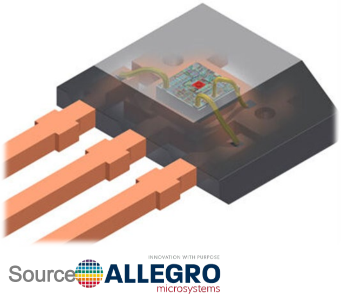

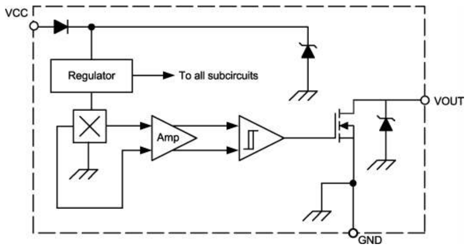

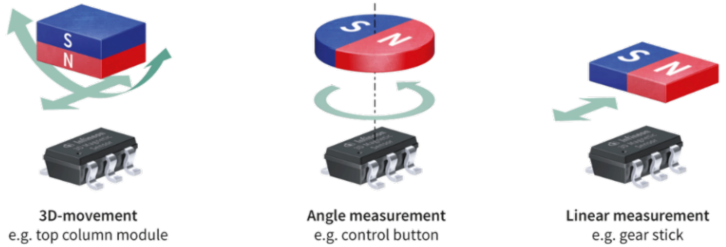

- Bandwidth: typically ≈ 10 kHz range | Resolution: can reach µm → sensor location is crucial!

Hall-Effect Sensors

- Typical use in Rotary Machines: 3 sensors, 120°^{el} displaced, detect (electrical) rotor angle
- Can use analogously for Linear Machines | Alternative: 2 sensors, 90°^{el} displaced (‘sin’ and ‘cos’)

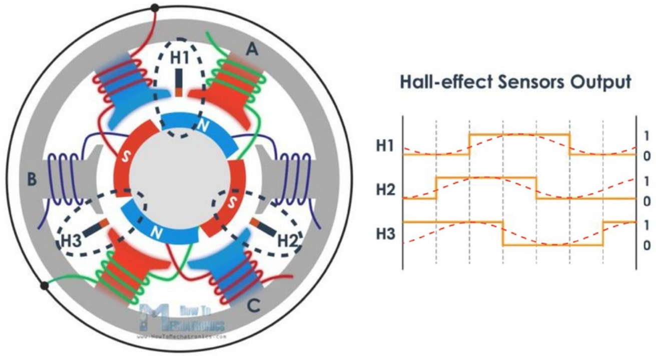

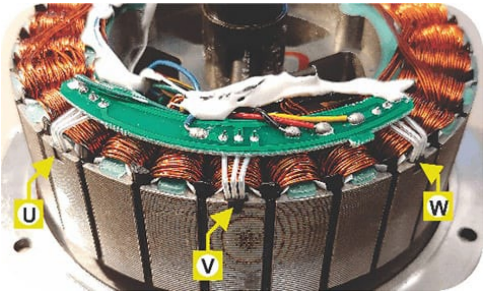

Source: digikey.com

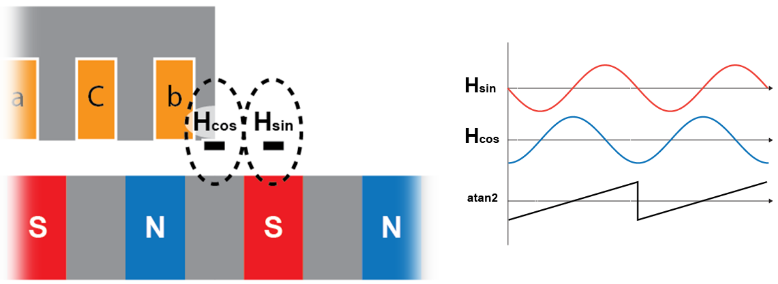

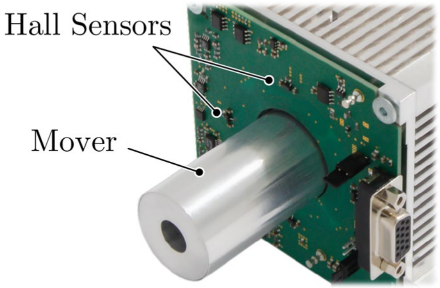

- Main drawbacks: depend on PMs magnetization (irregular, aging, external fields!) / thermal drift

Eddy Current Sensors (ECSs)

- Coil with high-frequency AC voltage excitation + conductive target → eddy currents induced
- Secondary field influences $Z_{c,in}$ (dep. on coupling factor!) → can measure distance δ (rule of thumb: range ≈ radius)

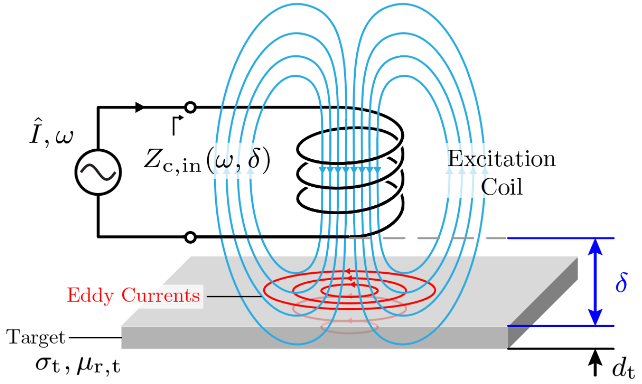

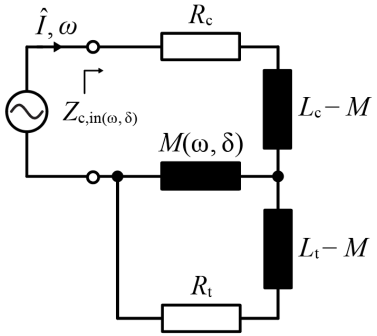

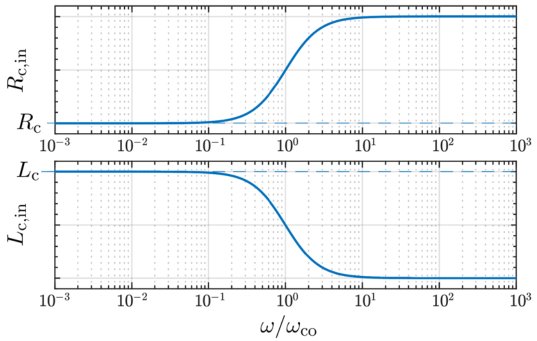

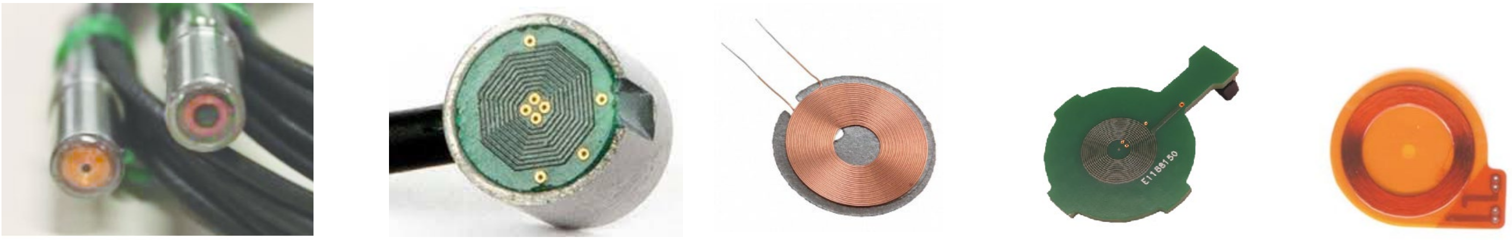

- Coil realization: typically spiral, one layer → low parasitic capacitance, higher SRF, can excite in MHz range
- High level of integration: PCB-embedded coils, also flexible

Eddy Current Sensors (ECSs)

- AC excitation, extract position information from impedance → sensor interface / post-processing circuit
- Extensive literature about ECS interfaces for high performance sensors. Examples:

ΔZ to ΔU

Example: Differential AC Wheatstone Bridge

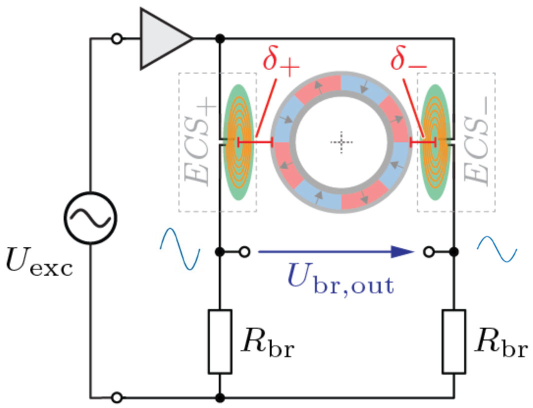

$U_{br,out}$ is AM-demodulated

ΔZ to Δf

Example: Difference Relaxation Oscillator

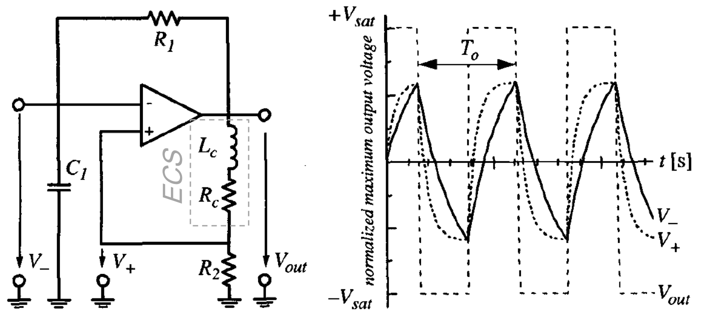

Source: Zoethout, 2002

- Sensor interface determines achievable sensitivity / resolution / bandwidth / (non-)linearity
- Integrated interface solutions are becoming available (e.g. LDC, Texas Instruments)

Eddy Current Sensor "Seeing Through Walls"

- Point of strength of ECSs: can tolerate objects in the air gap → suited for harsh / dirty environments
- Special application: ECS measuring through a conductive enclosure → high purity / sealed applications

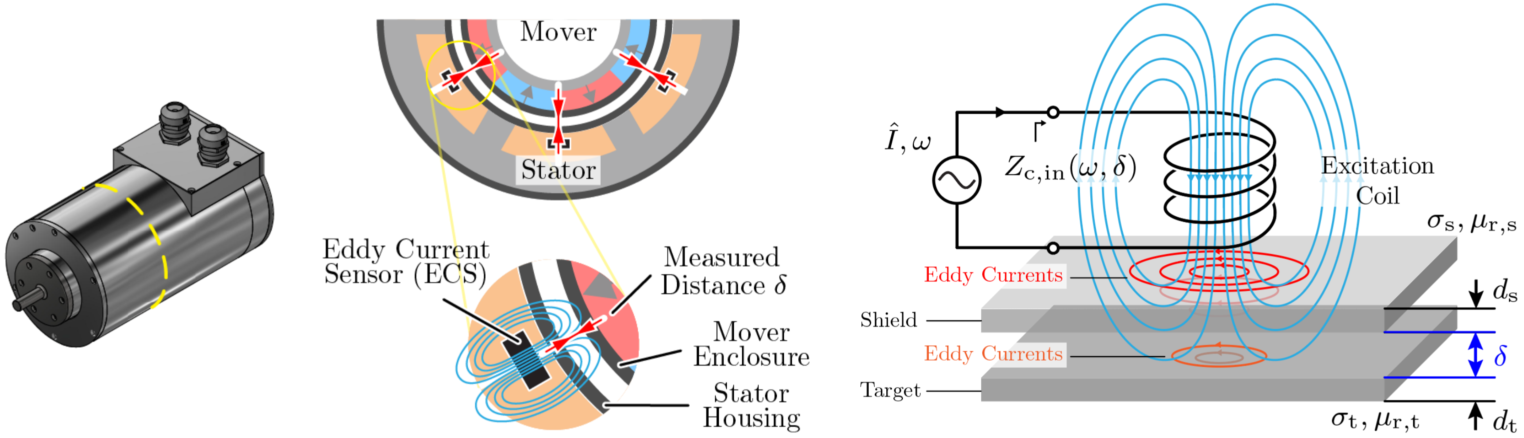

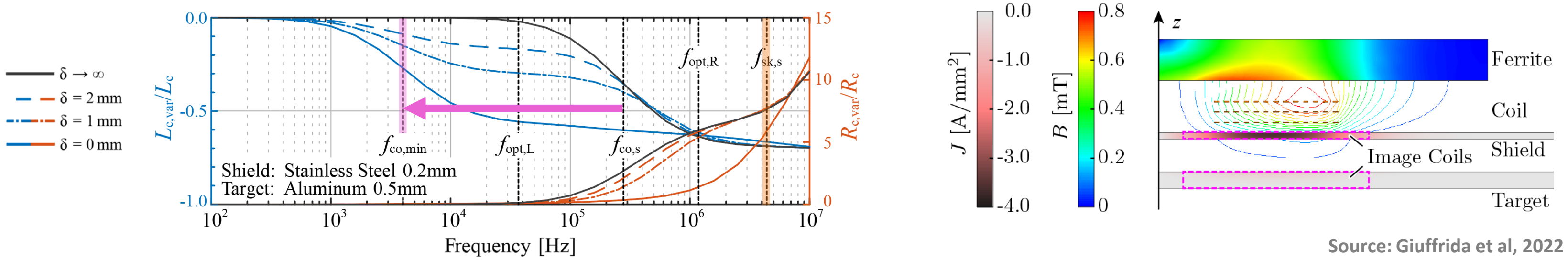

Source: Giuffrida et al, 2022

- Possible in a specific frequency range defined by shield and target properties
- Rule of thumb: make the enclosure thinner and/or of a less conductive material wrt the target

Eddy Current Sensor “Seeing Through Walls”

- Realized hardware prototype: PCB coil + evaluation board / analysis and verification of thermal drift
- Measurement circuit with quad. demod. → distinguish between distance δ and temperature T variations

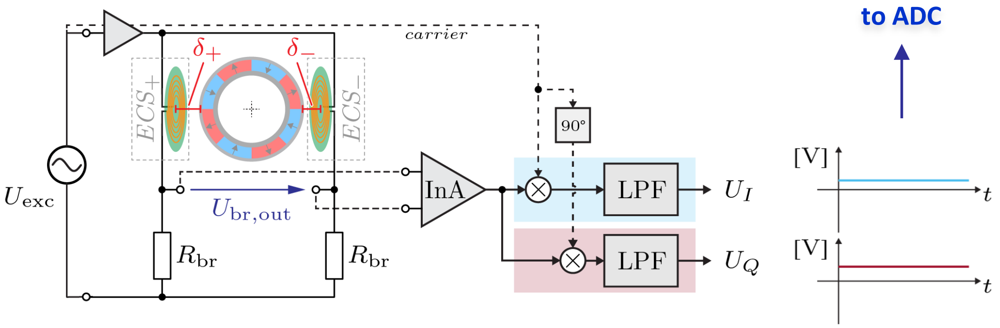

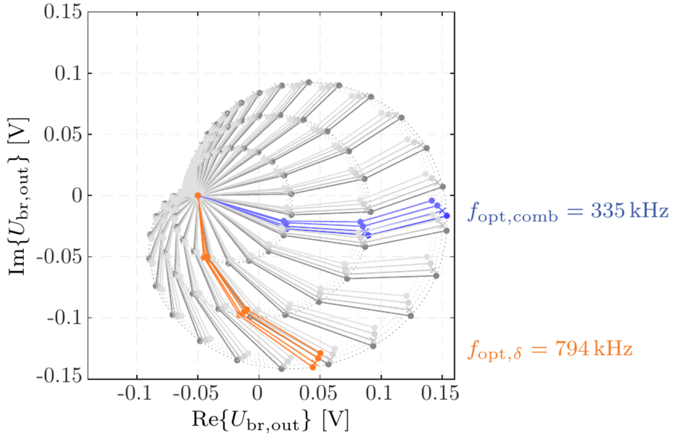

Source: Giuffrida et al, 2022

Temperature-controlled setup

Realized Evaluation Board

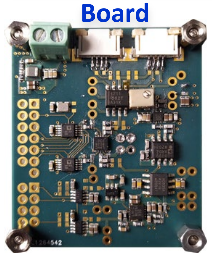

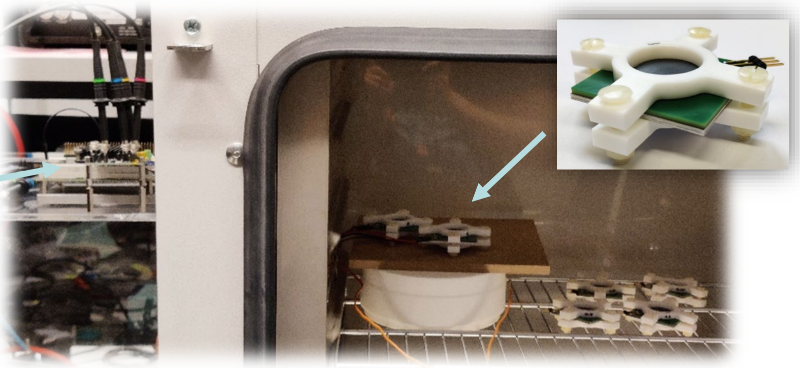

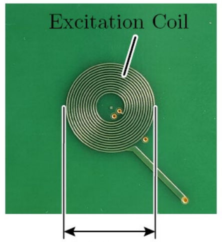

LiRA with HBs: ShuttlePump

Machine Design
Sensor System
Built Prototype

ShuttlePump

- Implantable TAH based on a LiRA → opening/closing of inlets/outlets @5 Hz → valveless!
- Pulsatile flow → physiological

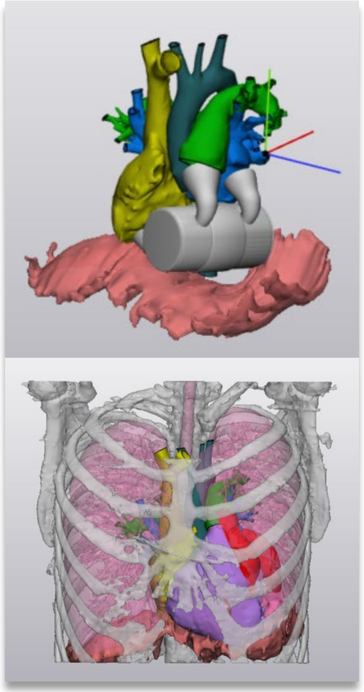

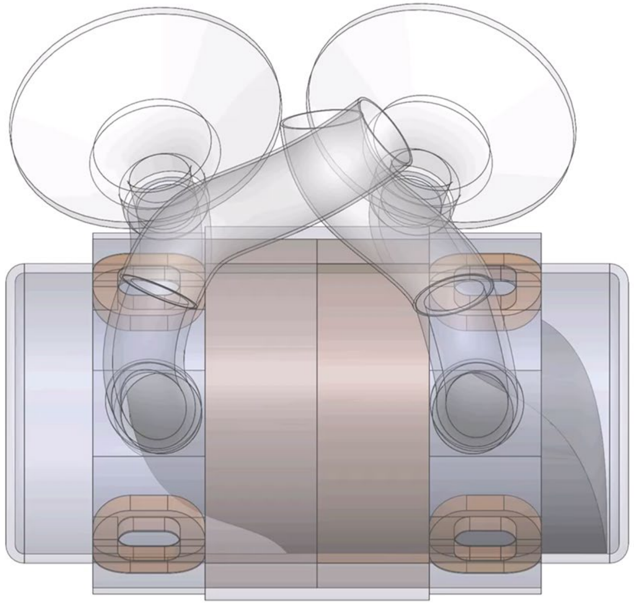

CHARITÉ UNIVERSITÄTSMEDIZIN BERLIN

MEDIZINISCHE UNIVERSITÄT WIEN

ETH zürich

- Design of the LiRA Motor Drive System @ PES – under realization

ShuttlePump

- Linear Actuator: push blood in circulation → motion profile with force requirement
- High power density (up to 10 W peak in 200 cm^3)

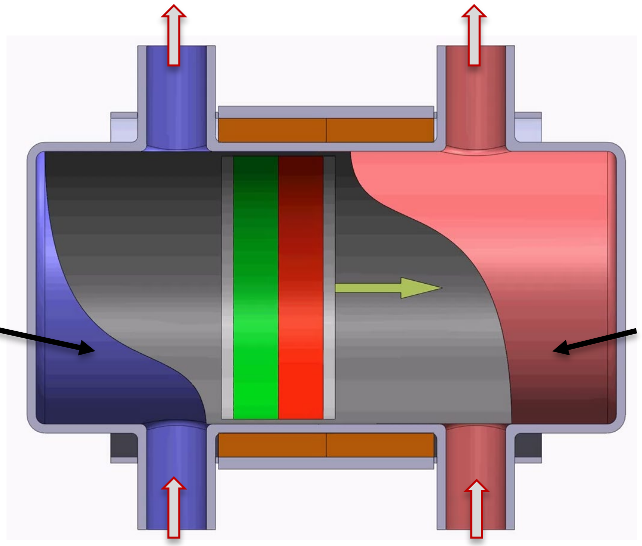

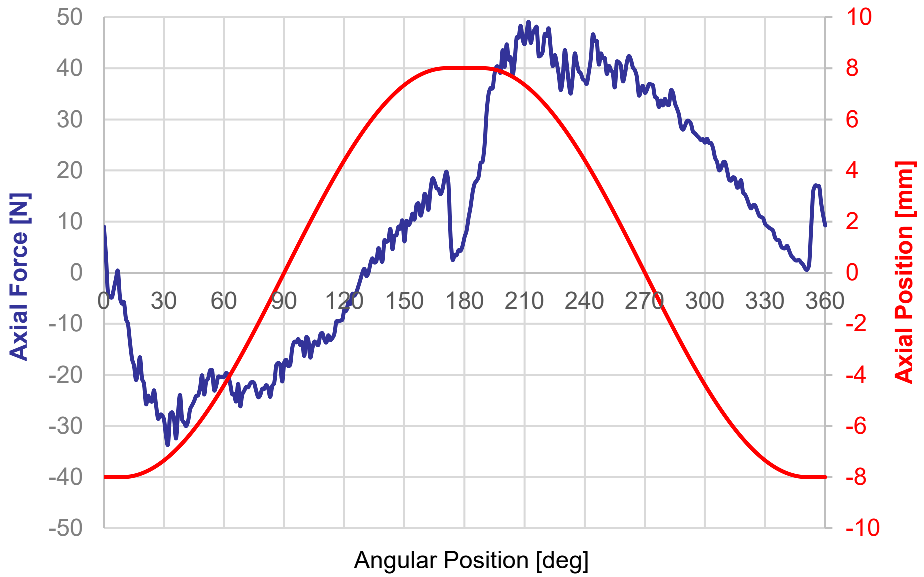

- Important constraints: 1) blood temperature increase < 2°C → minimize losses
  2) overall device weight < 900 g, minimize piston weight
  3) outer diameter < 70 mm

ShuttlePump – Hydrodynamic Bearing

- Rotary Actuator: continuous 3 mNm axial torque → establish journal HB
- CFD simulations from Medical University of Vienna / HB design

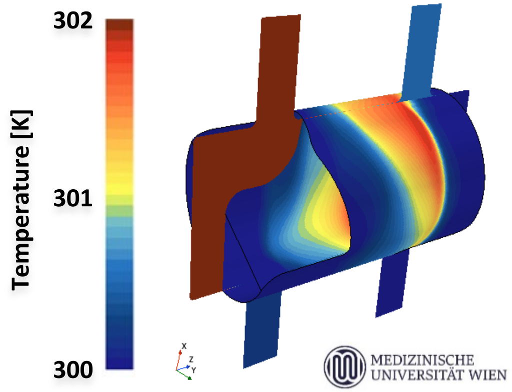

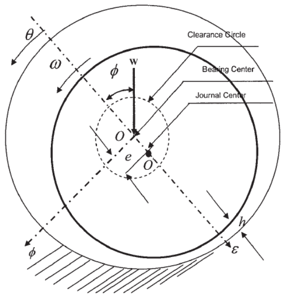

W – load
e – eccentricity
c - clearance
Φ – attitude angle
ε – eccentricity ratio e/c
ω – angular velocity
h – minimum film thickness

Source: Khonsari et al., 2017

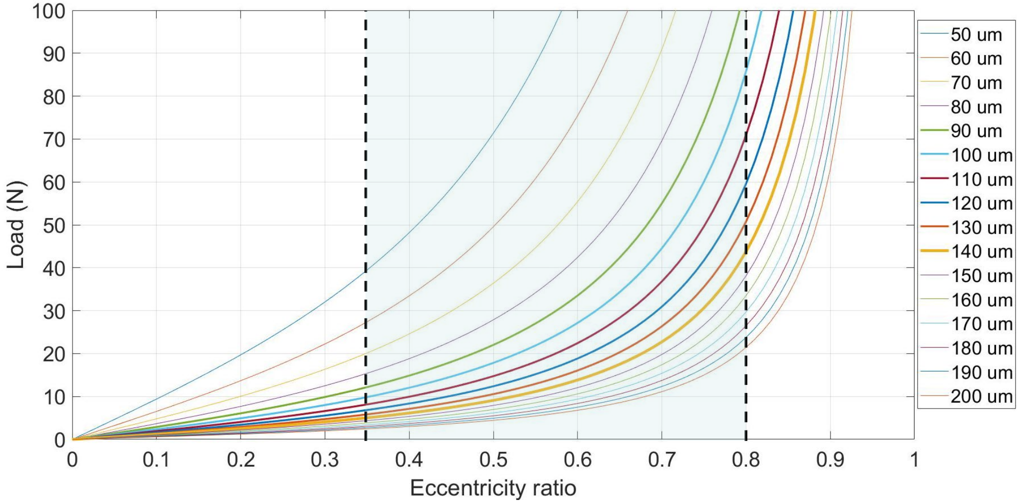

- Acceptable eccentricity ratio: 0.35 – 0.8
- May be unstable if $\varepsilon < 0.35$ or $\varepsilon > 0.8$

- Blood gap thickness: trade off radial load / blood heat-up → Suggested blood gap: 140 µm

ShuttlePump – Motor Concept

- Permanent Magnet Synchronous Machine (PMSM): high power density, PMs embedded in the piston
- Minimize drive unit's complexity, i.e. number of phases / half bridges

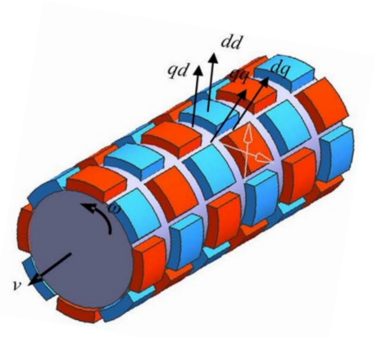

Source: Jin et al., 2012

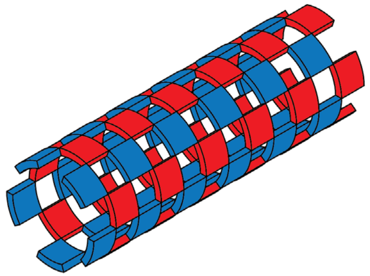

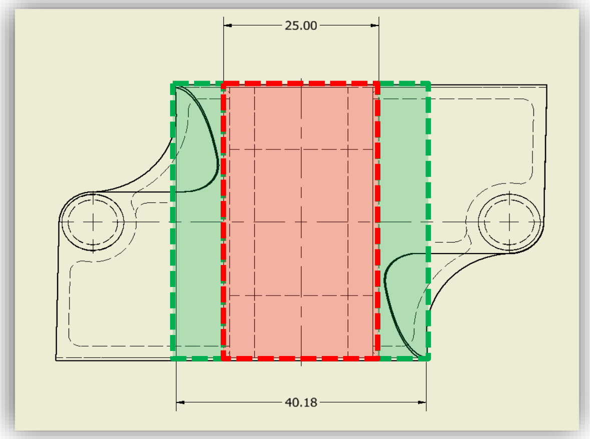

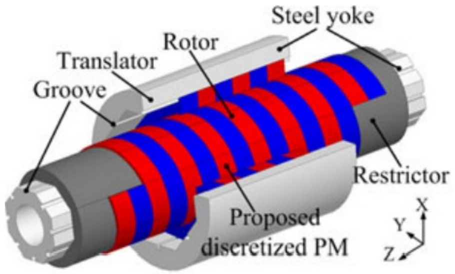

Source: Ling et al., 2018

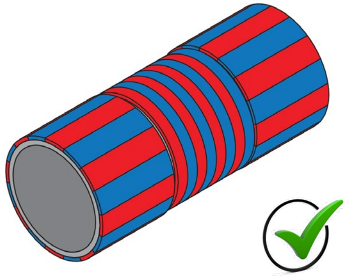

- Requirements for LA and RA highly differ → "Independent" machine design of LA and RA, 3 + 3 ph.
  → maximum lateral surface for LA

ShuttlePump – LA Design

- Tubular Linear Actuator (TLA), simplest possible stator / mover designs (1 pole pair)

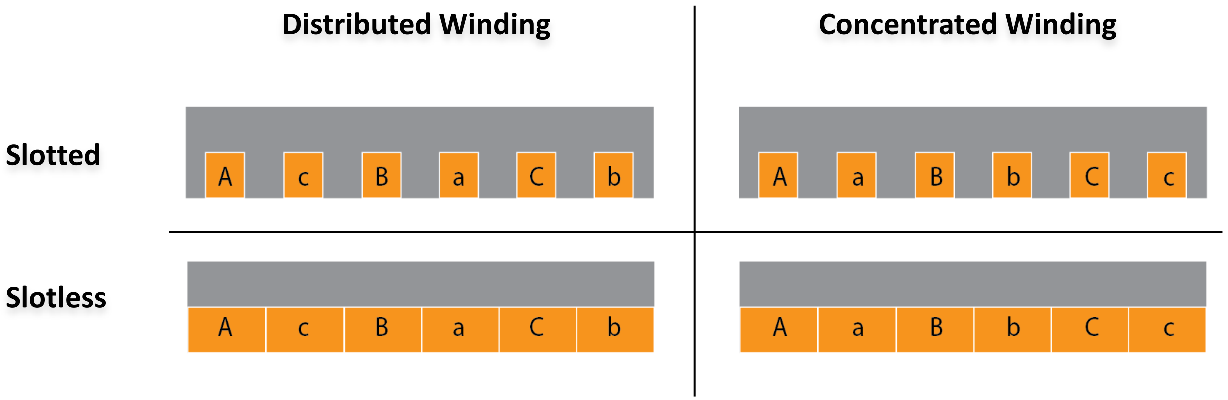

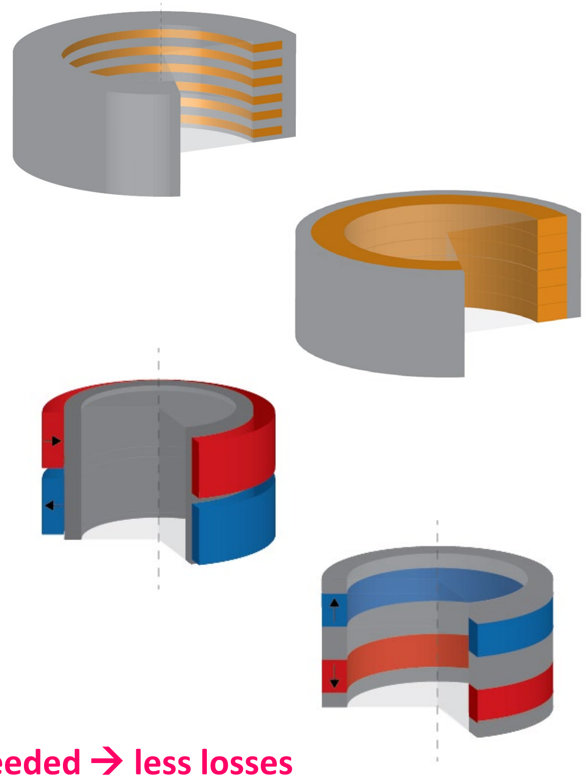

- Radial Magnetization: Surface PM

- Axial Magnetization: Interior PM

- Stator: if slotted → minimum air gap, higher flux density, less current needed → less losses
- Mover: both radial and axial magnetization possible, manufacturability

ShuttlePump – LA Design

- Parameterization + Optimization with Finite Element Methods (FEM) simulations
- For fixed output axial force (43 N), objectives: least losses | least weight

Ansys

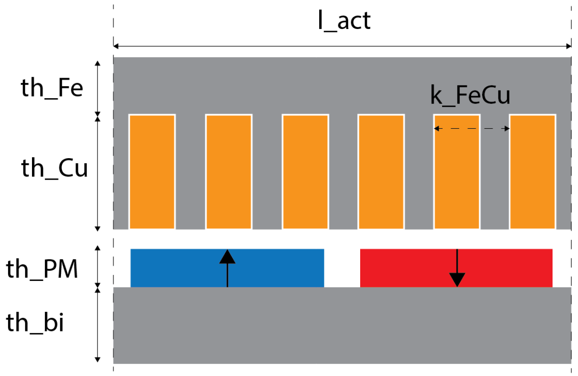

l_act	Actuator length
th_Fe	Stator back iron thickness
th_Cu	Copper layer thickness
k_FeCu	Ratio iron/copper per slot pitch (0 → slotless)
th_PM	Permanent Magnet thickness
th_bi	Mover back iron thickness

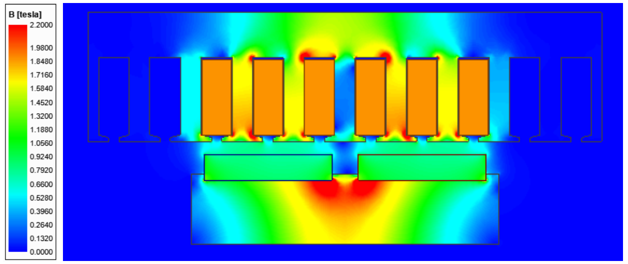

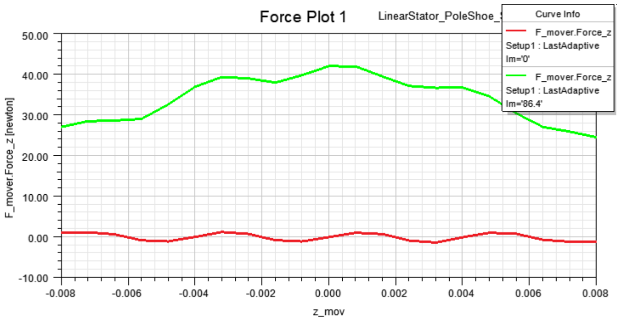

- Maximize copper cross-section, while guaranteeing that iron does not saturate
- Important: edge effects, reluctance shaping, pole shoes, iron extensions

ShuttlePump – LA Design and Radial Pull

- Stator: if slotted → minimum air gap, higher flux density, higher reluctance forces (radial pull!)
- Explore designs with increased air gap (min: 1 mm)

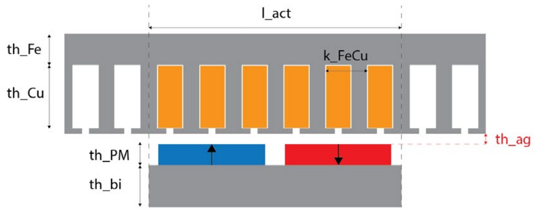

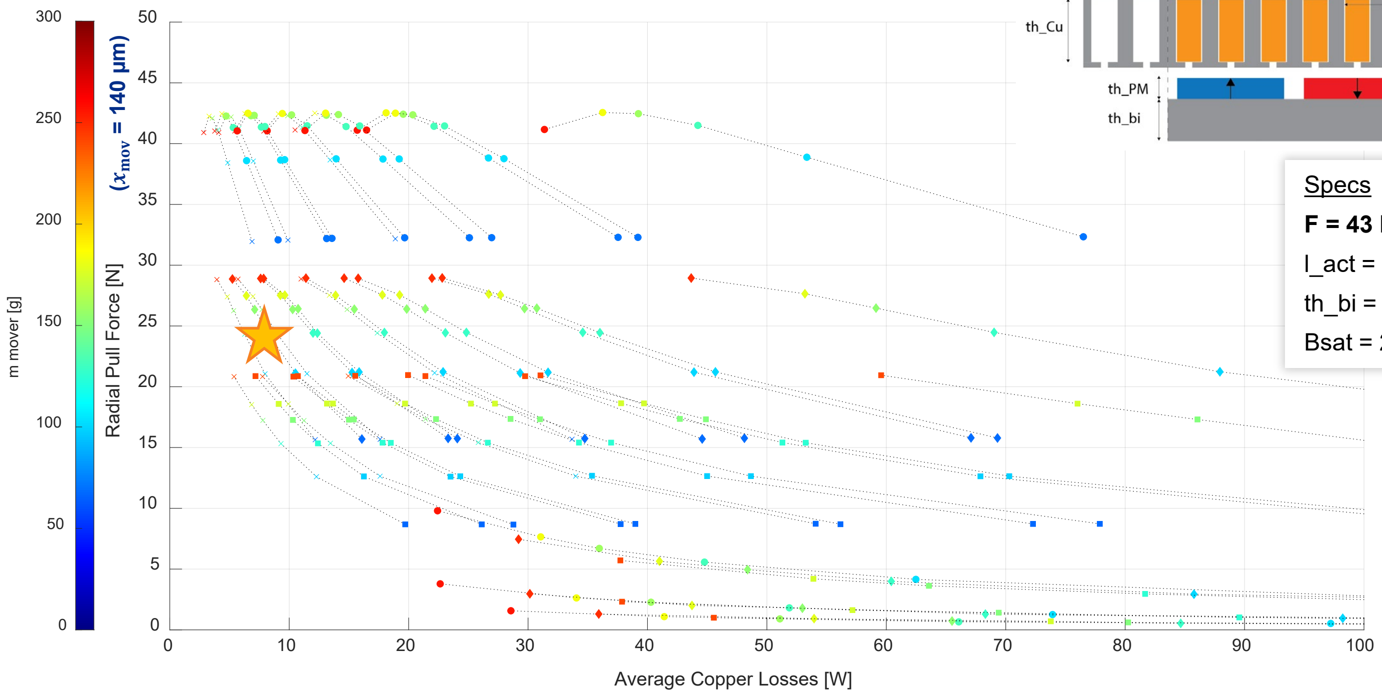

Specs
F = 43 N
l_act = 24 mm
th_bi = 2*th_PM
Bsat = 2.2 T

- Trade-off: radial pull force vs axial force, i.e. copper losses
- ☆Selected design: least copper losses (≈ 8 W) for maximum allowed radial pull (≈ 20 N)

ShuttlePump – LA Hardware Prototype

- Stator realization: stacked rings, VACOFLUX50 (high B_{sat} = 2.3 T) + ring coils
- Mover realization: discrete N50 neodymium PMs on VACOFLUX50 back-iron rings


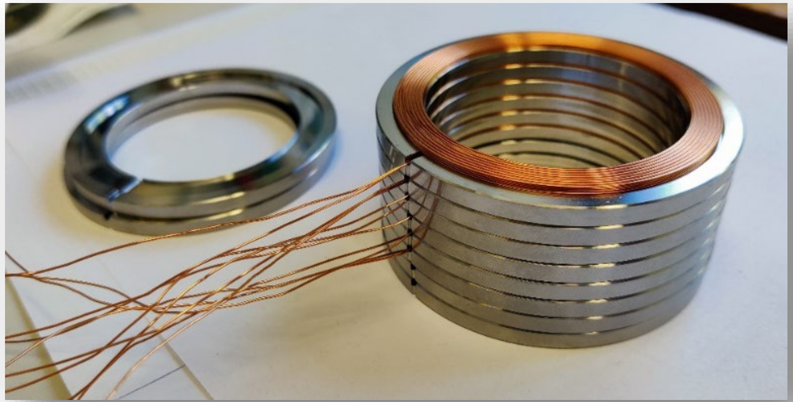

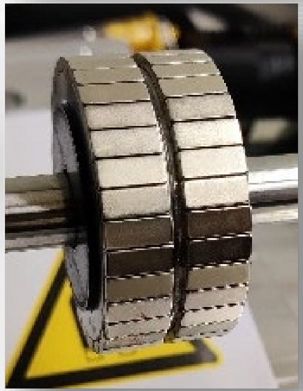


ShuttlePump – RA Design

- Spatial constraints: mover geometry → 4 poles, only magnets of the same polarity
  inlets/outlets location → split the stator into two independent ones

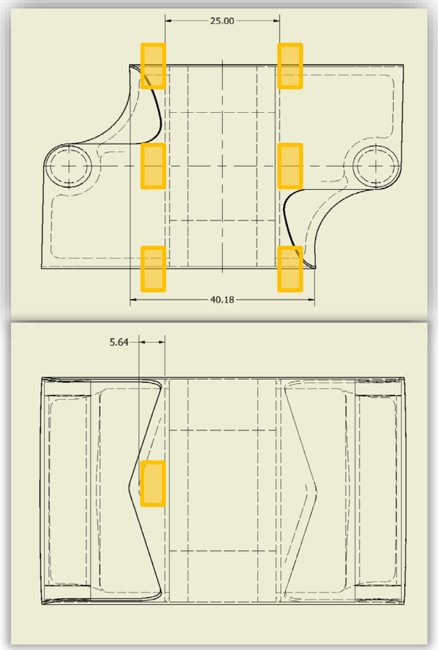

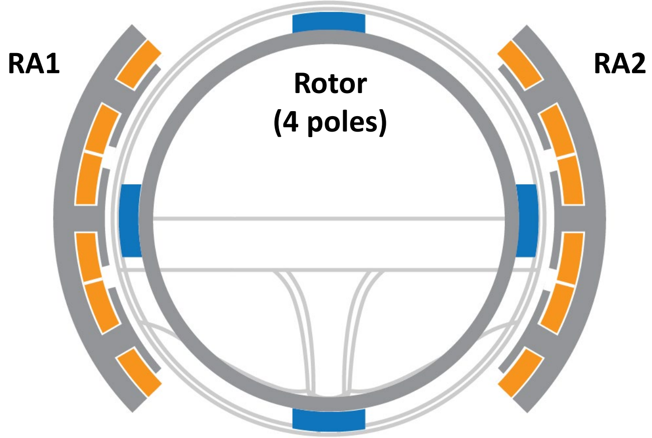

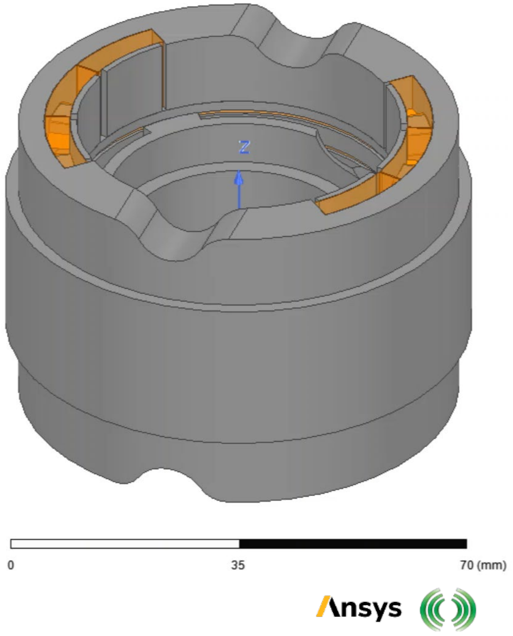

- Slotted design → air gap unchanged, axial reluctance profile kept, no edge effects for the LA
- Two steps optimization → 2D FEM for RA only, final 3D FEM together with LA (full LiRA)

ShuttlePump – Sensor Concept

- Contactless linear and rotary sensor needed. Enclosure: non-conductive
- Lateral surface occupied by LiRA stators. Far-away target: high sensitivity needed

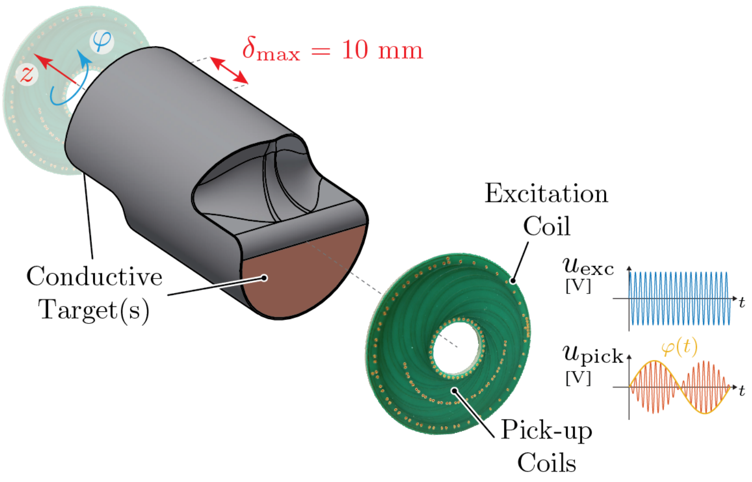

▸ **Renesas IPS2550**

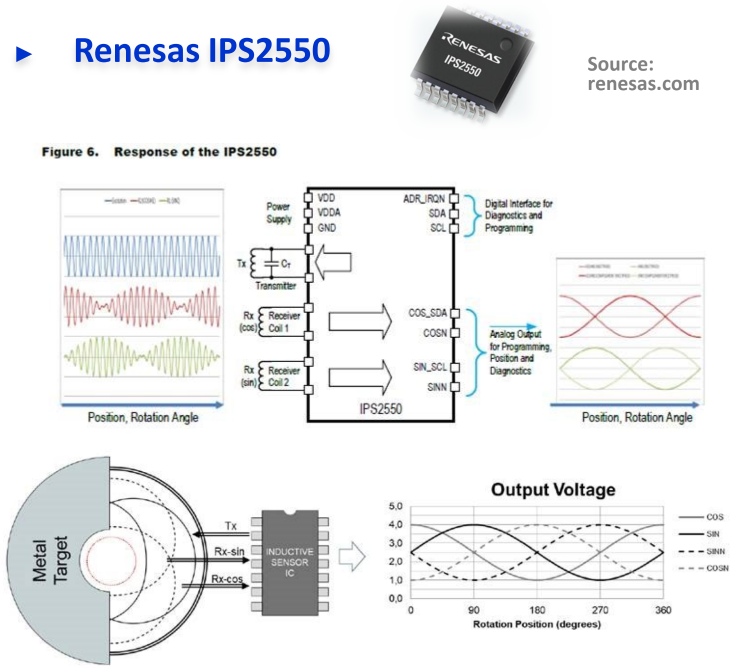

- Differential ECS system (from the cylinder bases) | Specially-shaped PCB-embedded pick-up coils
- Compact sensor interface: excitation + AM-demodulation in one chip, analog output

ShuttlePump – Sensor Concept

- Contactless linear and rotary sensor needed. Needed resolution ≈ 0.1 mm and ≈ 1 deg
- From rotary sensor can also extract linear position information (‘mag’ and ‘arg’)

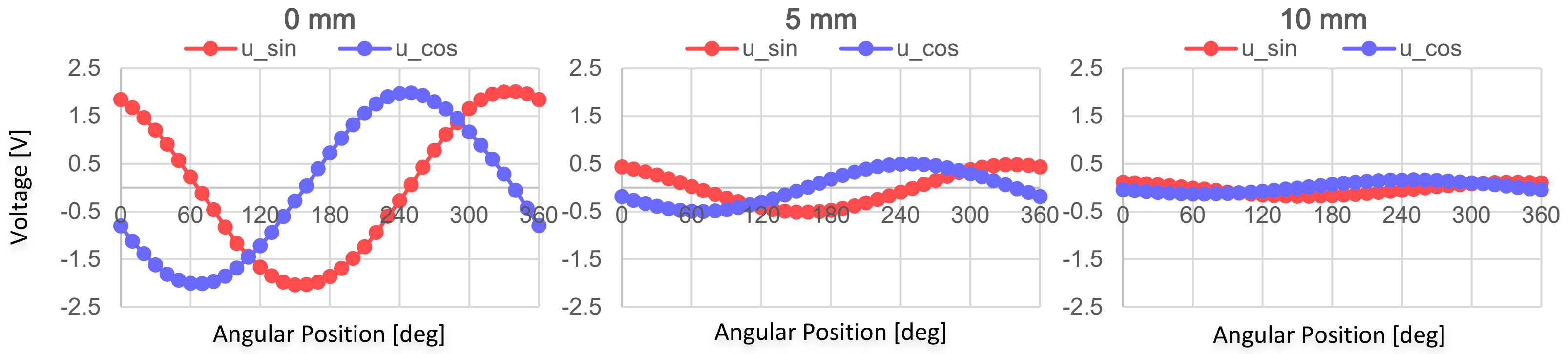

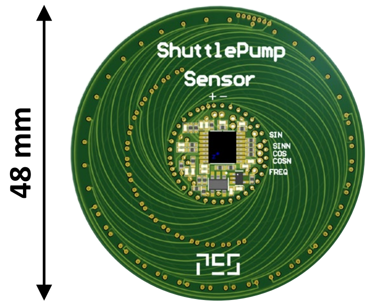

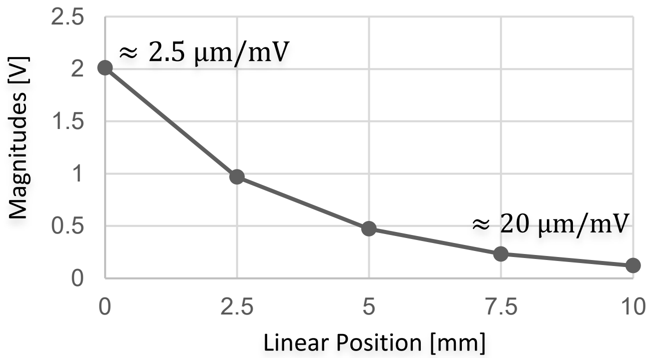

f_{exc} = 3 MHz

- Differential ECS system further enhances sensitivity and linearity

ShuttlePump – System Overview

- Inverter + Control PCB: hosts Zynq 7010 SoC / 2 inverter modules switching @1MHz with output filters
- First prototype: external drive → percutaneous cable connection

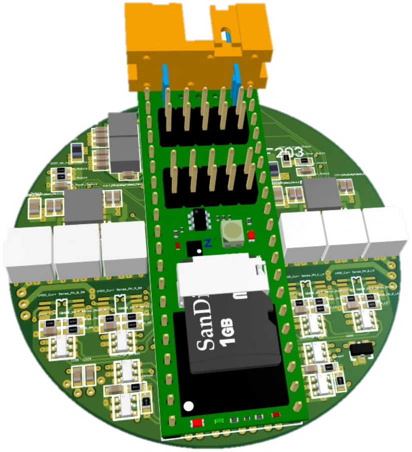

3 LA + 3 RA phases

Z_{cable}

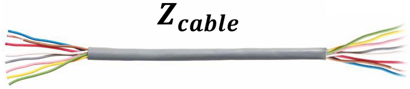

2 x 4 sensor signals
+ analog supply

= 16 wires

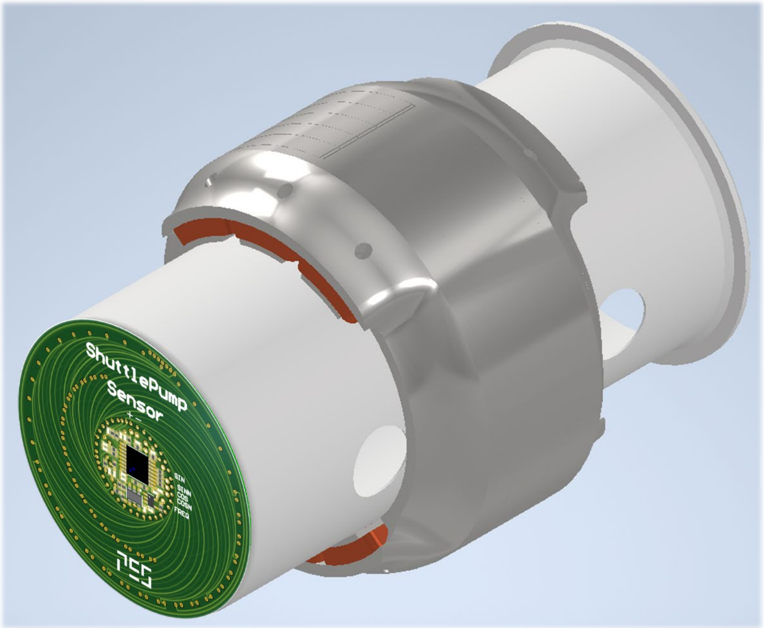

- ShuttlePump Firmware: current control / position + speed control / reference generation / fault detection / serial monitoring

ShuttlePump – Hardware Realization

- Inverter + Control PCB: hosts Zynq 7010 SoC / 2 inverter modules switching @1MHz with output filters
- First prototype: external drive → percutaneous cable connection

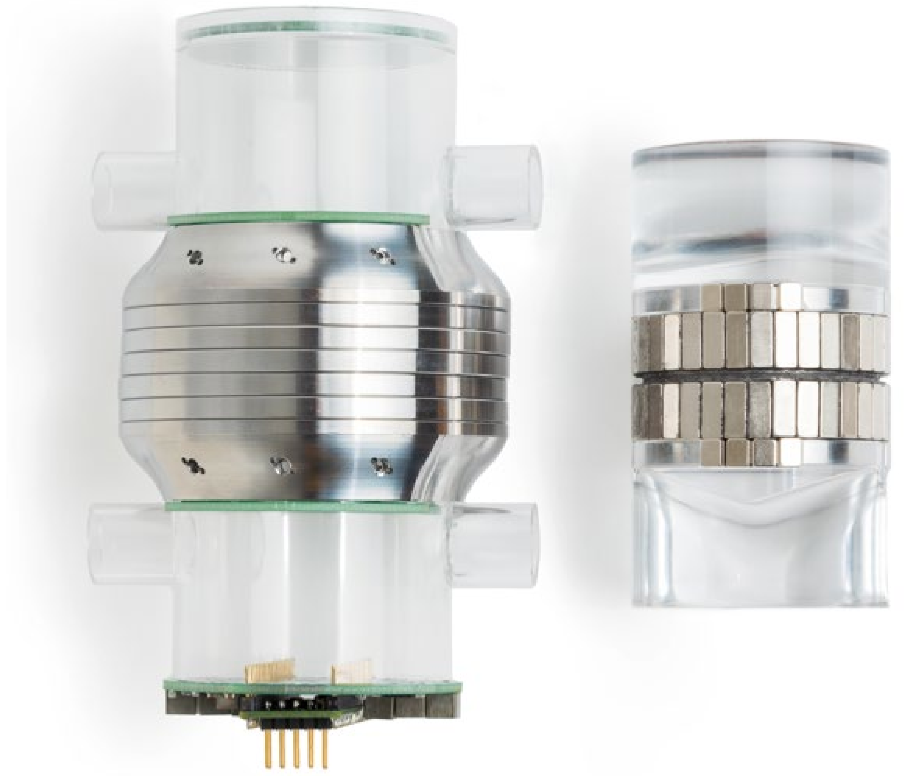

ShuttlePump – Experimental Verification

- Mechanical test bench: LiRA commissioning / machine constants and radial pull verification

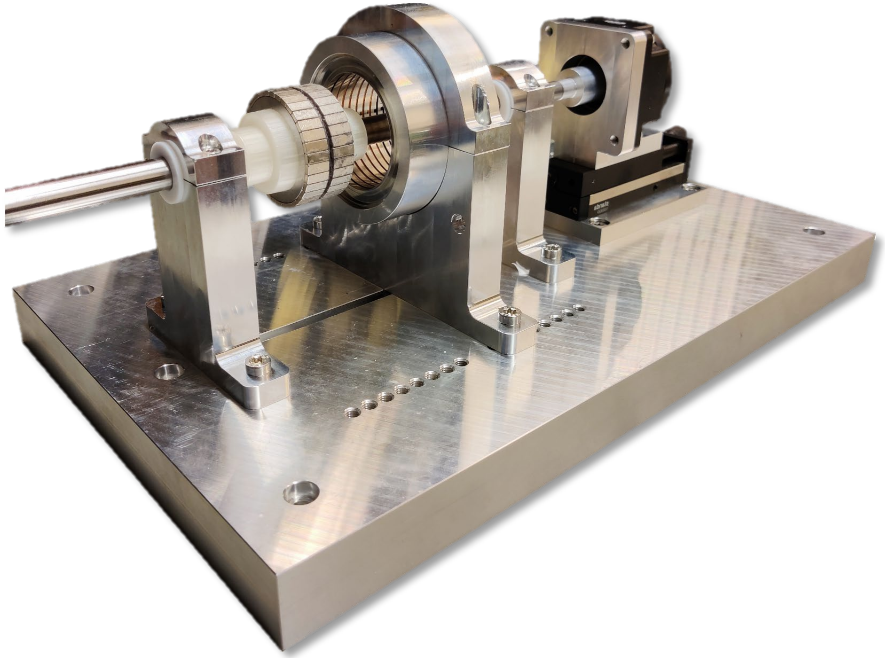

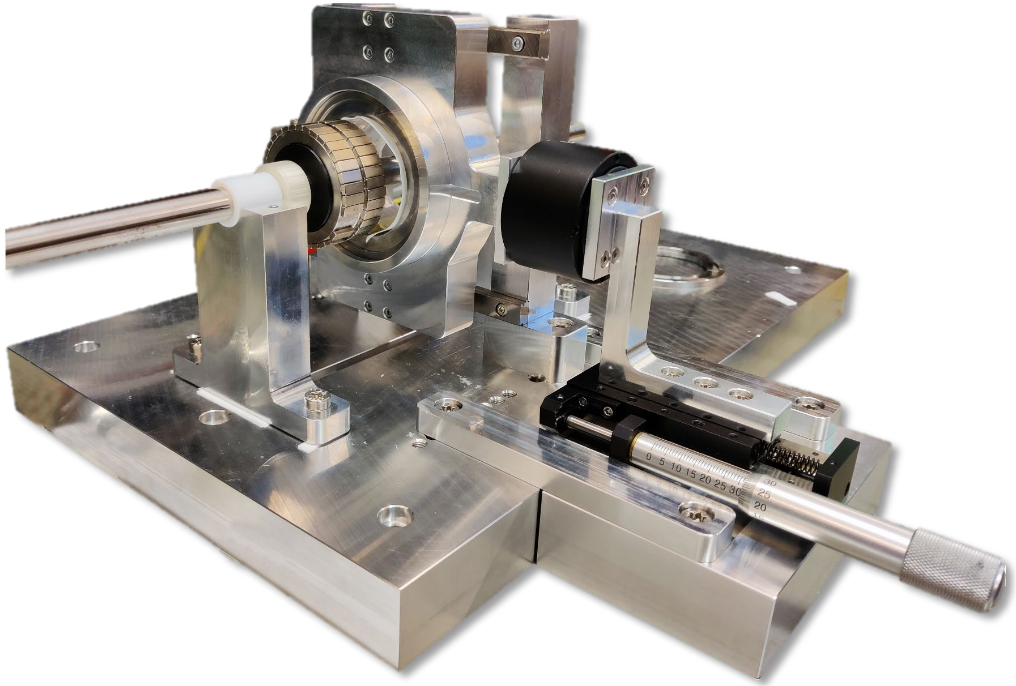

ShuttlePump – Experimental Verification

- Hydrodynamic test bench (Mock Circulatory Loop) @ Charite' Berlin
- Sealed tanks ≈ blood vessels' compliance | Pressure and flow-rate sensors

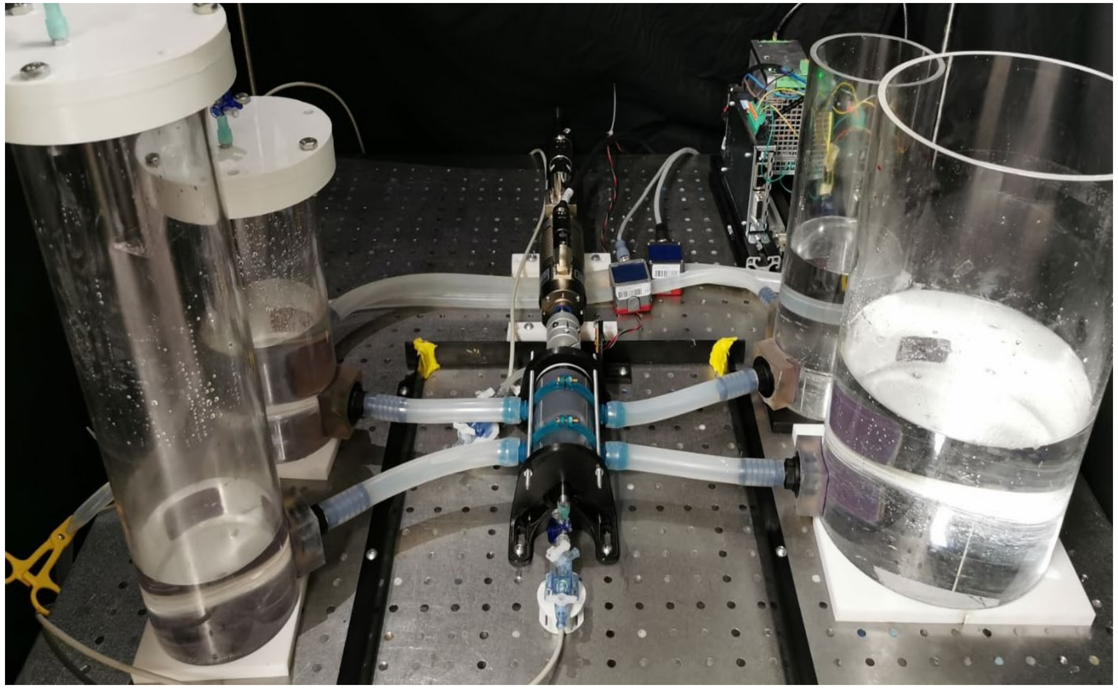

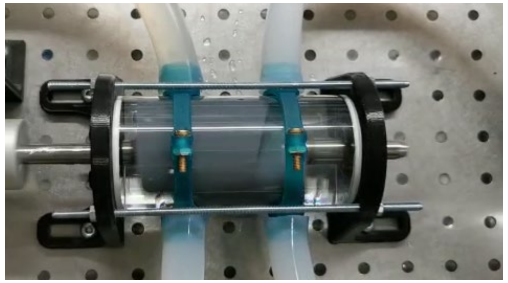

140 mmHg, up to 10 L/min

Source: CHARITÉ UNIVERSITÄTSMEDIZIN BERLIN

- Tested with external LiRA → next: with realized LiRA prototype

universität
innsbruck

Outlook

ETH zürich

International Electric Machines & Drives Conference
IEMDC 2023
San Francisco, CA May 15-18

Part 2 Outlook

- Overview on Blood Pumps: types, use, existing systems
- Overview on non-contact position sensors for SB-LiRAs: types, use in machines
- Example SB-LiRA with HB: ShuttlePump - LiRA design, sensor system, realization

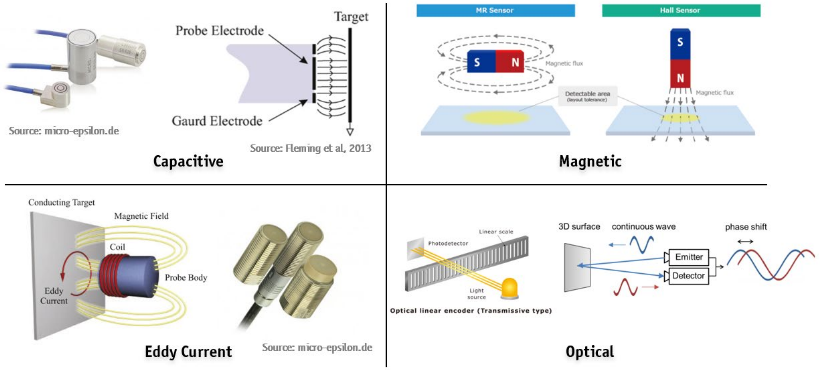

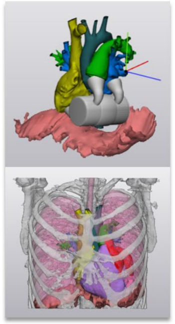

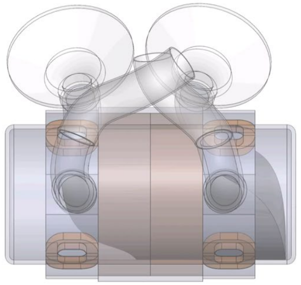

CHARITÉ — MEDIZINISCHE UNIVERSITÄT WIEN — ETH zürich

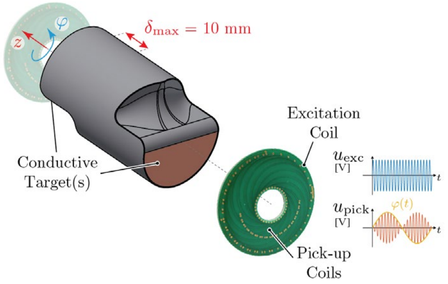

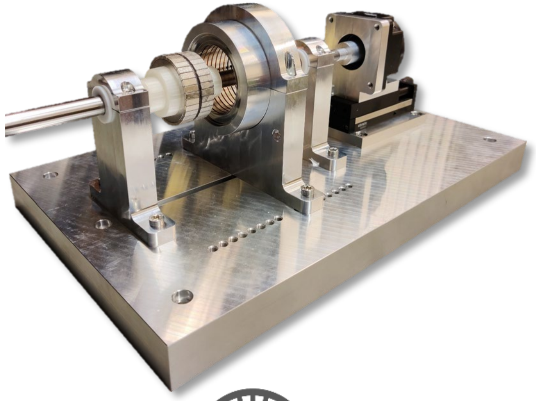

universität innsbruck

Outline

Part 1

- Introduction

- LiRA Examples / Applications
- Linear Actuator with Integrated MBs
- Position Sensors
- Dynamic Modeling, Controller Design
- Generalized Complex Space Vector
- Double Stator LiRA

- Outlook

Part 2

- Introduction

- Application: Blood Pumps
- Sensors for SB-LiRAs
- Design Example: the ShuttlePump

- Outlook

Part 3

- Introduction

- WPT to Linear Actuators
- Orthogonal and Parallel Field Concept
- Supplying Multiple Receivers
  Voltage & Current Impressed WPT

- Outlook

ETH zürich

Introduction

Motivation

- Supply power to a linear actuator which is enclosed in stainless steel (SS) housings.
- Highest hygiene in pharmaceutical, and semiconductor processing industries.

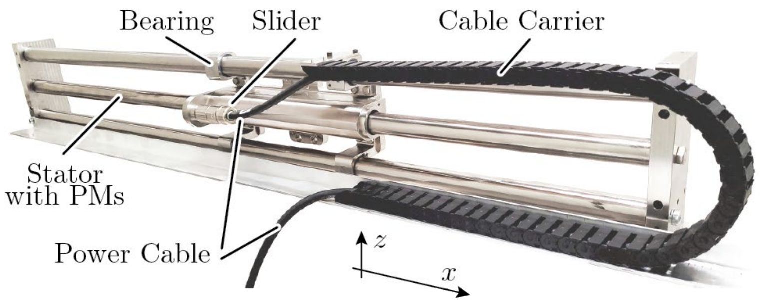

◄ SS-enclosed linear actuator with cable carriers.

- Supply cables and cable carriers → difficult to seal & thoroughly clean.
- WPT through SS allows the removal of cables and cable carriers.

Introduction

- $\boldsymbol{B}$ through the SS sheets → induced eddy current losses.
- Different types of WPT through SS → cause different eddy currents leading to different losses.

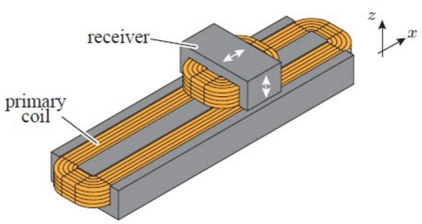

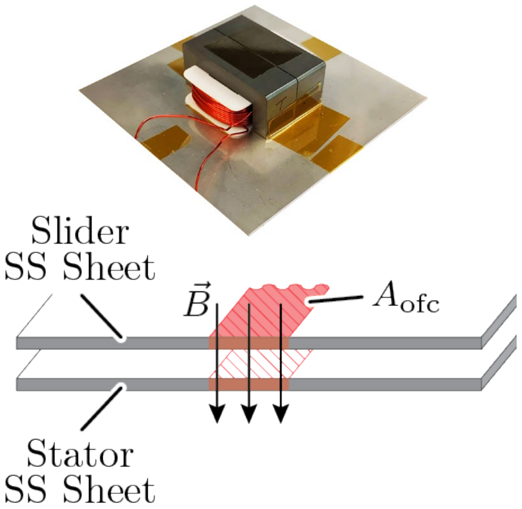

▲ Orthogonal-field Concept (OFC).

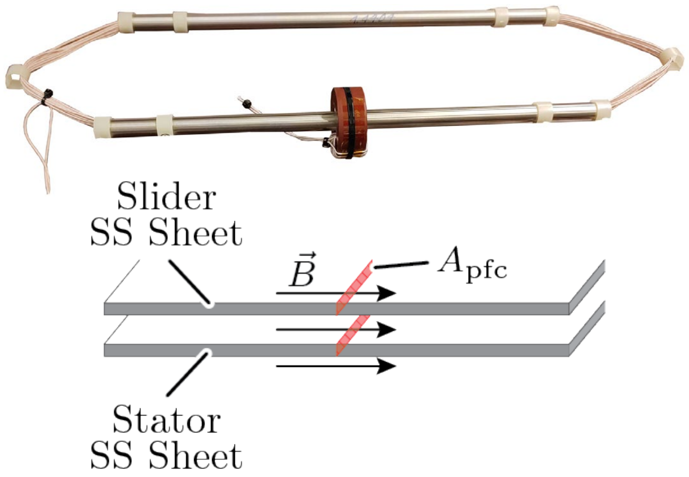

▲ Parallel-field Concept (PFC).

- In OFC, the magnetic material area A_{ofc} can be large → $p \propto A_{\mathrm{ofc}}$ → High losses (e.g. 72% efficiency).
- A_{ofc} is much smaller → eddy current induced is lower → high efficiency → PFC is studied.

Supply WPT

- Power supply for a single receiver → voltage impressed WPT
- Multiple receivers → voltage sharing or current impressed

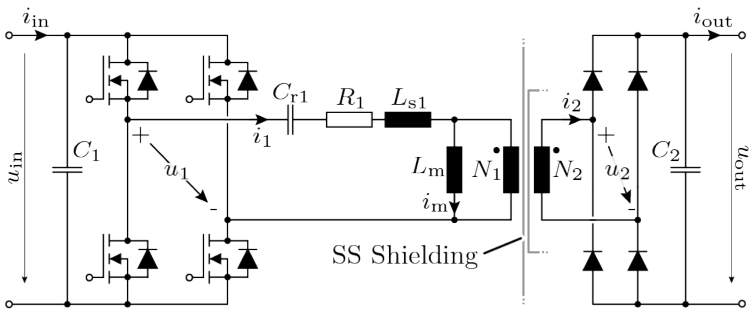

▲ Single Receiver

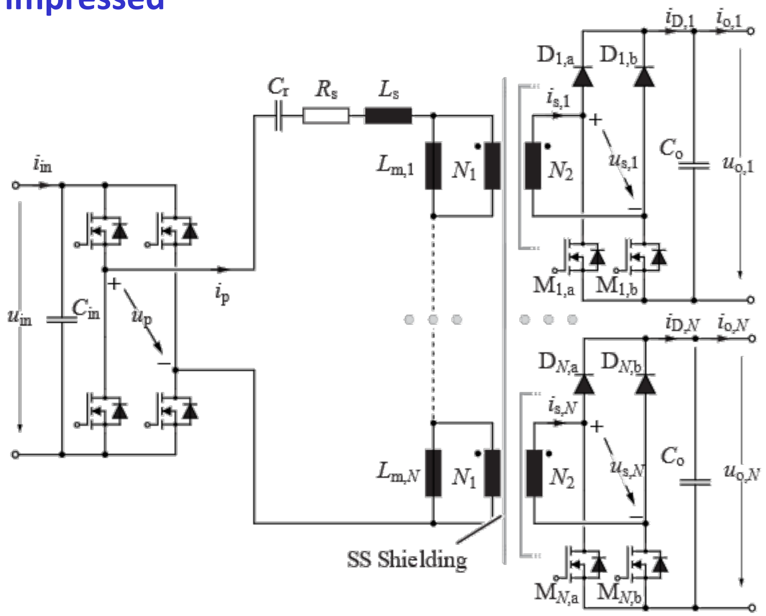

▲ Multiple Receivers

- In the case of PFC → high coupling due to closed toroidal core

universität innsbruck

Orthogonal Field Concept (OFC)

ETH zürich

International Electric Machines & Drives Conference
San Francisco, CA May 15-18

Field Orthogonal to the SS Enclosure

- Analyzed WPT through SS: E-core primary and secondary
- Transmitter & receiver: represented with W_1 and W_2

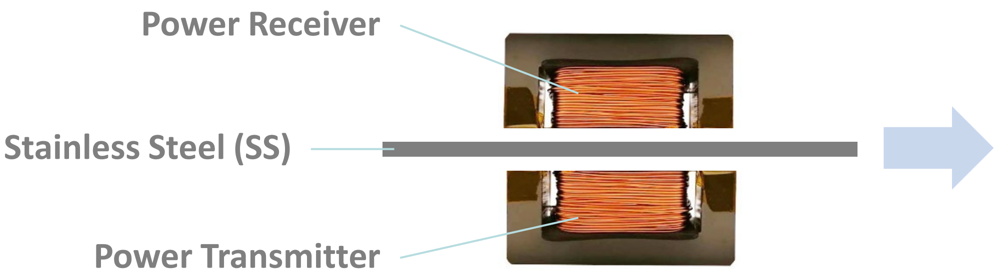

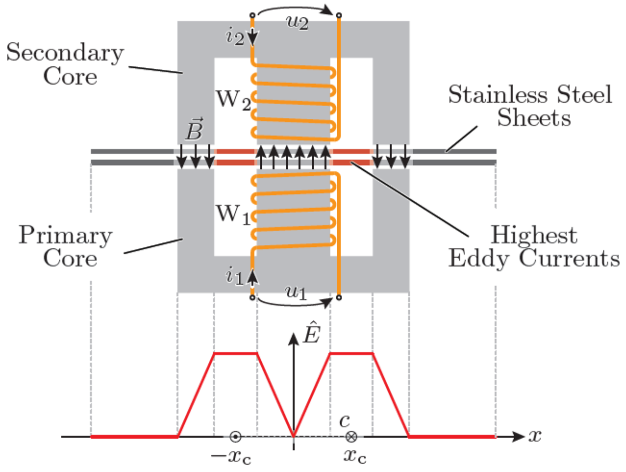

- Core flux density $\vec{B}$ penetrates through the SS sheets in the air gap
- Flux density integration → back emf $\hat{E}$ → induced eddy currents in SS

[ref] Miric, Spasoje, et al. ""Pushing Power Through Walls"-Wireless Power Transfer Through Stainless Steel." 2021 24th International Conference on Electrical Machines and Systems (ICEMS). IEEE, 2021.

SS Eddy Current Distribution

- Analysis of the eddy current distribution: 3D-FEM
- Simulation parameters: primary $100\ \mathrm{A-turns}$, secondary $0\ A - turns$, $1\ \mathrm{kHz}$ exc. freq.

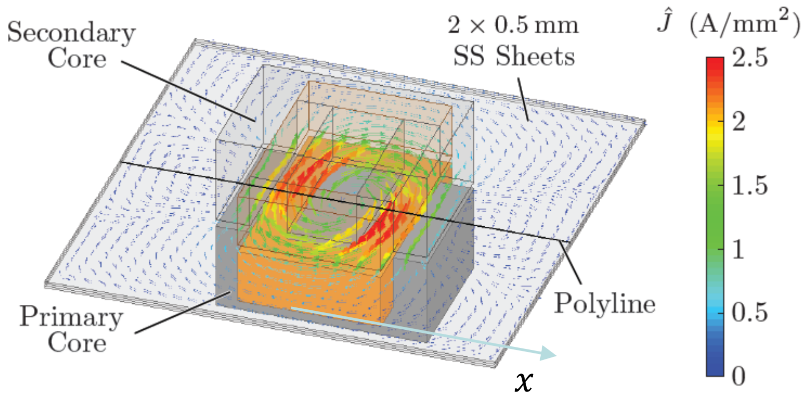

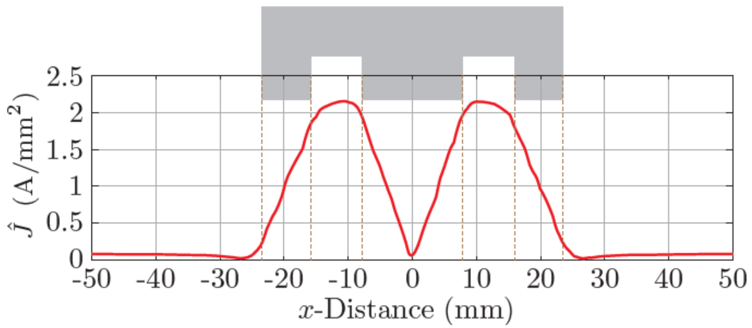

- Most of the current induced in the SS concentrated between the limbs

[ref] Miric, Spasoje, et al. "“Pushing Power Through Walls”-Wireless Power Transfer Through Stainless Steel." 2021 24th International Conference on Electrical Machines and Systems (ICEMS). IEEE, 2021.

WPT Through SS Modeling

- Most of the induced current between the limbs → replace SS with a short circuit winding W_3
- Windings W_1, W_2 and W_3 → three-winding transformer

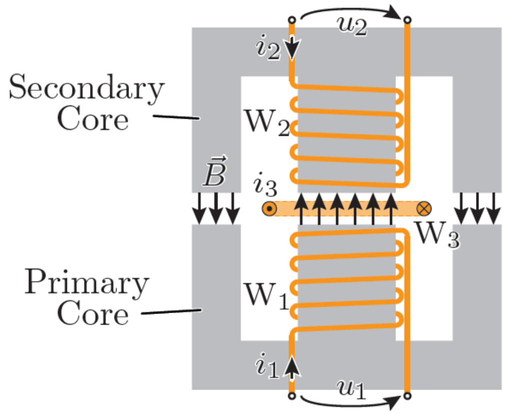

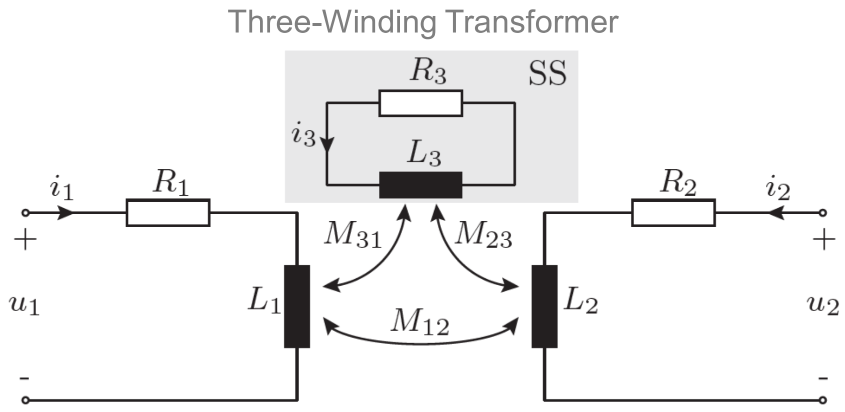

$$u_1 = R_1 i_1 + L_1 \frac{di_1}{dt} + M_{12} \frac{di_2}{dt} + M_{31} \frac{di_3}{dt}$$

$$u_2 = R_2 i_2 + L_2 \frac{di_2}{dt} + M_{12} \frac{di_1}{dt} + M_{23} \frac{di_3}{dt}$$

$$0 = R_3 i_3 + L_3 \frac{di_3}{dt} + M_{23} \frac{di_2}{dt} + M_{31} \frac{di_1}{dt}$$

- Impact of the SS in the air gap → a third short-circuited winding coupled with the primary & secondary
- Equivalent circuit of the WPT through SS system →

[ref] Miric, Spasoje, et al. "“Pushing Power Through Walls”-Wireless Power Transfer Through Stainless Steel." 2021 24th International Conference on Electrical Machines and Systems (ICEMS). IEEE, 2021.

WPT Through SS Equivalent Circuit (1)

- Mutual inductance per turn ($\boldsymbol{M_0}$) is equal for W_1, W_2 and W_3, otherwise mag. sym. is violated
- Equal M_0 assumption → scale mutual inductances with number of turns N_1, N_2 and N_3

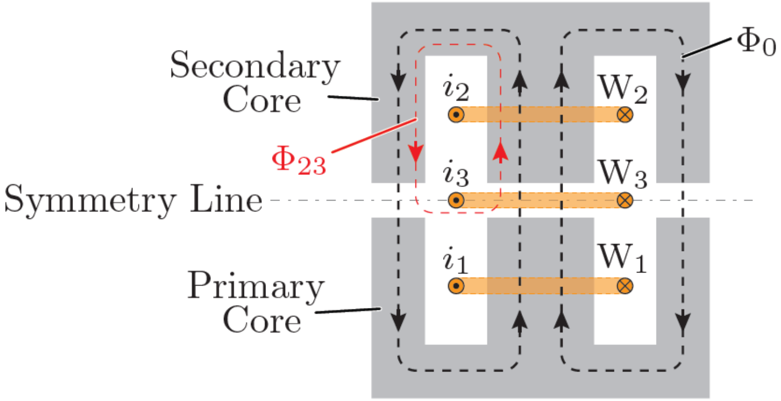

$$M_{12} = N_1 N_2 \cdot M_0$$
$$M_{23} = N_2 N_3 \cdot M_0$$
$$M_{31} = N_3 N_1 \cdot M_0$$

$$u_1 = R_1 i_1 + L_1 \frac{\mathrm{d}i_1}{\mathrm{d}t} + nM_{12} \frac{\mathrm{d}\frac{i_2}{n}}{\mathrm{d}t} + mM_{31} \frac{\mathrm{d}\frac{i_3}{m}}{\mathrm{d}t}$$

$$nu_2 = n^2 R_2 i_2 + n^2 L_2 \frac{\mathrm{d}\frac{i_2}{n}}{\mathrm{d}t} + nM_{12} \frac{\mathrm{d}i_1}{\mathrm{d}t} + nmM_{23} \frac{\mathrm{d}\frac{i_3}{m}}{\mathrm{d}t}$$

$$0 = m^2 R_3 \frac{i_3}{m} + m^2 L_3 \frac{\mathrm{d}\frac{i_3}{m}}{\mathrm{d}t} + nmM_{23} \frac{\mathrm{d}\frac{i_2}{n}}{\mathrm{d}t} + mM_{31} \frac{\mathrm{d}i_1}{\mathrm{d}t}$$

$$nM_{12} = mM_{31} = nmM_{23} = N_1^2 M_0 = M$$

Turns Ratios: $n = \frac{N_1}{N_2}$ $\quad m = \frac{N_1}{N_3}$

- Magnetization inductance M can be defined → equivalent circuit

[ref] Miric, Spasoje, et al. "“Pushing Power Through Walls”-Wireless Power Transfer Through Stainless Steel." 2021 24th International Conference on Electrical Machines and Systems (ICEMS). IEEE, 2021.

WPT Through SS Equivalent Circuit (2)

- Further rearranging of equations using magnetization inductance M
- The third equation has zero voltage → in the SS branch connected to '-' potential

$$u_1 = R_1 i_1 + (L_1 - M)\frac{\mathrm{d}i_1}{\mathrm{d}t} + M\frac{\mathrm{d}}{\mathrm{d}t}(i_1 + \frac{i_2}{n} + \frac{i_3}{m})$$

$$nu_2 = n^2 R_2 \frac{i_2}{n} + (n^2 L_2 - M)\frac{\mathrm{d}\frac{i_2}{n}}{\mathrm{d}t} + M\frac{\mathrm{d}}{\mathrm{d}t}(i_1 + \frac{i_2}{n} + \frac{i_3}{m})$$

$$0 = m^2 R_3 \frac{i_3}{m} + (m^2 L_3 - M)\frac{\mathrm{d}\frac{i_3}{m}}{\mathrm{d}t} + M\frac{\mathrm{d}}{\mathrm{d}t}(i_1 + \frac{i_2}{n} + \frac{i_3}{m})$$

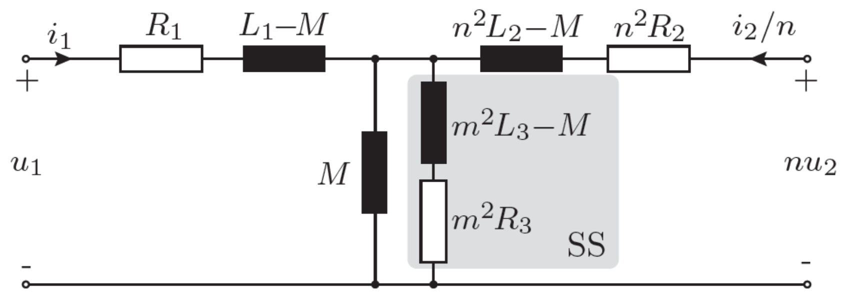

- Values of the parameters → from 3D-FEM eddy-current simulation

[ref] Miric, Spasoje, et al. ""Pushing Power Through Walls"-Wireless Power Transfer Through Stainless Steel." 2021 24th International Conference on Electrical Machines and Systems (ICEMS). IEEE, 2021.

WPT Through SS Equivalent Circuit Parameters

- WPT system geometry → determined such that 50 W can be transferred
- Primary/secondary core → two stacked E 47/20/16 N87 ferrite cores

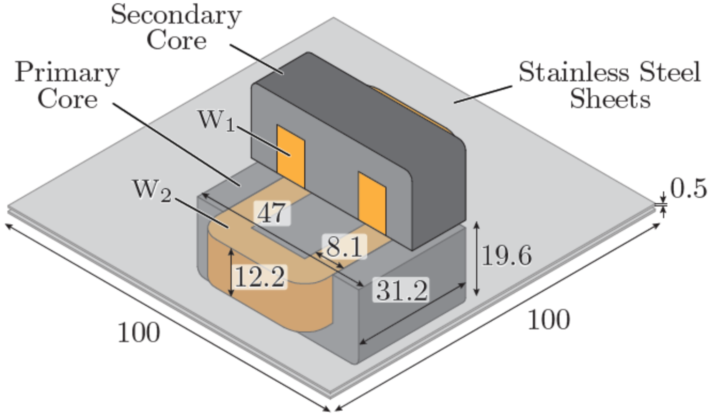

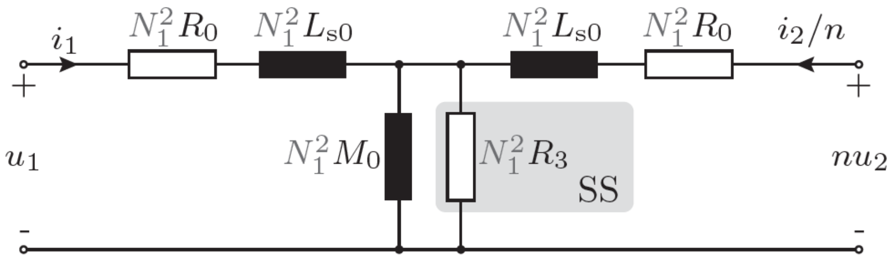

Per Turn Parameters
Valid for Exc. Freq. < 10 kHz

$R_0 = 55.6\ \mu\Omega$ $\quad R_3 = 4.97\ \mathrm{m}\Omega$

$L_{s0} = 77.16\ \mathrm{nH}$ $\quad M_0 = 172.84\ \mathrm{nH}$

$m^2 L_{s0} - M \approx 0$

$N_3 = 1$

- Parameters obtained from 3D-FEM simulation using $\underline{Z}_{11}$, $\underline{Z}_{12} = \underline{Z}_{21}$ and $\underline{Z}_{22}$ complex impedances

[ref] Miric, Spasoje, et al. "“Pushing Power Through Walls”-Wireless Power Transfer Through Stainless Steel." 2021 24th International Conference on Electrical Machines and Systems (ICEMS). IEEE, 2021.

Model Verification with 3D-FEM: Coupling k Calculation

- Coupling coefficient k calculated from the equivalent circuit
- Series equivalent of the magnetization branch: $L_{12} = (M_0 R_3^2)/(R_3^2 + (2\pi f \cdot M_0)^2)$

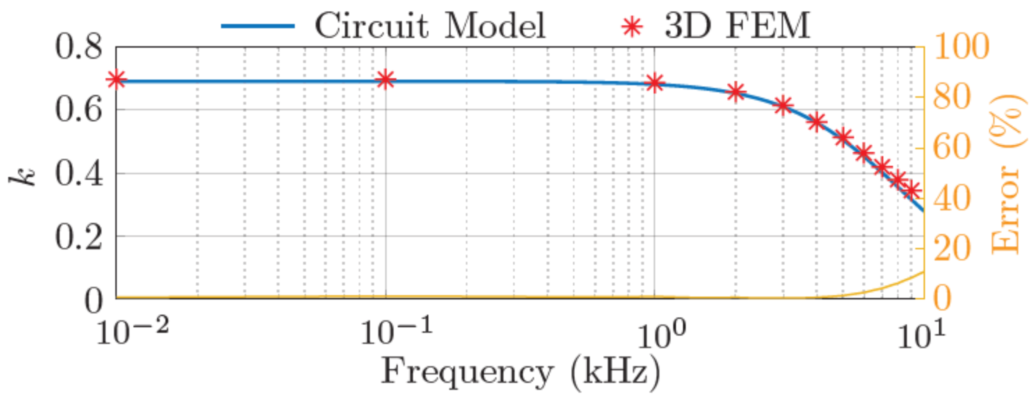

$$k = \frac{L_{12}(f)}{L_{12}(f) + L_{s1}}$$

$$k = \frac{M_0}{\omega^2 \cdot L_{s1}\left(\frac{M_0}{R_3}\right)^2 + L_{s1} + M_0}$$

if $R_3 \rightarrow \infty$ then: $k = \frac{M_0}{L_{s1} + M_0}$

- Coupling k dependence on frequency → second order low pass filter

[ref] Miric, Spasoje, et al. "“Pushing Power Through Walls”-Wireless Power Transfer Through Stainless Steel." 2021 24th International Conference on Electrical Machines and Systems (ICEMS). IEEE, 2021.

Analytic Calculation of Circuit Parameters

- Based on the current distribution in the SS → R_{ss} is calculated

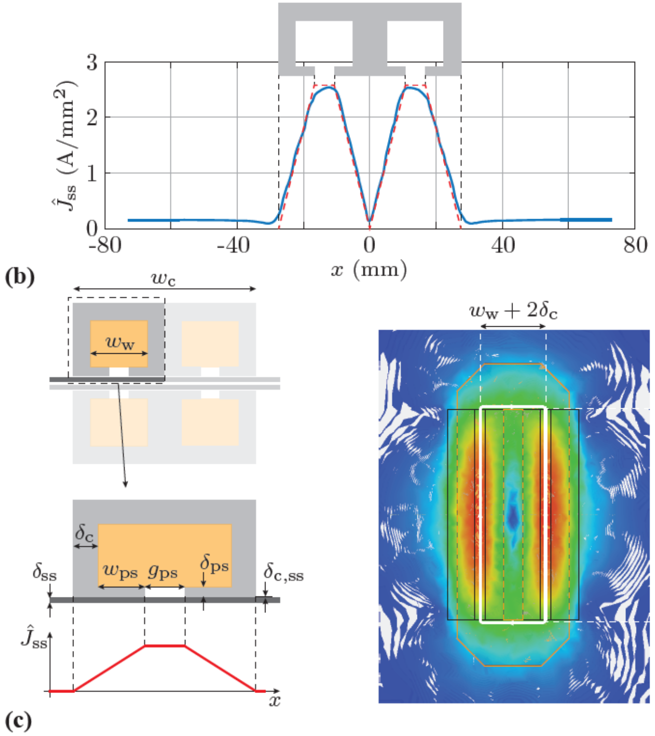

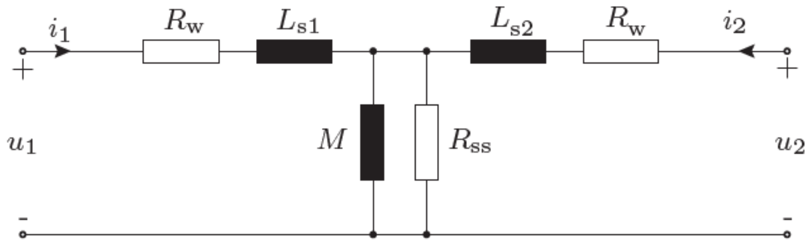

- Inductances calculated based on the magnetic circuit model

WPT Through SS Resonant Compensation

- Series resonant compensation → self-inductance $L_{11} = L_{s1} + L_{12}$ or stray inductance L_{s1}
- Rather low SS resistance value → self-inductances L_{11}/L_{22} are frequency dependent

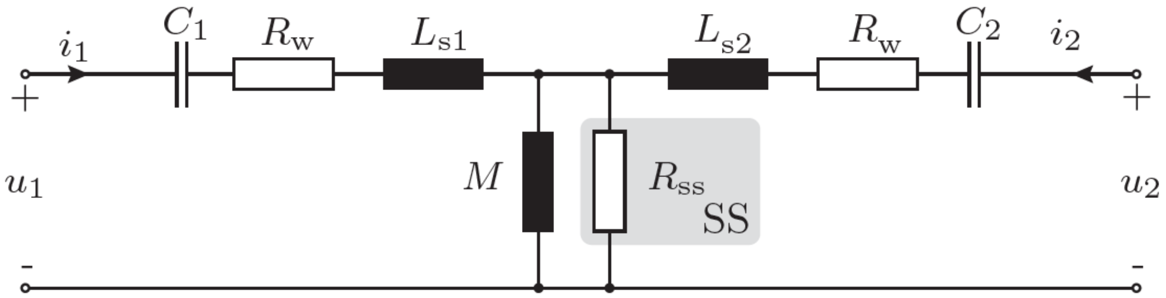

$$L_{12} = \Im(j\omega M||R_{ss})\frac{1}{\omega}$$

$$C_1 = \frac{1}{\omega^2 L_{s1}}$$

$$C_2 = \frac{1}{\omega^2 L_{s2}}$$

- Stray inductances L_{s1}/L_{s2} are not frequency dependent
- Compensation of stray inductances leads to higher efficiency

[ref] Miric, Spasoje, et al. "“Pushing Power Through Walls”-Wireless Power Transfer Through Stainless Steel." 2021 24th International Conference on Electrical Machines and Systems (ICEMS). IEEE, 2021.

Fundamental Frequency Modeling, Equivalent Load Resistance

- ‘Notch’-pass characteristic of the input impedance

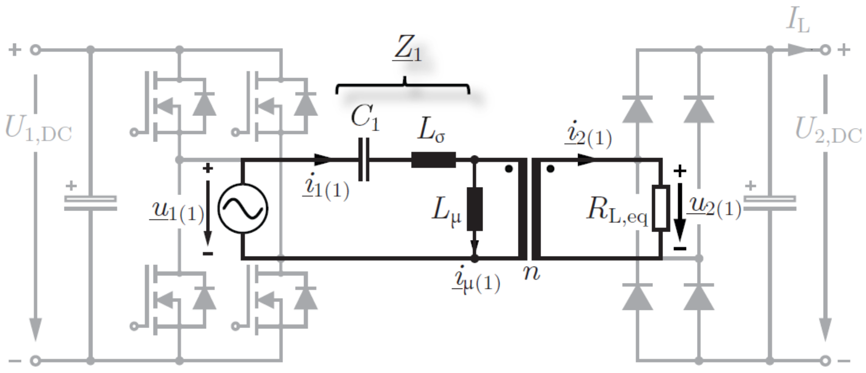

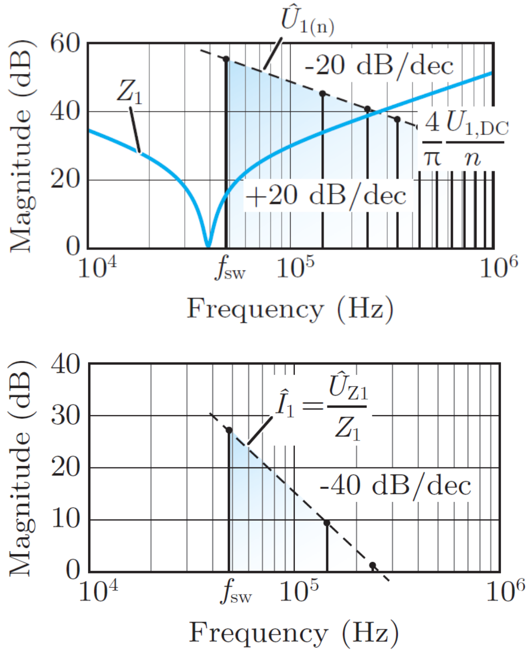

$$R_{L,eq} = \frac{8}{\pi^2}\frac{U_{2,DC}^2}{P_2}$$

- Pulsed input voltage → only fundamental component of the load current!
- Equivalent load resistance → models delivered output power P_2

[Source]: Roman Bosshard, ‘Multi-Objective Optimization of Inductive Power Transfer Systems for EV Charging’, PhD Thesis, ETH Zurich, 2015.

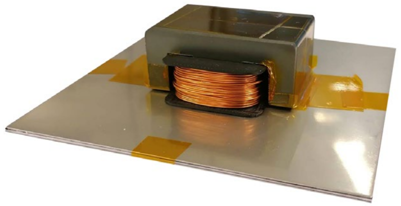

Prototype Design

Optimum Number of Turns

- In this work primary & secondary number of turns assumed equal, $N_1 = N_2$
- R_0, M_0, R_3 → parameters per turn ($N_1 = N_2 = 1$) determined by the core geometry

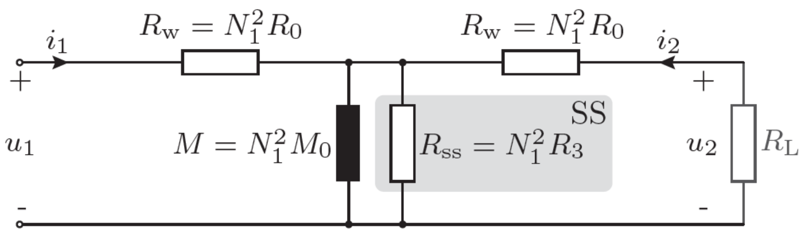

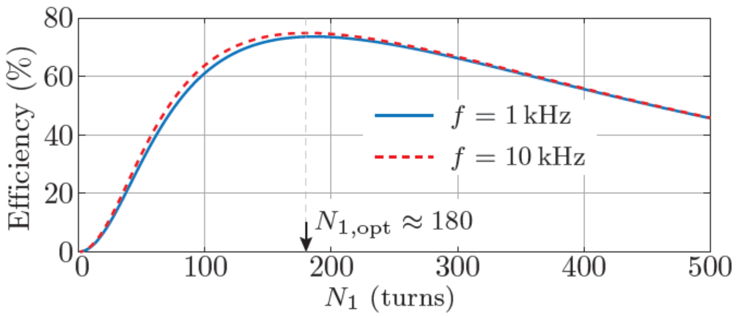

Input Voltage	Output Voltage	Output Power
$\hat{U}_1 = 50\,\text{V}$	$\hat{U}_2 = 50\,\text{V}$	$P_2 = 50\,\text{W}$

$$R_{L,nom} = \frac{\hat{U}_2^2}{2P_2} = 25\ \Omega$$

$$N_{1,opt} = \sqrt{\frac{R_{L,nom}}{\sqrt{R_0(R_0 + 2R_3)}}} \approx 180$$

- Optimum number of turns → $R_{L,nom} > R_w$ and $R_{L,nom} < R_{ss}$

[ref] Miric, Spasoje, et al. "“Pushing Power Through Walls”-Wireless Power Transfer Through Stainless Steel." 2021 24th International Conference on Electrical Machines and Systems (ICEMS). IEEE, 2021.

Hardware Prototype

- Primary & secondary cores → two stacked E 47/20/16 N87 ferrite cores
- Primary & secondary windings → $N_1 = N_2 = 180, 0.5$ mm wire diameter

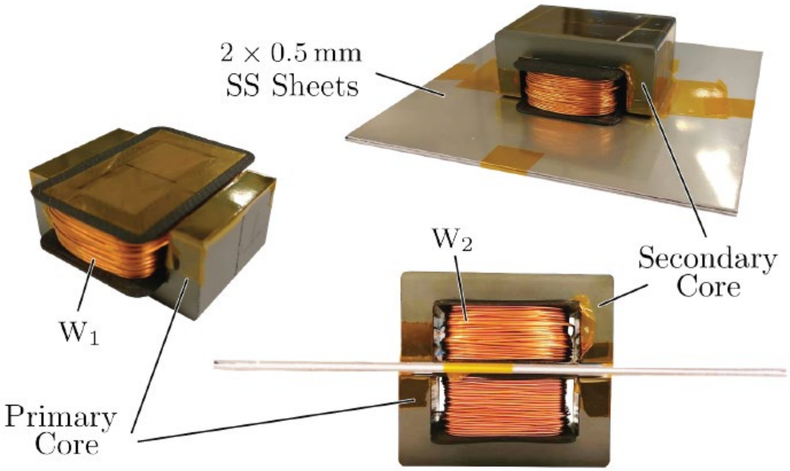

Parameter	3D FEM	Prototype	Rel. Error
$R_{w,dc}$	1.8 Ω	1.9 Ω	5.3 %
L_s	2.5 mH	2.62 mH	4.6 %
M	5.6 mH	5.4 mH	3.7 %
R_{ss}	160 Ω	155 Ω	3.2 %

- Model & prototype parameter values considered up to 10 kHz excitation frequency

[ref] Miric, Spasoje, et al. "“Pushing Power Through Walls”-Wireless Power Transfer Through Stainless Steel." 2021 24th International Conference on Electrical Machines and Systems (ICEMS). IEEE, 2021.

AC Winding Resistance

- Impedance measurements on the prototype → proximity effects in the windings
- Frequency dependent winding resistance $R_{\mathrm{w}}(f)$ → included in the model using $G_{\mathrm{R}}(f)$

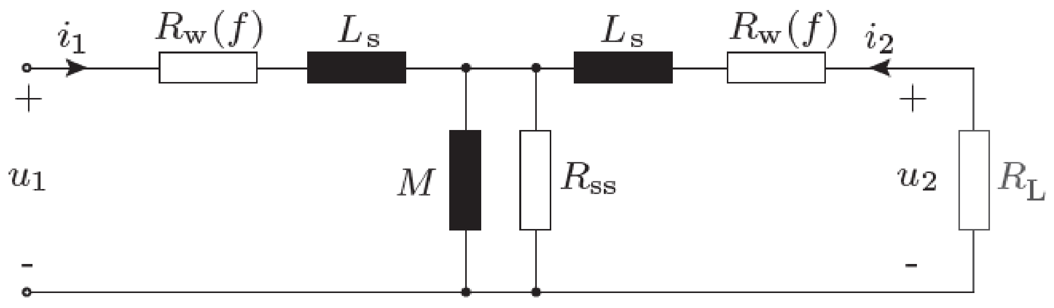

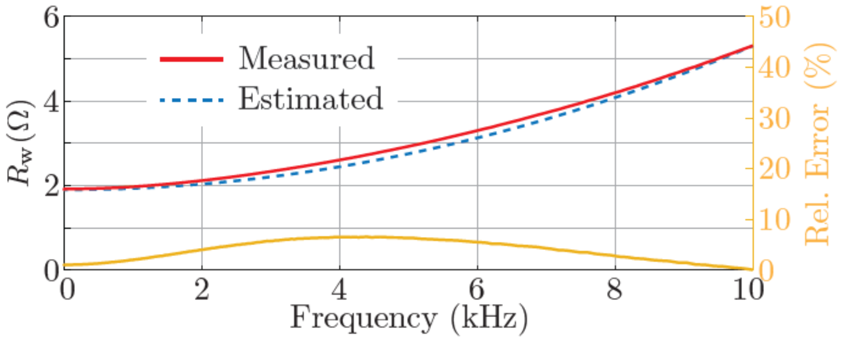

$$R_{\mathrm{w}}(f) = R_{\mathrm{w,dc}}(1 + 2G_{\mathrm{R}}(f) \cdot H^2)$$

$$H^2 = \frac{\frac{R_{\mathrm{w}}(10\ \mathrm{kHz})}{R_{\mathrm{w,dc}}} - 1}{2G_{\mathrm{R}}(10\ \mathrm{kHz})}$$

- Further details/references on $G_{\mathrm{R}}(f)$ can be found the in the paper manuscript

[ref] Miric, Spasoje, et al. "“Pushing Power Through Walls”-Wireless Power Transfer Through Stainless Steel." 2021 24th International Conference on Electrical Machines and Systems (ICEMS). IEEE, 2021.

Optimal Excitation Frequency f_{opt}

- Frequency dependent winding resistance $R_w(f)$ → there is f_{opt} s.t. efficiency is max.
- Frequency dependent winding resistance $R_w(f)$ → there is $R_L = R_{L,opt}(f)$ s.t. eff. is max.

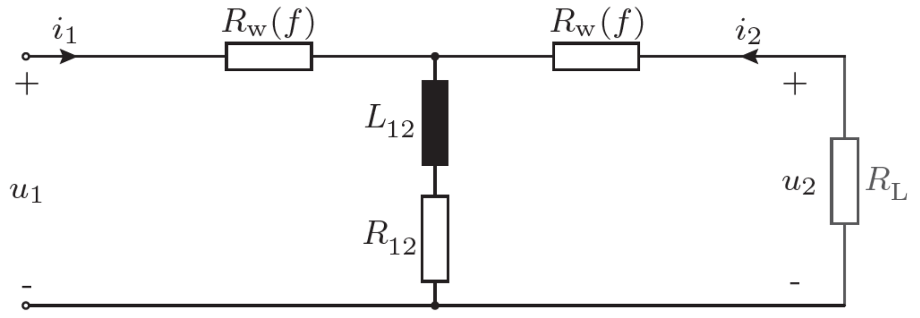

$$R_{L,opt} = \frac{\sqrt{R_w}\sqrt{R_w^2 + 3R_wR_{12} + 2R_{12}^2 + 2(\omega L_{12})^2}}{\sqrt{R_w + R_{12}}}$$

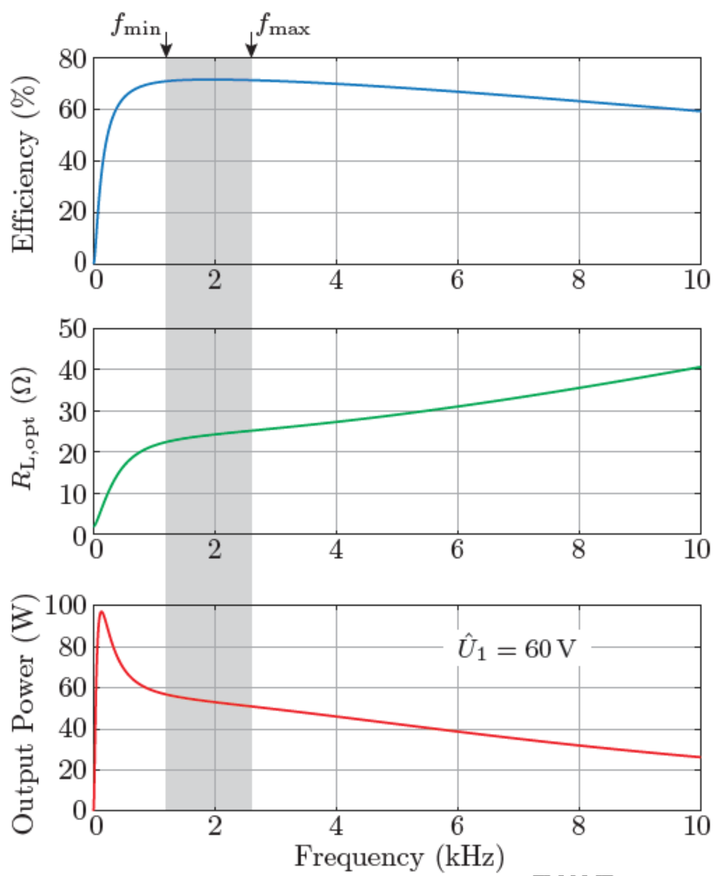

$f_{min} = 1.6$ kHz

$f_{max} = 2.3$ kHz

- 'Flat' eff. curve → range of freq.
- Res. comp. caps. → $C_1 = C_2 = 1.9$ μF
- Operation frequency → 2.25 kHz (71.2 % efficiency)

[ref] Miric, Spasoje, et al. ""Pushing Power Through Walls"-Wireless Power Transfer Through Stainless Steel." 2021 24th International Conference on Electrical Machines and Systems (ICEMS). IEEE, 2021.

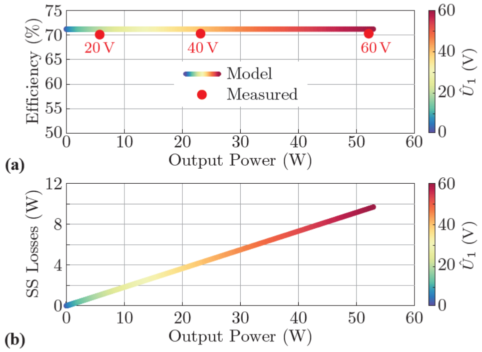

Power & Efficiency Measurements

Regulation of Power via Input Voltage

■ **Verification of the circuit model with the power & efficiency measurements**

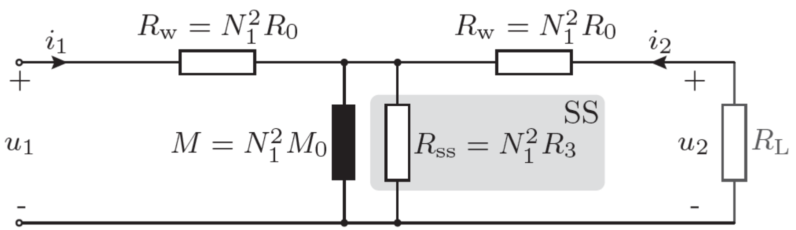

$R_L = 24\ \Omega$

$$\frac{P_{ss}}{P_2} = \frac{R_{12}(R_L + R_w)^2}{R_L(R_{12}^2 + X_{12}^2)}$$

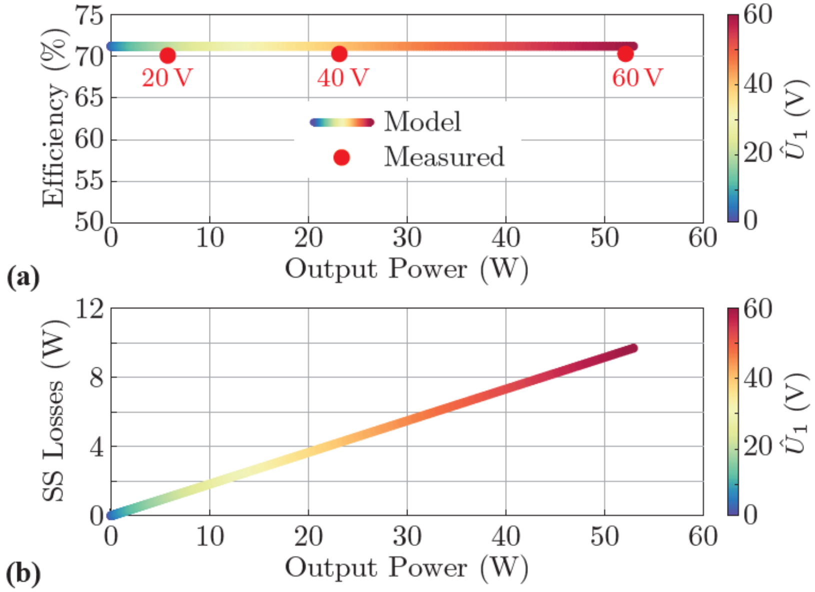

- **Efficiency does not depend on the input voltage**
- **SS losses P_{ss} increase linearly with the output power P_2 (R_L is constant!)**

[ref] Miric, Spasoje, et al. "“Pushing Power Through Walls”-Wireless Power Transfer Through Stainless Steel." 2021 24th International Conference on Electrical Machines and Systems (ICEMS). IEEE, 2021.

Regulation of Power via Load Resistance R_L

- Verification of the circuit model with the power & efficiency measurements

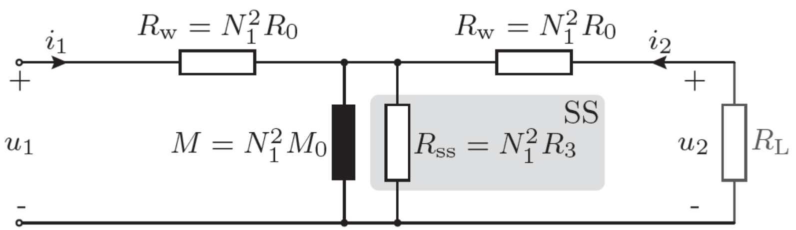

$$\hat{U}_1 = [20, 40, 60]\ \mathrm{V}$$

$$\frac{P_{ss}}{P_2} = \frac{R_{12}(R_L + R_w)^2}{R_L(R_{12}^2 + X_{12}^2)}$$

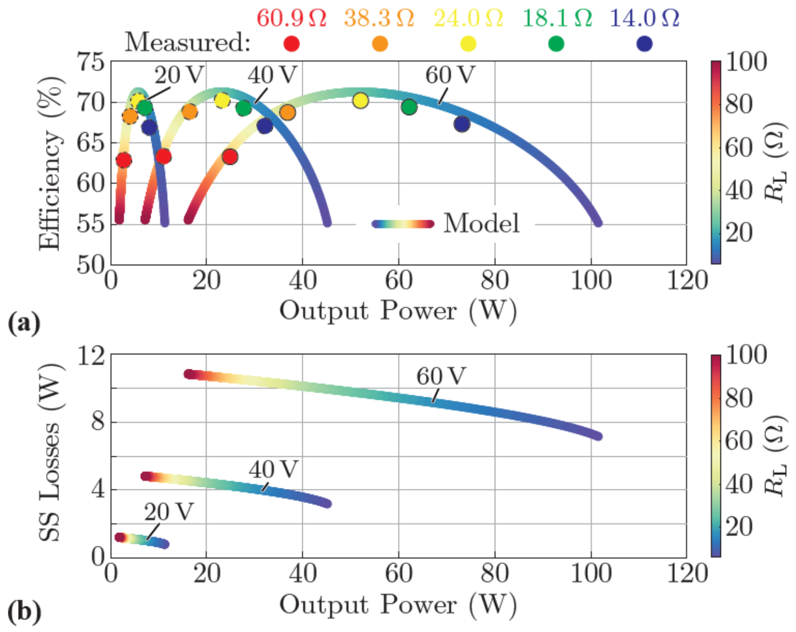

- Efficiency heavily depends on the load resistance R_L
- Larger output power P_2, while keeping the SS losses P_{ss} limited

[ref] Miric, Spasoje, et al. "“Pushing Power Through Walls”-Wireless Power Transfer Through Stainless Steel." 2021 24th International Conference on Electrical Machines and Systems (ICEMS). IEEE, 2021.

Coaxial WPT (PFC)

OFC and PFC

- $\boldsymbol{B}$ through the SS sheets → induced eddy current losses.
- Different types of WPT through SS → cause different eddy currents leading to different losses.

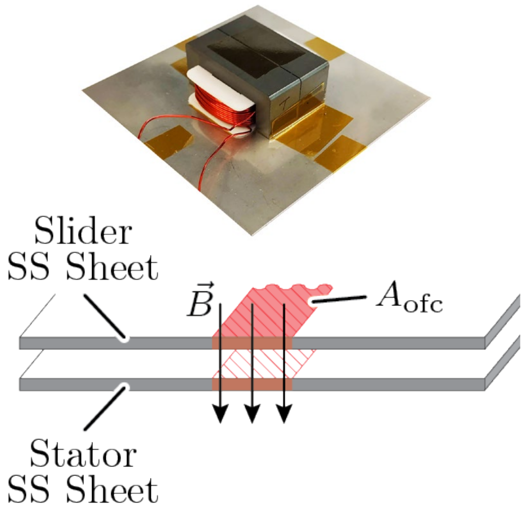

▲ Orthogonal-field Concept (OFC).

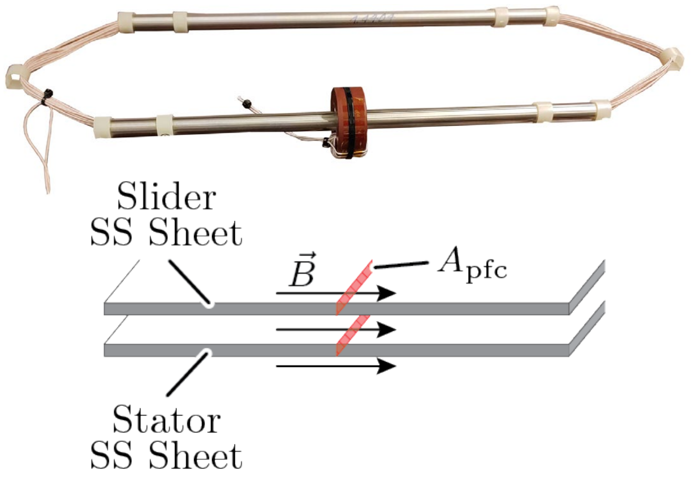

▲ Parallel-field Concept (PFC).

- In OFC, the magnetic material area A_{ofc} can be large → $p \propto A_{\mathrm{ofc}}$ → High losses (e.g. 72% efficiency).
- A_{ofc} is much smaller → eddy current induced is lower → high efficiency → PFC is studied.

Parallel-field Concept WPT

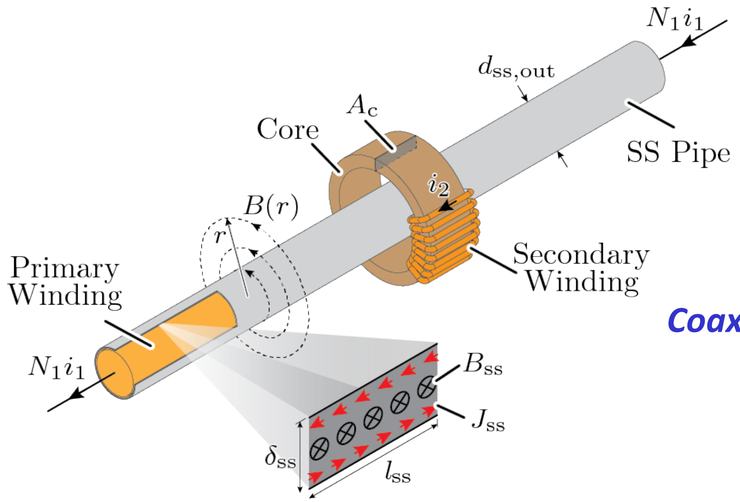

Coaxial arrangement

Parallel-field Concept WPT — SS Loss Model

- Calculation of eddy-current losses → $P_{ss} \propto V_{ss}, F(\chi), \sigma_{ss}, \delta_{ss}, \omega_{ss}, F(\chi), \hat{B}_{ss}$
- SS losses depend only on the primary current.

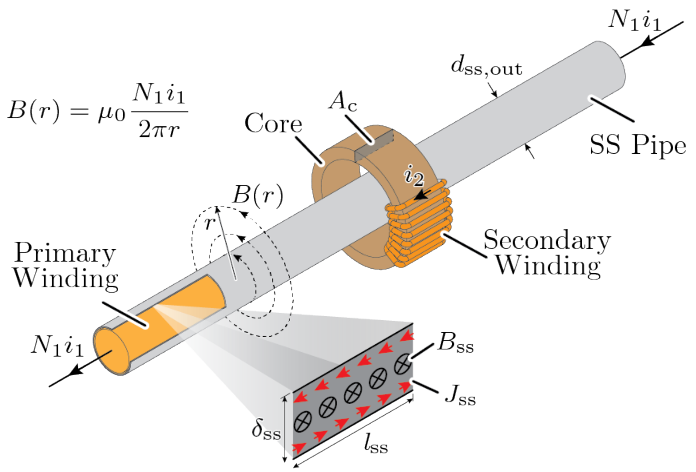

▲ Arrangement of the PFC WPT.

$$R_{ss} = \frac{V_{ss}}{12} \sigma_{ss} \omega_s^2 \frac{\mu_0^2 N_1^2}{4\pi^2} \ln^2\left(\frac{d_{ss,out}}{d_{ss,in}}\right)$$

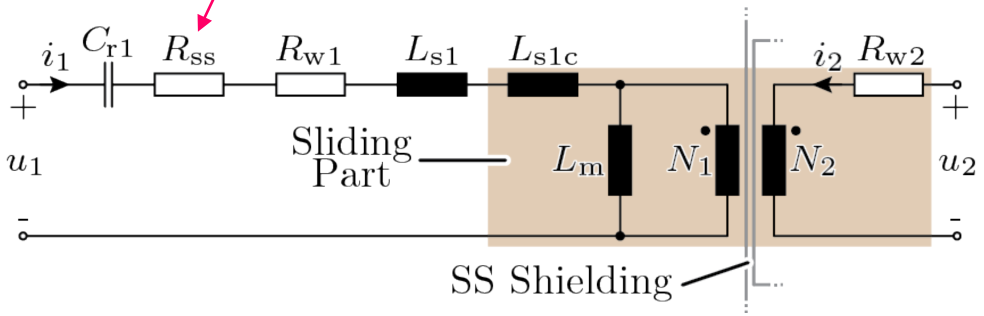

▲ Electrical equivalent circuit.

- The SS losses can be modeled in the same way as (primary-side) winding losses.

[ref] Mirić, Spasoje, et al. "Wireless Power Supply of Moving Linear Actuator Enclosed in Stainless-Steel." 2022 Wireless Power Week (WPW). IEEE, 2022.

Parallel-field Concept WPT — Primary Winding Design

- To find the best arrangement of the wires: 2D-FEM at $N_1 = 12$, $f_{sw} = 50$ kHz.
- Simulation parameters: Round → $d_w = 1.85$ mm ; Flat → $\delta_w = 0.9mm$, $b_w = 1.2mm$, and $d_w = 17$ mm.

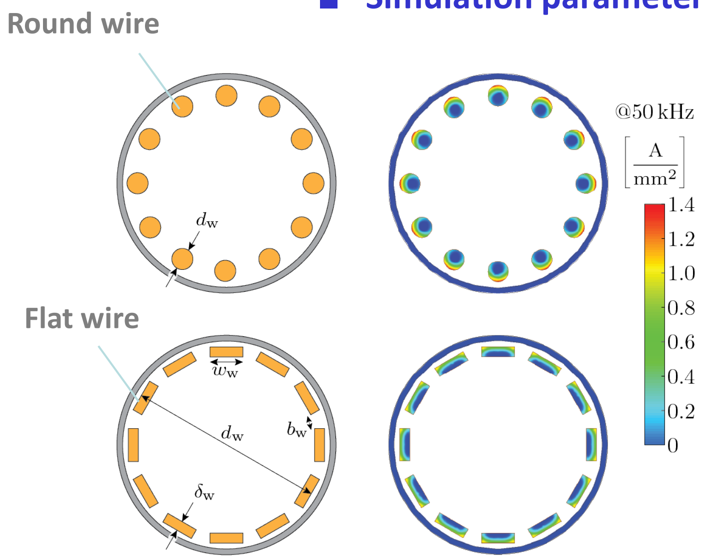

▲ 2D-FEM of analysis of different arrangement of wires.

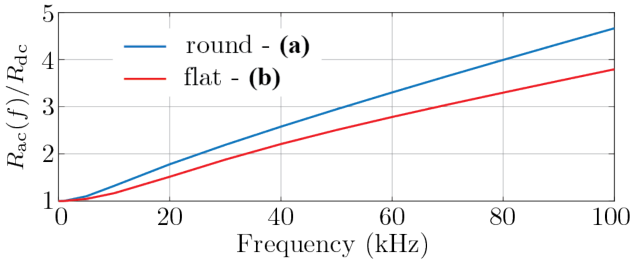

▲ R_{ac}/R_{dc} vs Frequency.

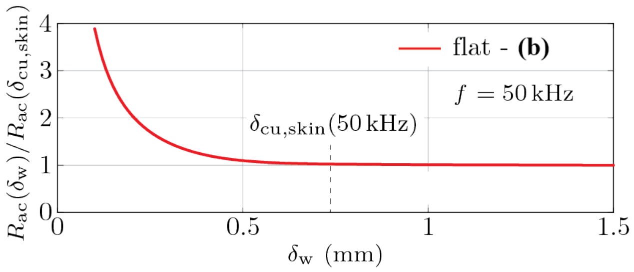

▲ Normalized Winding resistance vs Windign thinkness δ_w.

- The lowest AC resistance → the wires at the circumference, i.e., the flat wire should be used.
- Increasing δ_w above the skin depth does not lead to a further reduction of the winding resistance anymore.

[ref] Mirić, Spasoje, et al. "Wireless Power Supply of Moving Linear Actuator Enclosed in Stainless-Steel." 2022 Wireless Power Week (WPW). IEEE, 2022.

Parallel-field Concept WPT — SS Tube Thermal Model

- The SS surface T_{ss} should be kept below 60^oC.

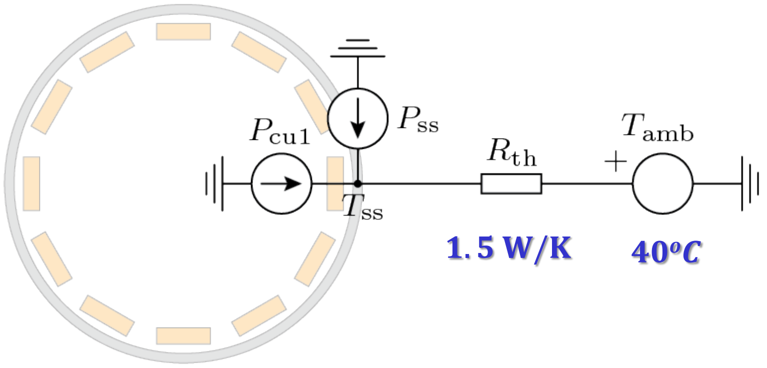

▲ Primary-side thermal model.

Circulate the current through the pipes, and measure the power and the temperature increase.

- To keep $T_{ss} < 60^oC$ at $T_{amb} = 40^oC$, the losses in the primary should be $P_{ss} + P_{cu1} < 13.3\ \mathrm{W}$.

[ref] Mirić, Spasoje, et al. "Wireless Power Supply of Moving Linear Actuator Enclosed in Stainless-Steel." 2022 Wireless Power Week (WPW). IEEE, 2022.

Parallel-field Concept WPT — Electric Equivalent Circuit

- $R_{\mathrm{w1,w2}}$ depends on the operating frequency and the winding geometry → $R_{\mathrm{w1,w2}} = R_{\mathrm{ac}}(f_{\mathrm{sw}})$.
- L_{s1} is the external stray inductance → $L_{s1} = \mu_0 \log[x_{s1}/(d_{\mathrm{w}}/2)] L_{\mathrm{SS}} N_1^2/\pi$.
- L_{s1c} is much smaller than L_{s1} → $L_{s1c} = L_{s1}(h/L_{\mathrm{ss}})$.
- L_{m} is calculated from the A_L value of the core → $L_{\mathrm{m}} = A_{\mathrm{L}} N_1^2$.
- C_{r1} is resonant capacitor → $C_{r1} = 1/[\omega^2 \cdot (L_{s1} + L_{sc1})]$.

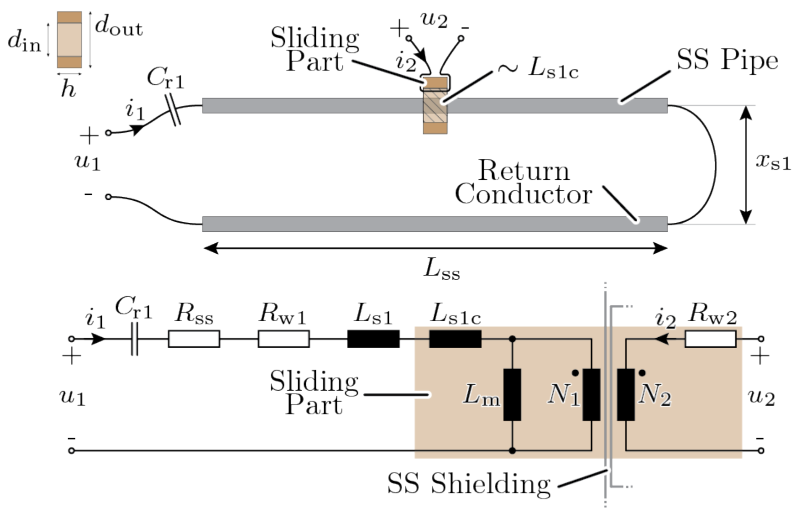

◄ PFC WPT system with a single receiver: conceptual physical arrangement and electrical equivalent circuit.

- Different from the OFC WPT, SS losses do not depend on the air gap field in PFC WPT.

[ref] Mirić, Spasoje, et al. "Wireless Power Supply of Moving Linear Actuator Enclosed in Stainless-Steel." 2022 Wireless Power Week (WPW). IEEE, 2022.

Mode of Operation

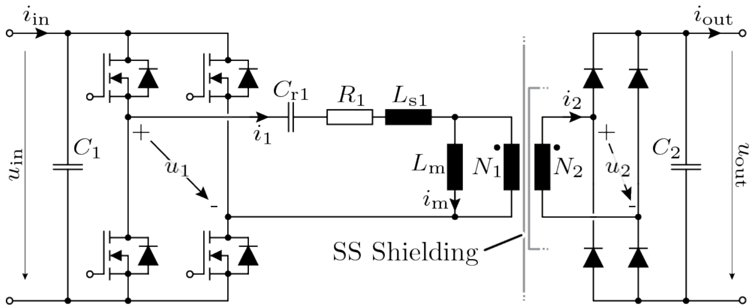

Parallel-field Concept WPT — Voltage-Impressed DCX Operation

- High magnetic coupling → operation of the WPT system as a series resonant converter.
- Switching frequency ≤ resonant frequency → soft switching achieved → “DC transformer” (DCX).

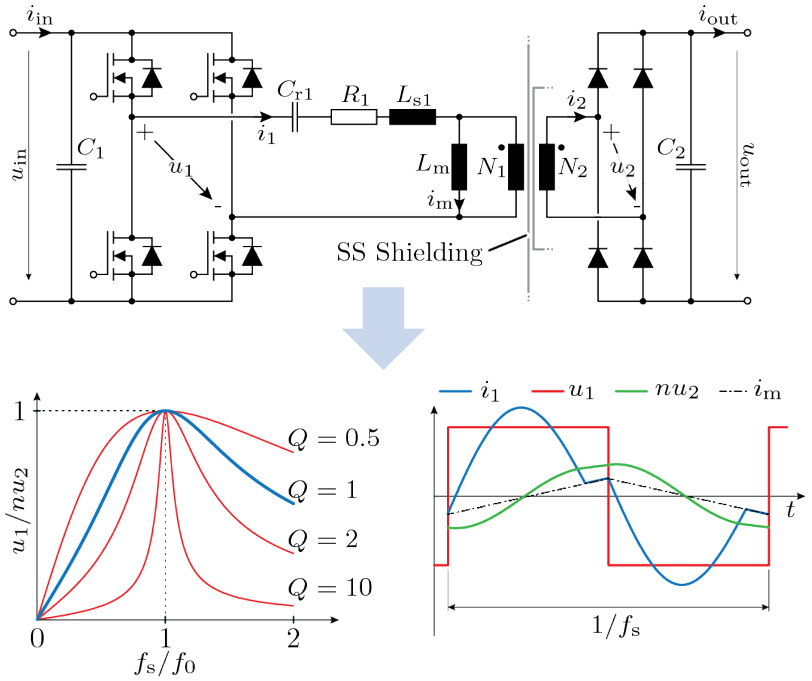

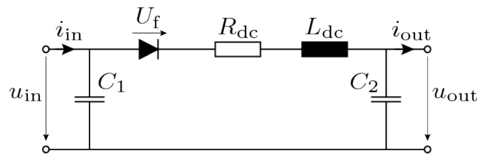

◄ Operation of the PFC WPT system as a “DC transformer”.

- The DCX couples the output voltage tightly to the input voltage without the need for closed-loop control.
- There is no need for a communication link between the primary and the secondary side.

[ref] Mirić, Spasoje, et al. "Wireless Power Supply of Moving Linear Actuator Enclosed in Stainless-Steel." 2022 Wireless Power Week (WPW). IEEE, 2022.

universität innsbruck

Hardware Prototype

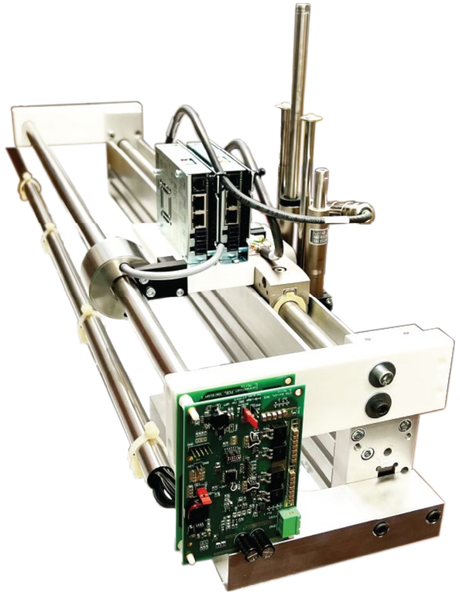

ETH zürich

International Electric Machines & Drives Conference

San Francisco, CA May 15-18

Hardware Prototype — Optimization result

- Swept parameters for different power levels: frequency $f_s = 5 \cdots 60$ kHz, turns $N_1 = N_2 = 4 \cdots 20$ turns.
- Number of secondary cores: $N_{\text{stacked}} = 1$.

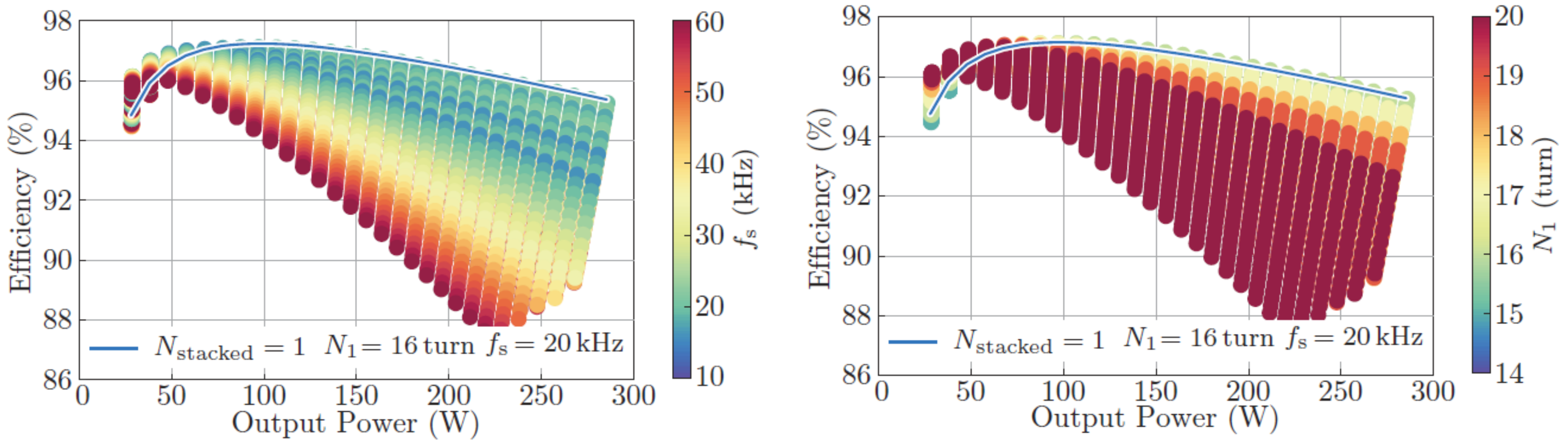

▲ Efficiency vs output power in dependence of the operating frequency f_s and the number of turns in the primary N_1.

- Optimum operation frequency → consequence of the core loss model: $P_{\text{core}} \propto B^a \cdot f^b$.
- The blue line indicates the best design with one stacked core ($N_{stacked} = 1$, $N_1 = 16$ turns, $f_s = 20\ kHz$).

[ref] Mirić, Spasoje, et al. "Wireless Power Supply of Moving Linear Actuator Enclosed in Stainless-Steel." 2022 Wireless Power Week (WPW). IEEE, 2022.

Hardware Prototype — Number of Cores on the Secondary

- The magnetic material area A_{fe} is increased by increasing the number of stacked cores $N_{stacked}$.
- 1 core → 90 gram, 2 stacked cores → 180 gram.

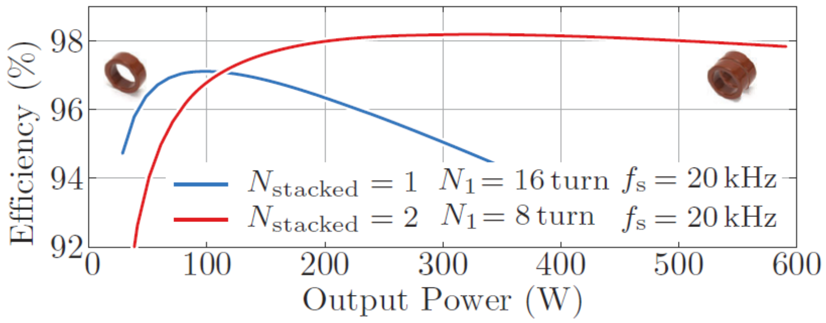

▲ Efficiency versus output power in dependence of the number of stacked cores.

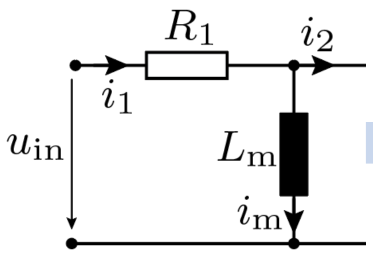

▲ Equivalent circuit.

$$\Psi_m = \frac{U_{in}}{4 \cdot f_s} = \frac{72}{4 \cdot 20k} = 0.9\text{mWb}$$

$$\Phi_m = \frac{\Psi_m}{N_1} = B_m \cdot A_{fe} = B_m \cdot N_{stacked} \cdot A_{core}$$

$$B_m = \frac{\Psi_m}{N_1 \cdot N_{stacked} \cdot A_{core}}$$

- Higher efficiency and/or power transfer can be achieved with two cores ($N_{stacked} = 2$).
- Stacking the cores → lower N_1 → reduce the R_1 accordingly → larger efficiency and output power.

[ref] Mirić, Spasoje, et al. "Wireless Power Supply of Moving Linear Actuator Enclosed in Stainless-Steel." 2022 Wireless Power Week (WPW). IEEE, 2022.

Hardware Prototype — Measurement

- Prototype of a linear $x - z$ actuator with a PFC WPT system → $V_{dc} = 72$ V, $f_s = 20$ kHz, and $P_{out} = 300$ W.
- The inverters supplying the linear motors move together with the linear actuator's slider (in the x-direction).

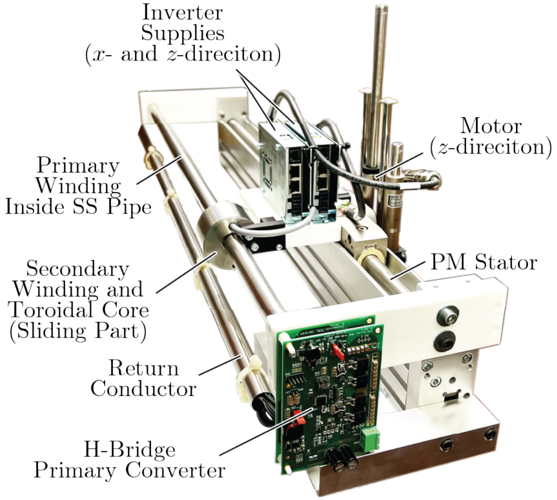

▲ Prototype

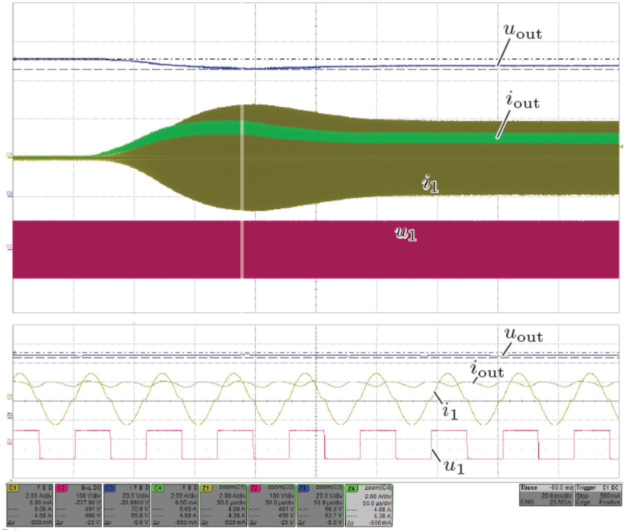

▲ Measured key waveforms during a mechanical load step

- The efficiency is up to 97% through SS (Wireless power transfer efficiency).
- Good load regulation without the need for a closed-loop control system.

[ref] Mirić, Spasoje, et al. "Wireless Power Supply of Moving Linear Actuator Enclosed in Stainless-Steel." 2022 Wireless Power Week (WPW). IEEE, 2022.

Hardware Prototype — Operation

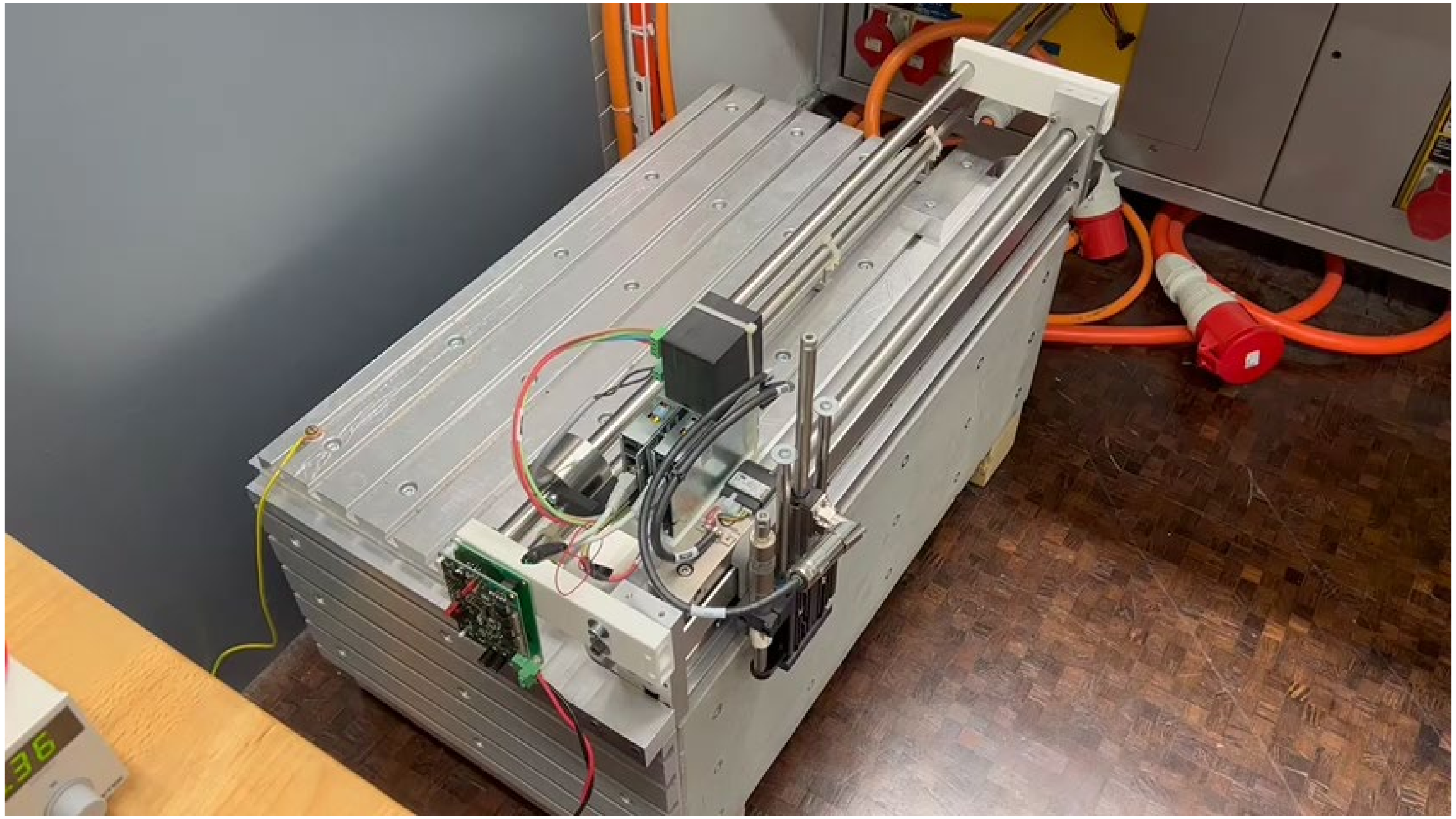

https://youtu.be/xQahtyX00Zo

Multi-Receiver PFC WPT

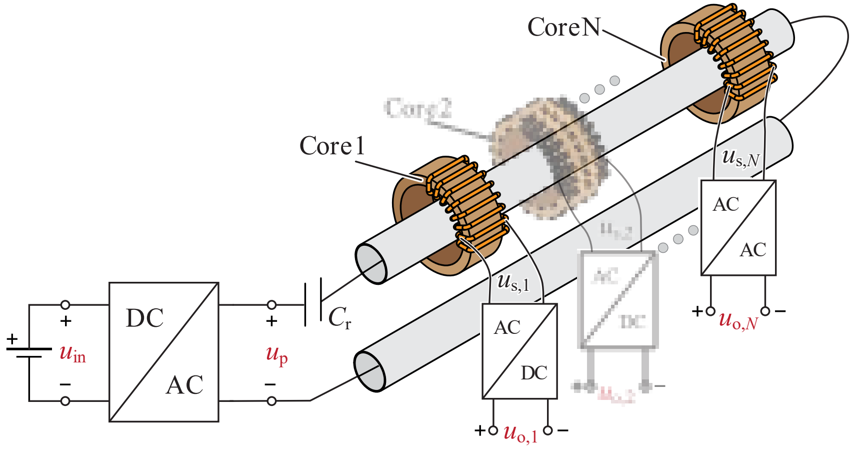

Multiple Receivers— Automatic Time-Sharing Operation

- More than one receiver → magnetic series connection of the secondary windings → the output voltage is uncontrollable (shared by the number of secondaries).
- Automatic time-sharing operation for the PFC WPT linked to multiple receivers without communication and close-loop control.

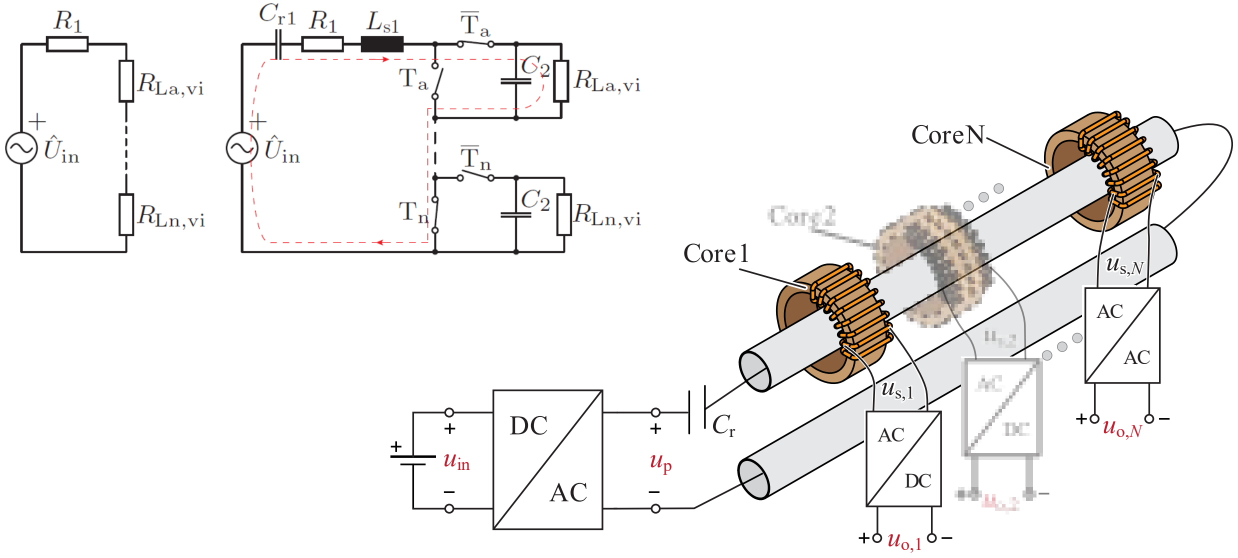

▲ Conceptual physical arrangement of multiple receivers

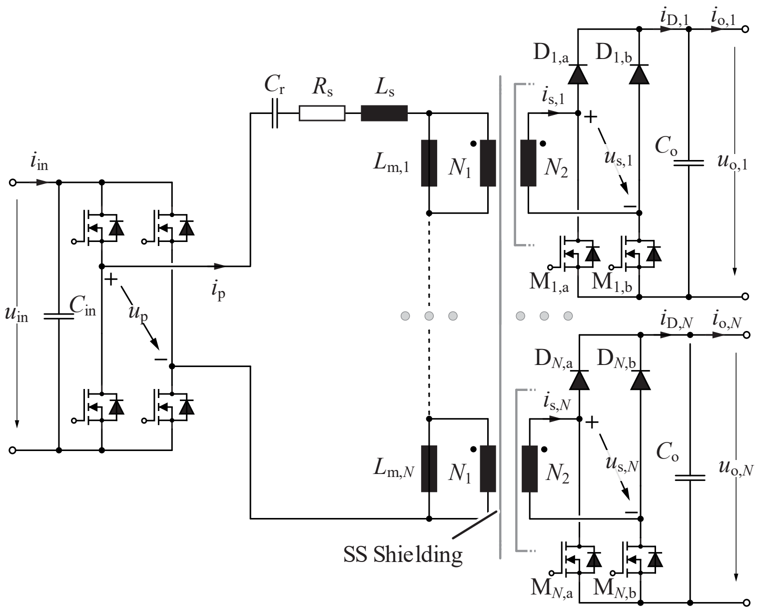

▲ Electronical equivalent circuit of multiple receivers

PFC WPT — Operation with Multiple Receivers

- Multiple independent drivers and power suppliers → coupling between the receivers.
- Time-sharing approach for multiple receivers.

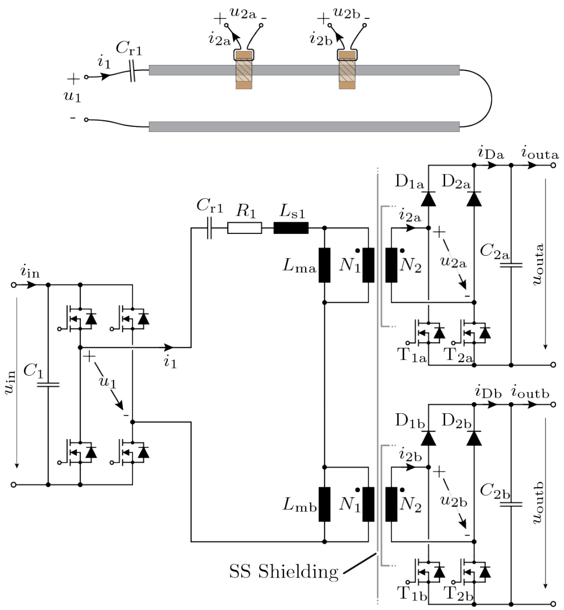

▲ Two receivers WPT circuit.

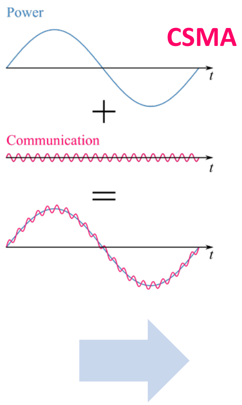

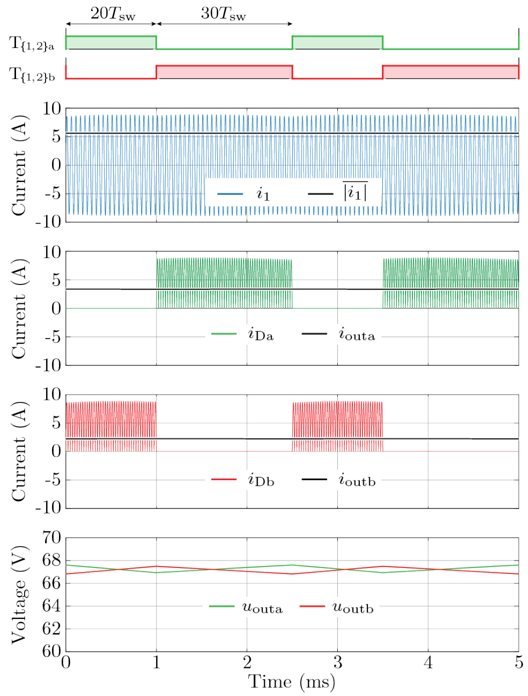

▲ Simulation results.

- The relative on-times depend on the respective output powers as: $D_{\mathrm{a\ or\ b}} = \frac{P_{a\ or\ b}}{P_{\mathrm{a}}+P_{\mathrm{b}}}$.

[ref] Mirić, Spasoje, et al. "Wireless Power Supply of Moving Linear Actuator Enclosed in Stainless-Steel." 2022 Wireless Power Week (WPW). IEEE, 2022.

Hardware Prototype — Two receivers

- Prototype of 2 linear $x-z$ actuators with a PFC WPT system → $V_{dc} = 72$ V, $f_s = 20$ kHz, and $P_{out} = 100$ W $*$ 2.
- Automatically adjusts switching duration of each module.

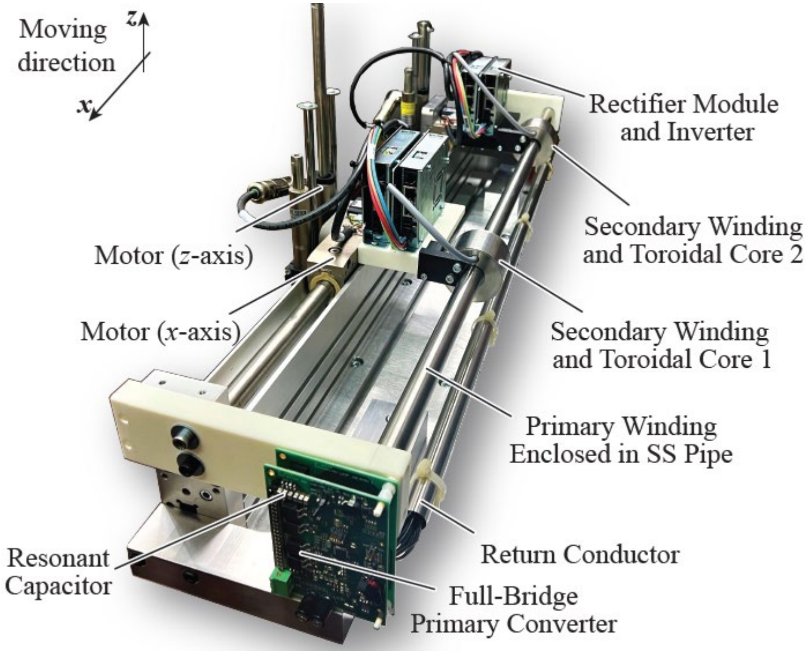

▲ Hardware prototype

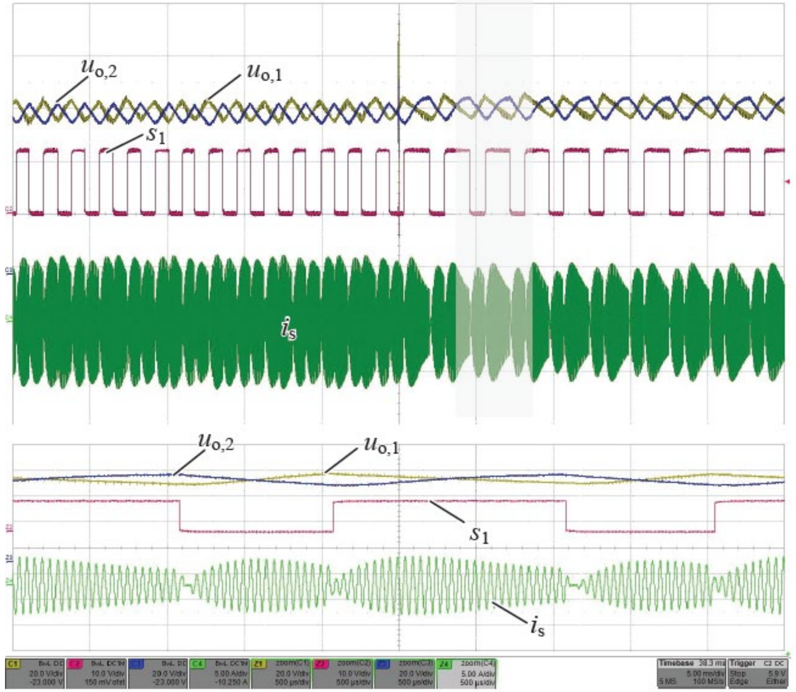

▲ Experimental result at transition.

(One module has a load step change from full load to half load, while the other is at full load.)

Hardware Prototype — Two receivers

- Video

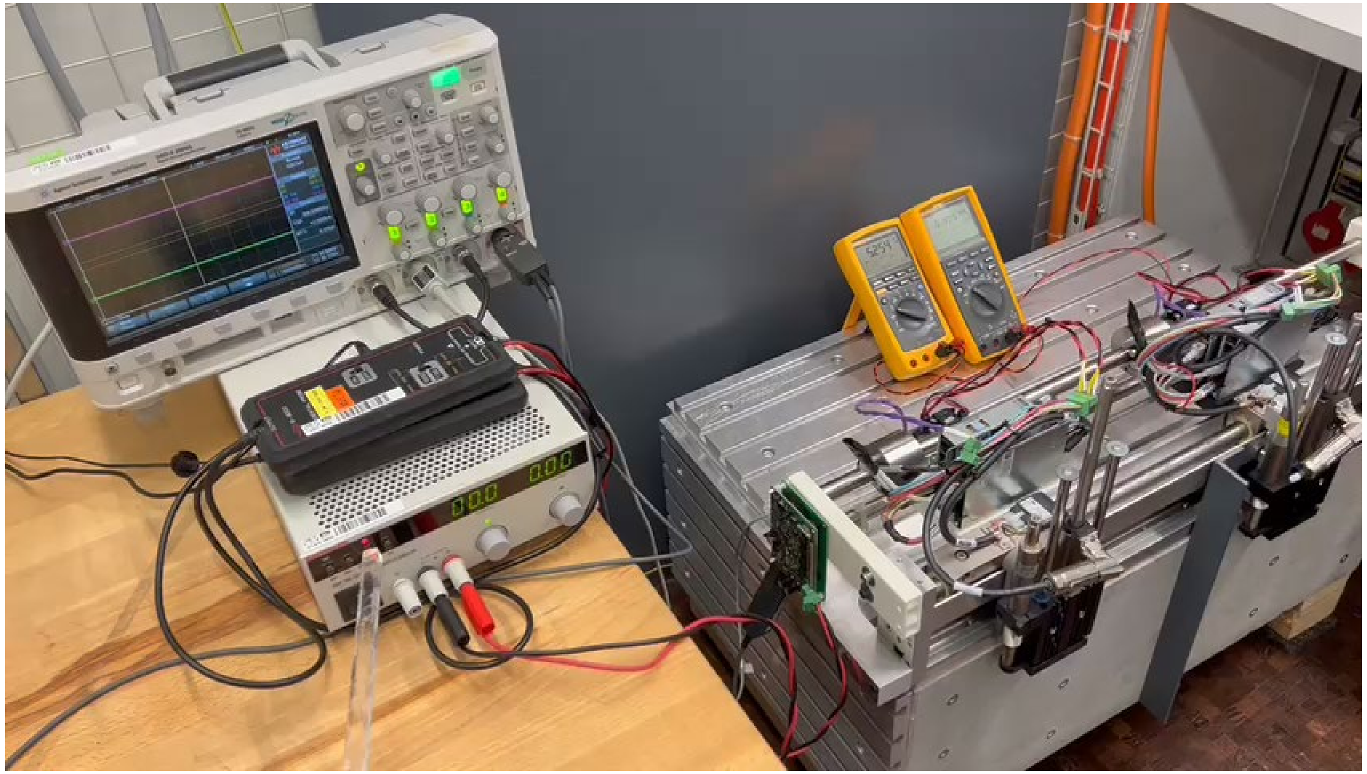

universität innsbruck

Current Impressed PFC

ETH zürich

International Electric Machines & Drives Conference
San Francisco, CA May 15-18

Voltage-Impressed WPT vs. Current-Impressed WPT

- Single receiver with voltage-impressed WPT (DC-X) → load-independent operation
- Multiple receivers → Equivalent to multiple loads connected in series
  - Voltage-impressed WPT → Voltage is shared between loads → time sharing control
  - Current-impressed WPT → load-independent operation

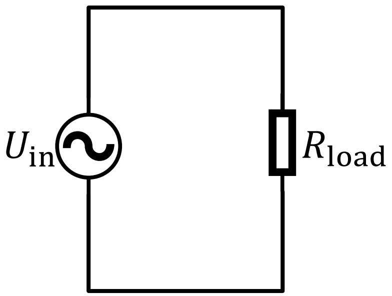

▲ Voltage-impressed WPT
▲ Single-receiver

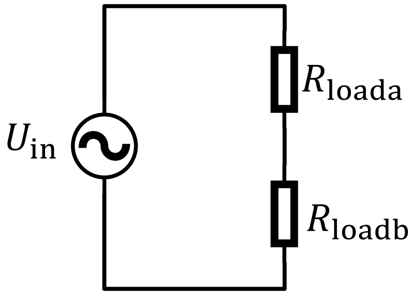

▲ Voltage-impressed WPT
▲ Multiple-receivers

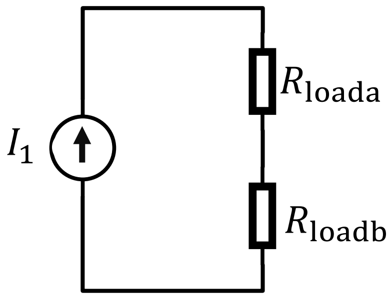

▲ Current-impressed WPT
▲ Multiple-receivers

- Voltage-impressed system can be converted to a current-impressed system
- Symmetric T-network:

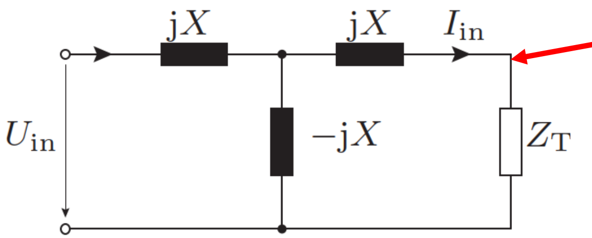

$$I_1 = \frac{U_{\text{in}}}{\mathrm{j}\,X}$$

Current-Impressed WPT, Single Receiver

- Current-impressed WPT for a single receiver → Active rectifier to keep constant U_{out} for different R_{L}
- The impressed current i_1 designed such that for the nominal load and $d_{\mathrm{r}} = 1$, $U_{\mathrm{out}} = U_{\mathrm{out,nom}}$

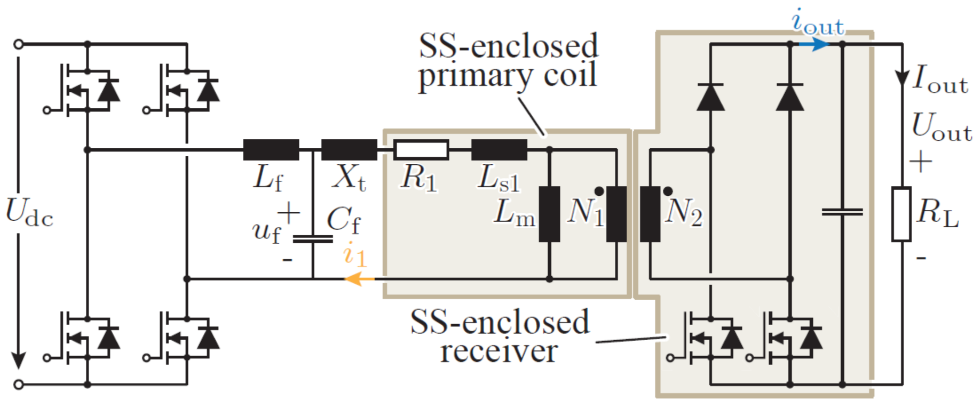

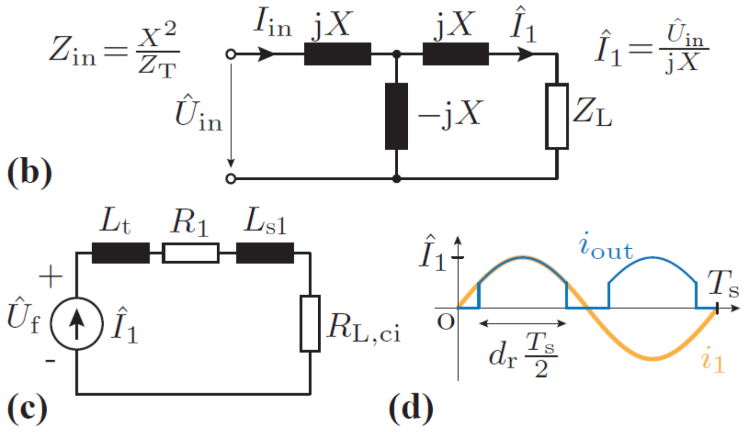

$$i_{\mathrm{out}} = \begin{cases} 0, & \text{MOSFETs are ON} \\ i_1, & \text{MOSFETs are OFF} \end{cases}$$

$$R_{\mathrm{L,ci}} = \frac{8}{\pi^2} \sin^2\left(\frac{\pi}{2} d_{\mathrm{r}}\right) R_{\mathrm{L}}$$

- The equivalent load resistance $R_{\mathrm{L,ci}}$ → depends on the duty cycle d_{r}
- The same current-impressed network can be used for any number of the receivers

Current-Impressed WPT, Multiple Receivers

- The current-impressed (CI) WPT network for a single receiver can be used for multi-receiver CI WPT

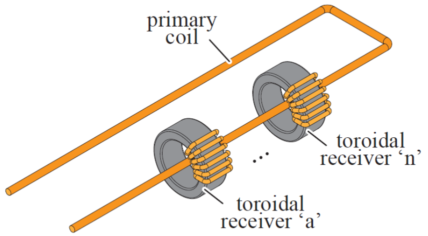

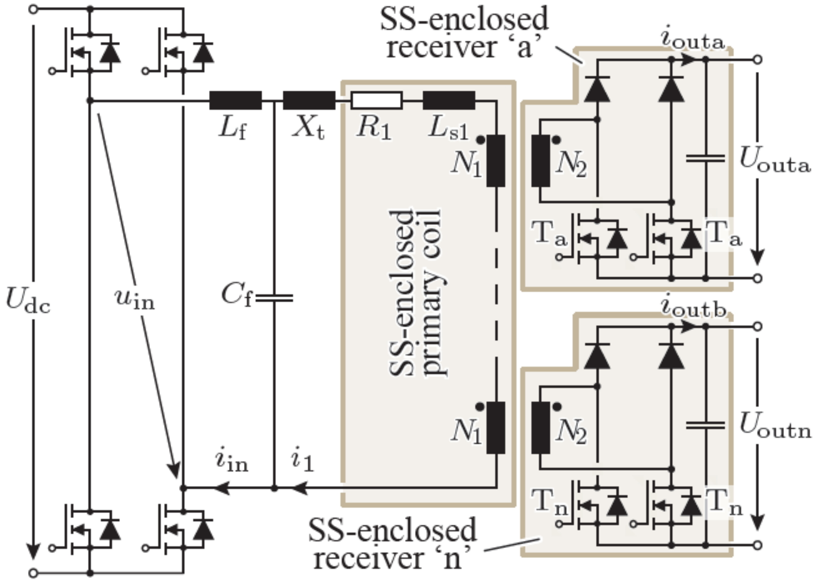

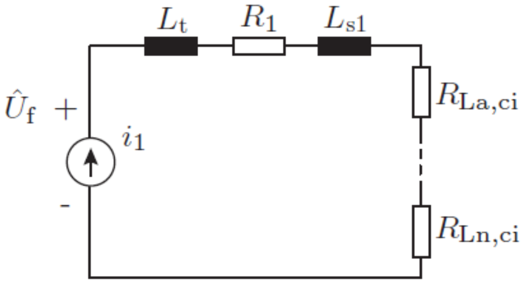

$$\hat{U}_f = \sqrt{(R_1 + n \cdot R_{L,ci,N})^2 + X^2} \cdot \hat{I}_1$$

$$\approx \sqrt{(n \cdot R_{L,ci,N})^2 + X^2} \cdot \hat{I}_1$$

- The voltage over C_f capacitor increases linearly with the number of receivers n

Voltage- vs Current-Impressed WPT

- Voltage-impressed → eq. load resistors in parallel; Current-impressed → eq. load resistors in series

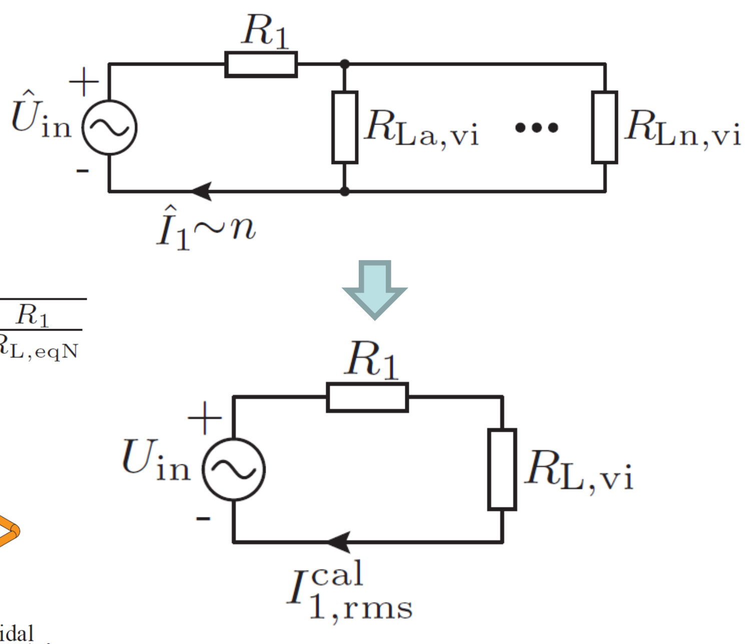

Voltage-impressed

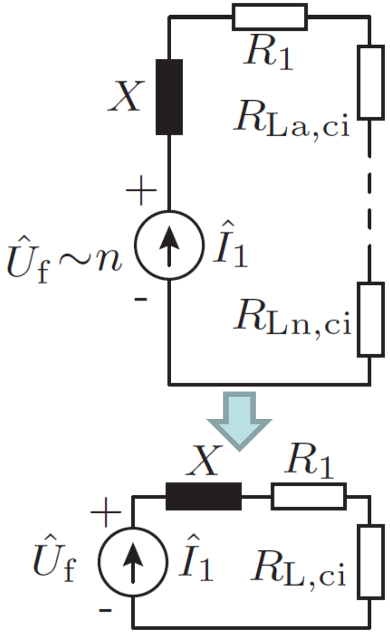

Current-impressed

$$\eta_{\text{vi,max}}(n) = \frac{1}{1 + n \cdot \frac{R_1}{R_{\text{L,eqN}}}}$$

$$\eta_{\text{ci,max}}(n) = \frac{1}{1 + \frac{R_1}{n \cdot R_{\text{L,eqN}}}}$$

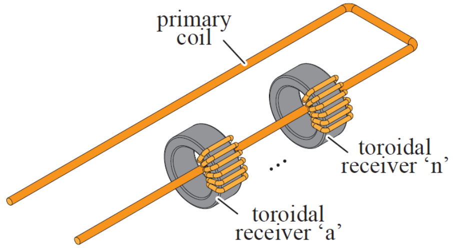

- Voltage-impressed → increased current i_1 over primary coil; Current-impressed → increased voltage over C_{f}

Voltage- vs Current-Impressed WPT

Specifications of the System

Parameter	Name	Value
Voltage-Impressed		
Specifications		
U_{out}	Desired output voltage	72 Vdc
ΔU_{out}	Maximum voltage ripple	4 V
$P_{out,a}$	Nominal output power	100 W
$P_{out,b}$	Nominal output power	50 W
Calculation and Simulation Results		
R_{La}	Load resistance	51.84 Ω
R_{Lb}	Load resistance	103.68 Ω
$R_{La,vi}$	Equivalent load resistance	42.02 Ω
$R_{Lb,vi}$	Equivalent load resistance	84.04 Ω
$R_{L,vi}$	Equivalent load resistance	28.03 Ω
$I_{1,rms}^{cal}$	Input current RMS	2.19 A
$I_{1,rms}^{sim}$	Input current RMS	2.14 A
Current-Impressed		
Specifications		
U_{out}	Desired output voltage	72 Vdc
ΔU_{out}	Maximum voltage ripple	4 V
$P_{out,a}$	Nominal output power	100 W
$P_{out,b}$	Nominal output power	50 W
Calculation and Simulation Results		
d_{ra}	Rectifier duty cycle	1
d_{rb}	Rectifier duty cycle	0.33
R_{La}	Load resistance	51.84 Ω
R_{Lb}	Load resistance	103.68 Ω
$R_{La,ci}$	Equivalent load resistance	42.02 Ω
$R_{Lb,ci}$	Equivalent load resistance	21.01 Ω
$R_{L,ci}$	Equivalent load resistance	63.03 Ω
I_1	Impressed current RMS	1.53 A
I_{in}	Input current RMS	2.37 A
$\hat{U}_f^{cal}$	Simulated peak C_f voltage (17)	167.8 V
$\hat{U}_f^{sim}$	Simulated peak C_f voltage	163.5 V

Parameter	Name	Value
Inverter		
U_{dc}	Input DC link voltage	72 V
f_s	Switching frequency	20 kHz
d_i	Inverter duty cycle	0.5
Compensation		
L_f	T-network inductance	334 µH
C_f	T-network capacitance	189 nF
L_t	X_t inductance	34 µH
Transformer		
R_1	Primary resistance	1.5 Ω
L_{s1}	Primary stray inductance	300 µH
L_m	Magnetization inductance	12 mH
N_1	Number of primary turns	16
N_2	Number of secondary turns	16
Rectifier		
U_{out}	Desired output voltage	72 Vdc
$P_{out,N}$	Nominal output power	100 W
$d_{r,N}$	Nominal rectifier duty cycle	1

Voltage- vs Current-Impressed WPT

- Voltage-Impressed (left) and Current-Impressed (right)

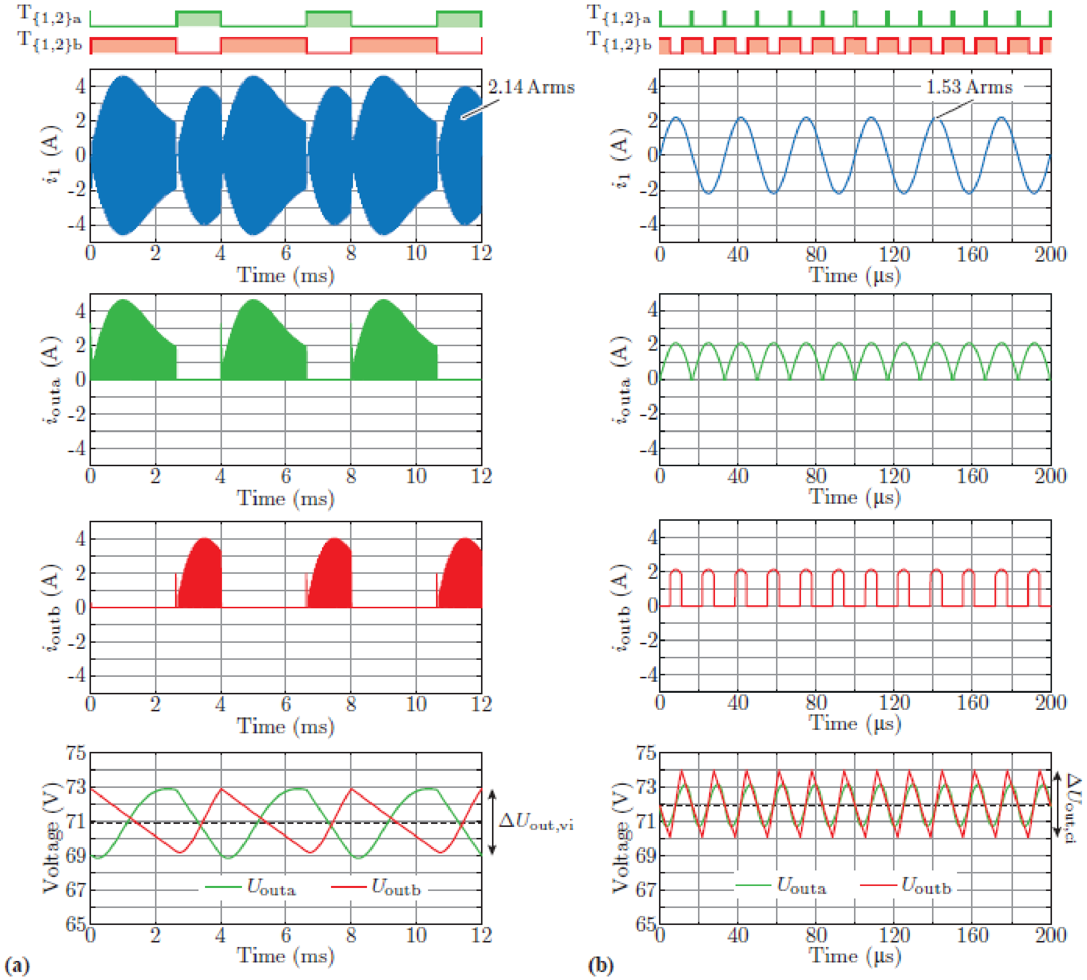

Part 3 Outlook

- OFC and PFC wireless power transfer
- Multiple receivers → Voltage impressed & Current impressed

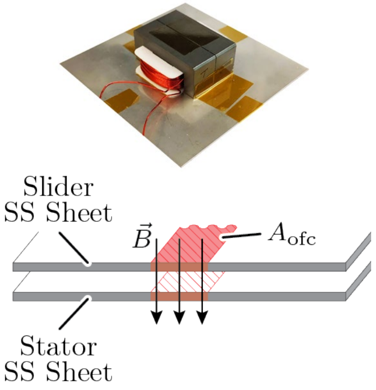

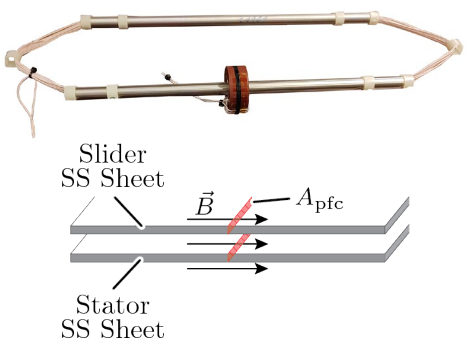

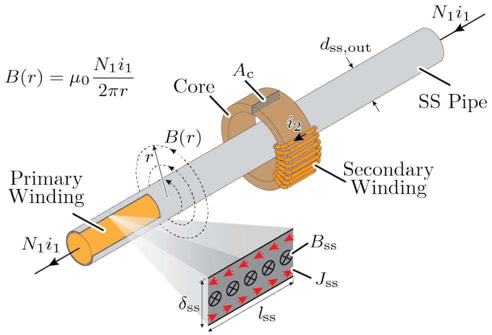

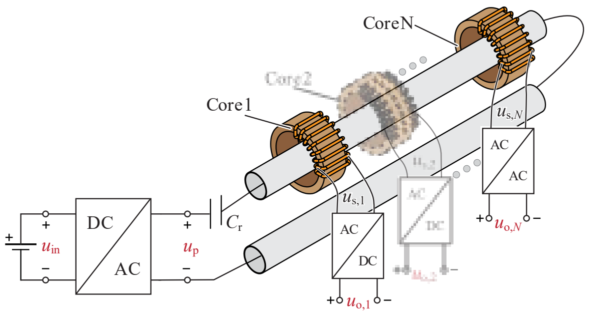

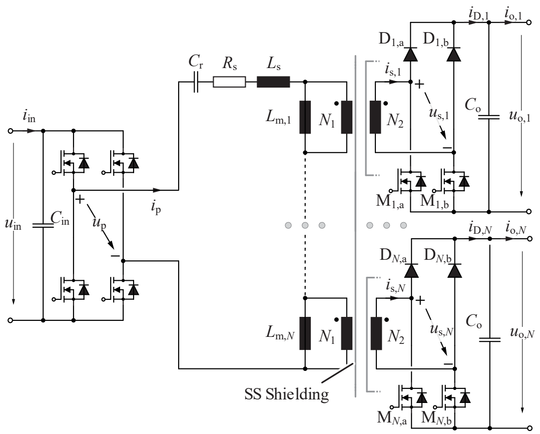

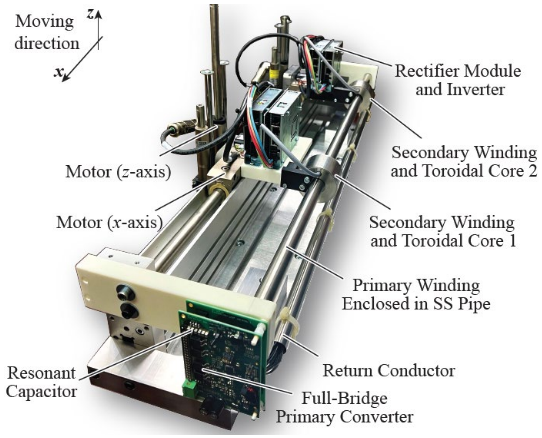

Biography

Biography of the Speaker

SPASOJE MIRIC (M') received B.Sc., M.Sc., and Ph.D. degrees in electrical engineering from the University of Belgrade, School of Electrical Engineering in 2012, 2013, and 2018 respectively, focusing on power electronics systems and drives. In 2021 he defended his second Ph.D. thesis at ETH Zurich at the Power Electronic Systems Laboratory (PES) in the advanced mechatronic systems area. More specifically, during his Ph.D. project, he focused on linear-rotary actuator systems with magnetic bearings, resulting in two new machine topologies patented. Since 2021, he has been with PES as a post-doc researcher, focusing on WBG power converter optimization with hard and soft-switching, new modulation techniques of flying capacitor converters, wireless power transfer systems, and eddy-current-based position sensor systems. He was appointed Ass. Professor and Head of the Innsbruck Drives and Energy Systems Laboratory at the University of Innsbruck (UIBK) on Jan. 1, 2023. DDr. Miric proposed a novel self-bearing actuator topology and a generalized complex space vector calculus for linear-rotary machines. He has published 20+ scientific papers in international journals and conference proceedings and filled 7 patents. He has presented 2 educational seminars at leading international conferences and received 5 IEEE Transactions and Conference Prize Paper Awards.

From 1st of January 2023 → TT Ass. Prof. @ University of Innsbruck

New Laboratory:

Drive and Energy Systems Laboratory (i-DES)

www.uibk.ac.at/mechatronik/ides/

innsbruck Drive and Energy Systems Laboratory

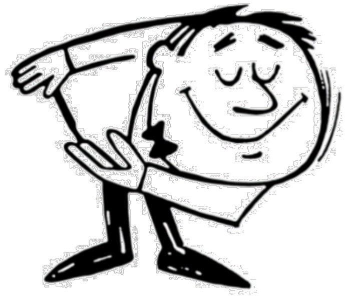

Thank you!